Transport of gases through concrete barriers. Task 3: Characterization of radioactive waste forms

Harris, A.W. , Atkinson, A. and Claisse, P.A.

Commission of the European Communities

nuclear science and technology

ransport of gases through concrete barriers
Task 3
Characterization of radioactive waste forms
A series of final reports (1985-89) — No 33

Report

Commission of the European Communities

nuclear science
and technology

Transport of gases through concrete barriers
Task 3
Characterization of radioactive waste forms
A series of final reports (1985-89) — No 33

A.W. Harris, A. Atkinson, P.A. Claisse [1]
Materials Chemistry Department
Materials and Manufacturing Technology Division
AEA Technology
Harwell Laboratory
Didcot, Oxon
OX11 0RA
United Kingdom

[1] University of Dundee
Department of Civil Engineering
Dundee
DD1 4HN
United Kingdom

Contract No FI1W-0187b

Final report

Directorate-General
Science, Research and Development
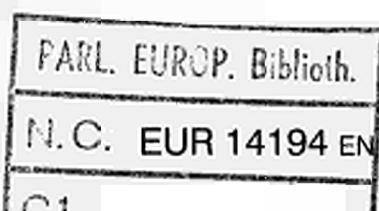
1993

LEGAL NOTICE

Neither the Commission of the European Communities nor any person acting
on behalf of the Commission is responsible for the use which might be made of
the following information

Cataloguing data can be found at the end of this publication

Printed in Belgium

Executive Summary

Objectives

The overall aim of the work described in this report is to improve the level of understanding of the way that gases migrate within the near-field barriers in a radioactive waste repository. In the United Kingdom, UK Nirex Ltd. is responsible for the development of such a repository for the disposal of low and intermediate level wastes. Within the repository, the space surrounding waste packages will be backfilled with materials based on hydraulic cements. Consequently, the migration of gases in cementitious materials is the primary concern of this work.

The generation of gas within the repository will occur by a variety of mechanisms. The principal mechanisms are the anaerobic corrosion of metals, yielding hydrogen, the degradation of organic wastes by microbial action to give methane and carbon dioxide and the radiolysis of water to give hydrogen and oxygen. The effects of the last are not considered to be significant. Consequently, the migration of hydrogen, methane and carbon dioxide have been studied. In addition, helium and argon have been used in experiments where the use of flammable gases would pose a significant risk.

The specific objectives of the work were to develop experimental methods for the measurement of gas migration in cementitious materials by both the bulk flow and diffusion mechanisms and to carry out such measurements. The gas migration rates for the gases listed above have been determined for a range of materials selected to be typical of those expected in a radioactive waste repository. The impact of a variety of parameters has been investigated, in particular the gas pressure, degree of water saturation of the material and the effect of interfaces within the specimens. The data have been interpreted in terms of the pore structures of the materials. A model has been developed which describes the cracking of the cementitious materials due to the stress generated by gas pressurisation. The experimental data have been used in the model to predict the behaviour of a repository.

Experimental Materials and Methods

Five materials were selected for investigation; typical structural concretes based on sulphate resistant Portland cement (SRPC) and a mixture of ordinary Portland cement and pulverised fuel ash (PFA/OPC), a grout consisting of a 9:1 mixture of blast furnace slag and OPC (BFS/OPC) and two high porosity backfilling grouts, referred to as the preliminary and reference backfill grouts. The designs of the two latter materials are the result of an exercise intended to produce backfilling materials with a high sorption capacity for radionuclides combined with the ability to condition the pore water within a repository to a high pH for an extended period, to be permeable to gases and to facilitate the retrieval of waste packages if this should ever be required. The effect of interfaces was investigated by producing specimens of the PFA/OPC-concrete containing reinforcement bars and preliminary backfill grout with a "construction joint".

Three different degrees of water saturation were used. These were achieved by conditioning

specimens in controlled humidity atmospheres. The nominal humidity conditions were dry and 75 and 100 % relative humidity. The last was intended to be representative of material which was completely water saturated, as would be expected eventually in a deep repository placed below the water table.

The pore structures of the materials were characterised by several techniques. The fractional porosity was measured by mercury intrusion porosimetry (MIP), by weight loss on drying and by the direct determination of the volume accessible by gas. The porosities of the concretes were of the order of 0.1 to 0.15 whilst the grouts exhibited porosities of 0.4 to 0.55. The gas accessible volumes were consistently lower than the fractional porosities measured by other means for all the materials in the dry condition. This was attributed to the retention of some water even after drying. The backfill grouts exhibited significant weight loss during conditioning at 100 % relative humidity and subsequent measurements indicated considerable gas accessible volume. This was attributed to the draining of water from the pore space under the influence of gravity. The 100 % relative humidity conditioned grouts may not therefore be representative of complete water saturation.

The pore structures were further characterised by the determination of pore size distributions from the MIP data. The PFA/OPC-concrete and the BFS/OPC-grout both gave quite symmetrical distributions with average pore sizes of about 0.01 μm. In contrast, the backfill grouts gave distributions significantly skewed to larger pore sizes with average pore sizes of about 0.5 μm.

The migration of gas by diffusion in dry SRPC-concrete was determined by the direct measurement of compositional changes due to diffusion through a membrane and from the magnitude of the pressure transient induced by the Kirkendall effect.

The bulk flow of the various gases under a pressure gradient was determined from the decay of a pressure difference established across a membrane. An analytical description of this decay was developed and subsequently modified to allow for the effect of the substantial volumes of porosity present in some specimens. The data were analysed to yield an effective permeability coefficient, as defined by the Darcy equation.

Experimental Results

The measured values of the argon-hydrogen inter-diffusion coefficient for the dry SRPC-concrete were of the order of 10^{-8} m^2s^{-1} for both experimental methods. This is very similar to data obtained by other workers for similar materials.

The permeability of the concretes was found to be strongly dependent on the degree of water saturation. The permeability coefficients were typically $3x10^{-17}$ m^2 and 10^{-21} m^2 for the dry and 100 % relative humidity conditioned materials respectively. The permeability of the dry material was found to depend on the average pressure; the permeability coefficient decreased by a factor of two or three as the average pressure was increased from 100 kPa to 7.5 MPa. This effect can be attributed to an increased contribution from Knudsen flow in fine pores at lower pressures. The BFS/OPC-grout exhibited a wider range of permeability coefficients; $4x10^{-16}$ m^2 when dry and 10^{-21} m^2 when water saturated.

The measured permeabilities of the backfilling grouts were significantly greater, in the range 6×10^{-17} m^2 to 10^{-14} m^2 for the preliminary backfill grout and 4×10^{-17} m^2 to 2×10^{-15} m^2 for the reference backfill grout. The higher permeability coefficients can be correlated with the greater fractional porosities and pore sizes of these materials. No significant variation in the permeability with pressure was observed.

The presence of a construction joint in the preliminary backfill grout increased the permeability coefficient by approximately an order of magnitude. In contrast, the reinforcement bar had no significant effect on permeability of water saturated concrete, although dried material specimens did exhibit an increased permeability coefficient. The increase is probably due to shrinkage away from the bar during drying.

Impact of Gas Generation and Migration

One possible impact of the generation of gas within a repository will be cracking induced by the subsequent pressurisation resulting from an imbalance between the rates of gas generation and migration. A model has been developed which relates the properties of the backfill materials and the gas generation to the likelihood of cracking. Cracking is assumed to occur when the stress induced by pressurisation exceeds the strength of the materials. The stress is dependent on the gas generation rate, the backfill porosity and Poisson's ratio and is inversely dependent on the permeability. The stress is also inversely dependent on the hydrostatic pressure. Consequently, the stress is a maximum prior to the re-saturation of the repository after closure, when the full hydrostatic pressure cannot be transmitted to the backfill.

The calculated stress due to gas generation is about 200 kPa when typical values of the appropriate parameters are assumed. This can be compared to an expected tensile strength of the reference backfill of the order of 400-500 kPa. The apparent draining of the water from the specimens conditioned at 100 % relative humidity may have led to an over-estimate of the permeability coefficients for the backfill grouts in these experiments. Consequently, it is possible that the stress may be significantly greater than 200 kPa and hence cracking due to gas pressurisation may occur.

CONTENTS

List of Tables

1. Summary of the permeability measurements performed in this work. The upper table refers to low pressure experiments (average pressure about 100 kPa) and the upper table to experiments performed with higher average pressures. In addition, measurements were carried out using hydrogen and argon in dry SRPC-concrete.

2. Water-cement and aggregate-cement ratios and total cement content used in the manufacture of the experimental materials. Data for backfill grouts are unavailable. All ratios are by weight.

3. Physical properties of the experimental materials. Average pore radius values obtained using mercury intrusion porosimetry (MIP). MIP measurements were not performed on the SRPC-concrete.

4. Fractional porosities obtained from the weight loss for each material during conditioning in the given relative humidity atmosphere (Wt.) and from the measurement of gas accessible volumes (GAV). Negative value is due to inaccuracy in the measurement.

5. Calculated values of the hydrogen-argon inter-diffusion coefficient for the dry SRPC-concrete at the average pressures shown. The appropriate values of the argon permeability coefficient used in the calculation, derived from Figure 14, are also given.

6. Results of the measurements of gas flow in dry PFA/OPC-concrete using varying average pressures. Data given are the means of best-fit values for the Klinkenberg equation. Low pressure data obtained for average pressures in the range 0 to 200 kPa. High pressure data obtained for average pressures in the range 0 to 7.5 MPa. Quoted errors are standard errors.

7. Measured permeability coefficients for a constant average pressure of 100 kPa in the experimental materials. All data are expressed as k / m^2.

8. Measured values of the infinite pressure permeability coefficient. Data for the dry conditioned specimens obtained for pressures in the range 0 to 200 kPa only. Quoted errors are standard errors. All data are expressed as k / m^2.

9. Measured values of the Klinkenberg constant for materials in the dry condition obtained using varying average pressure experiments. Where quoted, errors are standard errors. All data are expressed as $b / 10^5$ Pa.

10. Measured values of permeability coefficients for the flawed specimens. The constant average pressure data were obtained from experiments at an average pressure of 100 kPa. Where quoted, errors are standard errors. All data are expressed as k / m^2.

11. Measured ionic conductivities for the experimental materials saturated by a 3 M sodium chloride solution. Calculated equivalent sodium-chloride ion inter-diffusion coefficients are also given. Where quoted, errors are standard errors.

12. Pressure of 1 mole of gas when occupying quoted volume calculated from the Van der Waals equation. Percentage deviation from the pressure predicted by the ideal gas approximation for the same volumes are given in brackets. There is no significant deviation for a volume of $2 m^3$. Pressures expressed as $p / 100$ kPa.

List of Figures

13. Summary of the permeability coefficients measured for PFA/OPC-concrete conditioned under dry, 75 % relative humidity and 100 % relative humidity conditions. All measurements were performed using a constant average pressure of 100 kPa.

14. Variation in the permeability coefficients for hydrogen and argon in dry SRPC-concrete with average pressure. The curves demonstrate the fit of the Klinkenberg equation to the data. The permeability coefficients are expressed as $k / 10^{-17}$ m^2. Error bars illustrate the slight variation in average pressure which occurred during individual experiments.

15. Variation in the permeability coefficient for argon in dry PFA/OPC-concrete with average pressure. Each point is the mean of several experiments carried out at the same average pressure. The permeability coefficients are expressed as $k / 10^{-17}$ m^2.

16. Variation in permeability coefficient with average pressure in the BFS/OPC-grout during a single varying average pressure experiment. Measured values of the infinite pressure permeability coefficient and Klinkenberg constant were 3.64×10^{-16} m^2 and 7.31×10^4 Pa respectively.

17. Illustration of the spherical repository approximation used as the basis for the model of stress and crack generation in backfill.

18. Variation in spherical hoop stress at the void surface with gas generation rate, hydrostatic pressure, void radius and backfill permeability coefficient, calculated from the analytical solution to the stress generation model.

19. Summary of the conclusions of the stress generation model. The variation in tangential hoop stress at the void surface for three different void radii is plotted against permeability coefficient. The estimated tensile strengths for the materials investigated in this work are also plotted against the range of the permeability coefficients. A material is considered to crack if the calculated stress exceeds the tensile strength, as shown by the regions labelled "survive" and "crack".

Abbreviations

BFS	Blast furnace slag
GAV	Gas accessible volume
MIP	Mercury intrusion porosimetry
OPC	Ordinary Portland cement
PFA	Pulverised fuel ash
RH	Relative humidity
SRPC	Sulphate resistant Portland cement

A	Area (m^2)
b	Klinkenberg constant (Pa)
c	Concentration ($mol\ m^{-3}$)
c_0	Solubility of gas in water ($mol\ m^{-3}$)
D	Diffusion coefficient ($m^2 s^{-1}$)
e_r	Radial strain
E	Young's modulus (Pa)
g	Acceleration due to gravity ($9.81\ m\ s^{-2}$)
G	Volumetric gas generation rate ($m^3\ s^{-1}$)
G_0	Volumetric gas generation rate measured at atmospheric pressure ($m^3\ s^{-1}$)
h	Height of a column of water (m)
H	Relative humidity
J	Molecular flow rate ($mol\ s^{-1}$)
k	Permeability coefficient (m^2)
k_{sd}	Permeability coefficient equivalent to the solution-diffusion mechanism (m^2)
k_∞	Infinite pressure permeability coefficient (m^2)
l	Thickness (m)
n	Quantity of substance (mol)
p	Pressure (Pa)
p	Hydrostatic pressure (Pa)
p_{av}	Average pressure (Pa)
p_{final}	Final pressure after completion of an experiment (Pa)
p_H	Pressure measured in the hydrogen reservoir (Pa)
p_p	Average pressure in the pore space of a specimen (Pa)
p_v	Pressure in void (Pa)
p_0	Atmospheric pressure (101325 Pa) and pressure at which gas solubility is defined (Pa)
p_1	Pressure in low pressure reservoir of experimental apparatus (Pa)
p_2	Pressure in high pressure reservoir of experimental apparatus (Pa)
Q	Volumetric gas flow rate ($m^3 s^{-1}$)

r	Correlation coefficient
r_p	Pore radius (m)
R	Ideal gas constant ($8.31\ \mathrm{Jmol^{-1}K^{-1}}$)
R	Void radius (m)
Re	Reynold's number
S_r	Radial stress (Pa)
S_θ	Tangential hoop stress (Pa)
T	Thermodynamic temperature (K)
V	Volume ($\mathrm{m^3}$)
V_m	Molar volume ($\mathrm{m^3}$)
V_p	Volume of the pore space in specimen ($\mathrm{m^3}$)
V_1	Volume of the low pressure reservoir in the experimental apparatus ($\mathrm{m^3}$)
V_2	Volume of the high pressure reservoir in the experimental apparatus ($\mathrm{m^3}$)
V'	Ratio of V_2 to V_1
x	Position (m)

α	Initial pressure in low pressure reservoir of experimental apparatus (Pa)
β	Initial pressure in high pressure reservoir of experimental apparatus (Pa)
γ	Constant in Van der Waals equation ($\mathrm{Pa\ m^6\ mol^{-2}}$)
δ	Constant in Van der Waals equation ($\mathrm{m^3\ mol^{-2}}$)
ε	Fractional Porosity
λ	Mean free path (m)
μ	Viscosity (Pa s)
ν	Poisson's ratio
ρ	Density ($\mathrm{kg\ m^{-3}}$)
σ	Ionic conductivity ($\mathrm{\Omega^{-1}m^{-1}}$)
σ	Surface tension ($\mathrm{N\ m^{-1}}$)
ζ	Radius of the spherical repository (m)

1 Introduction

1.1 The Role of Cementitous Materials in a Repository

In the United Kingdom, UK Nirex Ltd. is responsible for the development of a deep underground repository for the disposal of low and intermediate level radioactive wastes. In the repository, the spaces around waste packages will be backfilled with a cementitious grout and structural concretes will also be used. Being below the water table, the contents of the repository will relatively quickly become more-or-less water-saturated after the cessation of operations and final closure.

Gas will be generated within the repository by several mechanisms. Conditions will become anaerobic soon after closure following the consumption of oxygen by the oxidation of metal and aerobic microbial processes. Subsequently, the principal gas generation mechanisms are the anaerobic corrosion of metals, generating hydrogen, microbial degradation of organic wastes and other materials, generating methane and carbon dioxide, and the radiolysis of water, producing hydrogen and oxygen. The effects of the last are insignificant.

The gas pressure within the repository will rise locally above the ambient hydrostatic pressure to a value determined by the relative rates of generation and migration through the repository structure into the surrounding geosphere. It is conceivable that this pressure rise may be sufficient to affect the repository structure and properties and may drive contaminated water into the geosphere without it having been fully chemically conditioned to a high pH. Thus, information on the movement of gases through the repository structure is required to determine the magnitude of these effects and the need to accommodate them in the repository design and safety calculations.

Cementitious materials may be utilised for three main purposes in the construction of the United Kingdom radioactive waste repository; the manufacture of structural components, the backfilling of the repository vaults and the encapsulation of materials within the actual waste packages. The materials selected for study in this work were chosen to be typical of those which may be adopted for each of these three applications [1].

The structural concretes studied were relatively conventional materials based on either sulphate resistant Portland cement (SRPC) or a mixture of ordinary Portland cement (OPC) and pulverised fuel ash (PFA), together with both fine and coarse limestone aggregates. The waste encapsulation material was represented by a grout based on a 1:9 mixture of OPC and blast furnace slag (BFS) containing no aggregate.

The backfilling material requires a high porosity both to provide a readily-accessible capacity for the sorption of radionuclides and to condition fully the chemistry of the mobile water in the repository. Cementitious materials condition the pore water to a high pH by the dissolution of the various mineral phases present. A high pH has beneficial effects on the solubilities of many radionuclides. Two materials that fulfil these criteria, but differing in composition and compressive strength, have been studied in this work. They are referred to in the text as the preliminary backfill grout and the reference backfill grout.

1.2 Experimental Work

This study has investigated the migration of a range of gases in the five different experimental materials detailed in Section 1.1. The magnitude of the rate of migration by both bulk flow and diffusion has been characterised. The impact on gas migration of a range of variables has been investigated. These were as follows:

     (i)   Nature of the cementitious material;

     (ii)   Type of gas migrating;

     (iii)   Degree of water saturation of the cementitious material;

     (iv)   Gas pressure;

     (v)   Presence of potential short-circuit pathways within the cementitious materials.

The cementitious materials and gases were as detailed in Section 1.1. The impact of water saturation was determined by conditioning materials in controlled humidity atmospheres to achieve a known level of water saturation. The conditions were selected to give specimens with zero, 75 and 100 % of the pore volume occupied by water. Measurements were carried out with a range of pressure gradients and average pressures. The ranges of pressure gradient and average pressure were 1 to 75 MPa m^{-1} and 100 kPa to 7.5 MPa respectively.

The cementitous materials within a repository will necessarily contain interfaces which may act as "short-circuit" pathways, providing a route for more rapid gas migration. The effect on gas migration of such interfaces due to the process of construction has been assessed for concrete containing reinforcement and backfill grout containing a construction joint.

The experimental measurements of the permeability coefficient were carried out at what can be described as either low pressure (typical pressures of the order of 100 kPa) or high pressure (pressures typically well in excess of 100 kPa). The entire matrix of measurements required to fully investigate the effects of five parameters discussed above was not performed. The experiments actually performed are summarised in Table 1.

In addition to the experiments detailed in Table 1, permeability measurements were performed on the SRPC-concrete using hydrogen and argon as the migrating gases. The diffusion of hydrogen and argon in the SRPC-concrete was also investigated.

A discussion of previously reported experimental techniques for the measurement of gas migration and the results obtained is provided to allow comparison with the data obtained from the present work. A wide range of measurements have been reported but few are directly relevant to the description of the migration of gases in the water-saturated cementitious materials likely to be present in a radioactive waste repository. The experimental methods developed for the experimental work detailed in this report are described and related to the techniques used by other workers.

The implications of the results for the behaviour of gases, in particular gas migration, within a radioactive waste repository are considered using a simple model of stress generation and

cracking based on the behaviour of a hollow spherical body. The actual experimental results and discussion of various additional factors which may influence the results are given in the appendices.

2 Background

2.1 Mechanisms of Gas Migration

The migration of gases within porous media is the subject of an extensive literature and has been reviewed on several occasions [2-5]. The fundamental mechanisms of gas migration are flow due to an imposed pressure gradient and flow due to a composition gradient. These are termed bulk, or permeable, and diffusive migration respectively.

The steady-state viscous flow of a fluid in a capillary under an imposed pressure gradient at sufficiently low Reynolds numbers (Re<2100) is governed by the Hagen-Poiseuille law [2, 3]. In a real porous medium the Hagen-Poiseuille law must be modified to allow for the convolutions of the pore structure, resulting in Darcy's equation for the bulk, or viscous, flow of an effectively incompressible fluid such as water [2, 3, 6];

$$Q = -\frac{kA}{\mu}\frac{dp}{dx} \qquad ....(1)$$

where Q is the volumetric flow rate, k the permeability coefficient, A the cross-sectional area of the medium perpendicular to the direction of flow, μ the fluid viscosity and dp/dx the applied pressure gradient. The permeability coefficient is considered to be a property specific to the porous material and hence should be independent of the both the properties of the fluid and the specific transport mechanisms. In a highly compressible fluid, that is a gas, the pressure gradient cannot be considered to be independent of position in a material and, even in a steady state, the volumetric flow rate is significantly different at every point in the medium. Under steady-state conditions, the molecular flux must be conserved throughout the medium and consequently Darcy's equation can be re-cast in terms of the molecular flow rate, J [2];

$$J = -\frac{kAp_{av}}{\mu RT}\frac{\Delta p}{l} \qquad ....(2)$$

where p_{av} is the average pressure in the medium and Δp the pressure difference imposed across specimen thickness l.

It has been frequently observed that the gas permeability of a porous medium is dependent on the gas pressure. Hence, the permeability coefficient for a gas in a particular medium will generally differ from that measured for an incompressible fluid. This effect was noted by Klinkenberg from investigations of migration of gas in oil reservoirs [7]. An empirical equation was proposed to describe these observations;

$$k = k_\infty (1 + b/p_{av}) \qquad (3)$$

- 4 -

where k is the gas permeability coefficient measured at average pressure p_{av}, k_∞ the gas permeability coefficient which would be observed at infinite pressure and b a constant termed the Klinkenberg constant. Hence, the measured gas permeability coefficient decreases with increasing average pressure. The infinite pressure permeability coefficient should be equal to the permeability coefficient for an incompressible fluid. Klinkenberg also observed that the value of the constant was dependent on the water permeability coefficient.

The Klinkenberg effect is due to an additional contribution to the assumed viscous flow from Knudsen or "slip" flow at low pressures [2, 3, 9]. Hence, at some particular range of pressure the mechanism of gas flow will be transitional between viscous and Knudsen flows. The Knudsen flow regime becomes significant when the mean free path of the gas is of the same order as or greater than the size of the capillary or pore in which the gas is flowing. The consequent reduction in the interaction between the gas molecules and the capillary wall results in a non-zero flow adjacent to the capillary walls, increasing the overall flow relative to the purely viscous flow regime. The mean free path is inversely dependent on pressure and hence the contribution from Knudsen flow in a particular medium is reduced at higher pressures.

The migration of a species under a composition gradient, as opposed to a pressure gradient, is characterised by a material dependent parameter known as the diffusion coefficient. For one-dimensional diffusion with a constant diffusion coefficient, the diffusion coefficient is determined by Fick's laws of diffusion [10];

$$J = -D \frac{\partial c}{\partial x} \qquad ....(4)$$

$$\frac{\partial c}{\partial t} = D \frac{\partial^2 c}{\partial x^2} \qquad ....(5)$$

where c is the concentration and D the diffusion coefficient. In an unconfined system, the rate of diffusion of a gas is determined by the molecular velocity and hence, at a given temperature, the rate of diffusion is inversely dependent on the square root of the molecular mass. In a confined system, such as a porous medium, the inter-diffusion of two gases at a constant pressure results in a shift of the centre of mass of the system because the lighter gas diffuses more rapidly. Consequently, the migration of gases at constant pressure must be effectively described as the sum of a diffusive flow and a non-segregative bulk flow [2]. Alternatively, if the pressures are not constrained to remain equal to the initial pressure, the differing diffusive flow rates result in an imbalance in the pressures and a pressure difference arises. This is known as the Kirkendall effect [3, 11]. The resulting bulk flow exactly counter-balances the difference in diffusive flows and the rate of change in composition of each gas is equal. Hence, only a single diffusion coefficient can be determined, the inter-diffusion coefficient for the pair of gases utilised.

The movement of molecules during the diffusion of a gas in a porous medium can occur by

both the normal, "viscous" type flow and by Knudsen flow [12]. Consequently, gas diffusion coefficients may be dependent on the pressure in similar manner to permeability coefficients discussed above.

The migration of gases within the pore structure of the cementitious materials intended for use in repository construction will be complicated by the presence of pore water. Under fully water saturated conditions the pores will be effectively blocked and, for lower gas pressure gradients, the only plausible mechanism of gas migration will be the aqueous phase diffusion of gas molecules which have become dissolved in the water. It is currently not known whether the conditions within a repository will result in completely water-saturated material or whether some air will be trapped initially. At a sufficient excess internal pressure difference the gas should be able to expel a proportion of the pore water from the porosity of even fully-saturated material, allowing migration in what is effectively a small volume fraction of open porosity. Under such conditions, the migration will in reality be a two-phase flow. In the current work this complication is ignored and the gas migration treated as a simple single phase situation.

The production of gas within a radioactive waste repository subsequent to closure and re-saturation by water will result in an increase in pressure above the prevailing hydrostatic pressure. Consequently, it is expected that gas migration will be primarily driven by excess pressure. Some degree of migration will occur by the solution-diffusion mechanism. On the basis of available information, it is not expected that gaseous diffusion will be significant in the post-closure situation although it may be of greater relevance during the operating period.

2.2 Review of Experimental Measurements of Gas Migration
2.2.1 Gas Permeability of Cementitious Materials

Measurements of the permeability of cementitious materials to fluids have been extensively reported. However, experimental measurements of the permeability of such materials to gases in particular are less widely available. Previously reported data are generally concerned with the development and validation of experimental techniques intended for determining gas permeability for model cement pastes [13] or structural concretes [8, 14-18] and as a parameter to be correlated with the durability of structural concretes, often as an *in situ* technique [19].

The techniques employed for the measurement of gas permeability differ substantially in detail but are all based on the determination of the flow rate of a gas under an applied pressure gradient. The most common technique utilises a membrane-type arrangement with a specimen of material separating two gas reservoirs at different pressures. The flow rate into the lower pressure reservoir is monitored with a flow meter, generally of the bubble-type [8, 14, 16-18, 20]. Typical applied pressures utilised lie in the range 0.2 to 1 MPa, resulting in pressure gradients of the order of 1 to 20 MPa m^{-1}. The determination of the permeability from the measured flow rate is relatively straightforward for this "membrane" technique. An alternative technique utilises the decay of a known pressure due to the flow of gas to determine the permeability [15, 19]. Martin describes the implementation of such an experimental technique but this method of data analysis

provides only a qualitative indication of permeability [15].

The actual gas permeability coefficients for cementitious materials cover a wide range, depending on the composition and condition of the material. This range is typically about 10^{-21} to 10^{-15} m^2. The lower permeability coefficients are those measured for water-saturated materials where the flow rates for such materials are often too low to be measured in the membrane technique. Hence, the majority of reported measurements of permeability are for dried materials.

The intrinsic permeability coefficient of a porous material is generally considered to be determined by the properties of the material and hence should be independent of the permeating fluid. However, at the pressures typically utilised for gas permeability measurements, the gas permeability coefficient is generally found to be significantly in excess of that for water. Bamforth has found that the gas permeability lies between 5 and 80 times that for water in a variety of concretes [8]. This phenomenon is attributed to the additional contribution to the flow of a gas provided by Knudsen flow. Bamforth compared his experimental data for gas and water permeabilities with the relationship proposed by Klinkenberg for oil reservoir sands [7]. He observed a similar dependence of the Klinkenberg constant on the water permeability coefficient for the cementitious materials although the experimental data indicated a slightly different relationship to that observed for the sands [8].

Daimon *et al* measured the permeability coefficients of vacuum-dried OPC-sand mortars using hydrogen and nitrogen as the migrating gases [21]. An expression for the measured permeability coefficient in terms of the relative contributions of viscous and Knudsen flow was derived and applied to the experimental data. Both the viscous and Knudsen contributions were found to decrease with curing time. The change in the viscous contribution was significantly greater, indicating a relative increase in the contribution from Knudsen flow as the pore structure became finer with increased curing. The viscous and Knudsen contributions for hydrogen were respectively greater and less than those for nitrogen.

The relative contribution of Knudsen flow to the overall rate of gas migration is dependent on the pore size of the porous medium, and hence on both the composition and conditioning of a cementitious material, and on the mean free path of the permeating gas. Consequently, the simple comparison of gas permeability coefficients for different materials at a single pressure is of limited utility in a more fundamental study of gas migration. However, much of the published data on gas permeation is limited to such a comparison due to the requirements of the particular authors for simple tests related to, for example, concrete durability [16, 17, 19].

Grube and Lawrence have determined the repeatability of membrane permeability measurements on dried concretes and find that, for a single specimen, repeated measurements give a coefficient of variability of 3-4 % [17]. Similarly, Cabrera and Lynsdale measured variabilities of between 0.3 and 1.5 % for a single specimen [16]. In contrast, the coefficient of variability for measurements on different specimens of the same material is considerably greater; measured values vary from 7.5 % [16] to a range of 15-24 % [17]. Such values are typical of the inter-specimen variability in measurements of other mass-transport parameters for cementitious materials [22].

The gas permeability of concrete has been found to vary substantially with the age of the material. Cabrera and Lynsdale found a decrease in the permeability coefficents by factors of around 20 in a period of 90 days after casting for several different mortars [16]. The final permeabilities of dried materials were typically 2×10^{-17} m^2. Grube and Lawrence have reported a similar decrease in oxygen permeability with curing time for a range of different concretes examined in a study performed in several laboratories. The absolute values of the gas permeability coefficients showed considerable variability between the different laboratories participating in the measurements. The range of measured values was about 2×10^{-18} to 2×10^{-16} m^2 [18]. This range of permeability coefficient is typical of the values obtained for dried structural materials [8, 13].

The gas permeability of water-saturated material has not been widely reported due to experimental difficulties. The behaviour of a 3:1 BFS/OPC grout has been measured after drying to various weight losses [23]. The measured permeability was strongly correlated with the weight loss. Specimens with a nominal 90 % water saturation (specimens dried to give 10 % of the weight loss observed on full drying) gave a permeability coefficient of about 10^{-18} m^2 whereas fully saturated material had a permeability coefficient below the limit of resolution of the technique; 10^{-20} m^2. Chou Chen and Katz report that the permeability coefficient for methane in wet concrete is several hundred times smaller than that measured in dry material [20]. The permeability coefficients were 8.3×10^{-17} and 4.7×10^{-14} m^2 respectively. The water permeability coefficient for the wet material was substantially lower than that for methane even in the wet material.

It is apparent that the majority of published data on gas permeability are determined for either hardened cement pastes or structural materials in a dry condition. Consequently, there are little data relevant to the type of high porosity material envisaged as the Nirex repository backfill.

2.2.2 Gaseous Phase Diffusion in Cementitious Materials

The diffusion of gases in porous materials has been extensively measured but published data directly relevant to cementitious materials are scarce. Daimon *et al* [20] measured the inter-diffusion of hydrogen and nitrogen in vacuum-dried OPC-sand mortars at constant pressure. The diffusion coefficients obtained were dependent on curing time and initial water-cement ratio. After 28 days, the diffusion coefficients were 4.8×10^{-7} and 1.9×10^{-7} m^{2}s^{-1} for water-cement ratios of 0.65 and 0.5 respectively. The diffusion coefficients showed a significant decrease with increasing average pressure, indicative of the contribution of Knudsen flow at low pressures.

Lawrence [24] measured the inter-diffusion of nitrogen and oxygen in a range of concretes as a function of various parameters. The experiments were performed at a constant pressure using an oxygen sensor to determine the concentration within the flowing nitrogen gas. Specimens were cured at 55% relative humidity and allowed to surface dry prior to measurement. Subsequent drying caused changes in the diffusion coefficients until constant values were reached. The diffusion coefficients were strongly dependent on curing time and water-cement ratio, as observed by Daimon *et al* [21]. The measured values lay in the approximate range 2×10^{-9} to 2×10^{-7} m^{2}s^{-1}. The values were quite well correlated with measured water permeability coefficients. Tuutti [25]

has reported a series of measurements of the diffusion coefficient for oxygen in concrete based on Portland cement both with and without the addition of BFS. The unmodified material was studied under a variety of relative humidity conditions and the diffusion coefficient was found to decrease from about 7×10^{-8} m^2s^{-1} in the dry condition to about 3×10^{-10} m^2s^{-1} after conditioning at 100 % relative humidity. The slag-modified materials were found to have diffusion coefficients which were a factor of 2 to 5 times lower than the unmodified material under the same conditions.

The diffusion of radon gas through concrete structures has also been studied. In general, experiments were performed on actual structures and hence the condition of the concrete was not well defined. It is assumed that it was relatively dry. Measured diffusion coefficients lay in the range 7.5×10^{-7} to 1.9×10^{-7} m^2s^{-1} [26, 27]. The diffusion of methane in wet and dry structural concretes has been investigated by Chou Chen and Katz [20]. The diffusion coefficients for dry material were in the range 3.6×10^{-8} to 3.1×10^{-7} m^2s^{-1} whereas those for wet material lay between 1.3×10^{-9} and 1.8×10^{-8} m^2s^{-1}. The values for wet material are somewhat greater than those reported by Tuutti for 100 % relative humidity [25]. This may indicate that the "wet" material does not represent full water saturation.

The above measured values for diffusion coefficients are all similar in magnitude and hence the approximate range of values for the diffusion coefficient for dry material can be given as about 10^{-9} to 10^{-7} m^2s^{-1}.

2.2.3 Aqueous Phase Diffusion of Dissolved Gases

Page and Lambert directly measured the aqueous diffusion of oxygen derived from the gaseous phase in hardened cement pastes using an electrochemical technique [30]. The measured diffusion coefficients were dependent on the water cement ratio of the material and were in the range 1.3×10^{-12} to 2.2×10^{-12} m^2s^{-1} at 25 °C. The activation energy for the diffusion was typically half that for chloride ions.

The diffusion of chloride ions derived from ionic compounds have been reported for migration in hardened cement pastes [22, 28, 29]. Although there is no direct evidence that the aqueous phase migration of chlorine gas occurs exclusively via the diffusion of chloride ions, it is likely that some ions will be produced on dissolution and hence chloride ion diffusion data has some relevance to the consideration of gas migration. The measured chloride ion diffusion coefficients were of the order of 10^{-11} m^2s^{-1}.

3 Experimental Method

3.1 Experimental Materials

3.1.1 Manufacture and Physical Properties

The ratios of water to cement and aggregate to cement and the total cement contents for the concretes, where available, are given in Table 2. The materials were mixed in pan or shear mixers as appropriate and vibrated into moulds. The SRPC and PFA/OPC-concretes and the BFS/OPC-grout were cured for 24 hours at 20 °C prior to de-moulding then cured underwater at ambient temperature for 28 days. All materials were subsequently stored underwater at ambient temperature until required for use. The resulting compressive strengths and densities of all the experimental materials are given in Table 3.

The pore structures of all materials except the SRPC-concrete were investigated using mercury intrusion porosimetry (MIP) using a Carlo Erba Strumentazione Porosimeter 2000 with a maximum operating pressure of 200 MPa. The sample of the PFA/OPC-concrete was prepared by taking a number of 10 mm cores from a larger specimen and breaking these up and mixing to ensure a representative sample was achieved. Simple cores were used for the remaining materials. The porosity and the average pore radius were obtained from the MIP and these data are given in Table 3. In addition, the porosity was calculated from the weight loss on drying, given in Table 4, using the measured density of water-saturated material from Table 3. The discrepancies between the two methods of obtaining the porosity may be due either to the MIP failing to intrude fine pores or the drying causing the loss of some water of hydration. It is likely that the MIP data are the more accurate.

The MIP results revealed that the PFA/OPC-concrete and the BFS/OPC-grout have relatively narrow and symmetrical pore size distributions in the range 5 to 50 nm. In contrast, the preliminary and reference backfill grouts have broad pore size distributions ranging from 5 nm to greater than 1 μm. Typical pore size distributions for all materials except the SRPC-concrete are illustrated in Figures 1 to 4. These distributions are quite strongly biassed towards the larger pore sizes as shown by the average radii given in Table 3.

The pore structure of the materials can also be assessed by the measurement of mass transport properties. The diffusion coefficients for ionic diffusion in all materials except the reference backfill grout have been reported previously [22, 31]. The ionic conductivities of all materials have been measured and the results are discussed in Appendix 1. There is an strong correlation between the measured average pore size and the conductivity, demonstrating the dependence of mass transport on the pore structure.

3.1.2 Specimen Conditioning

The specimens were conditioned prior to use in a controlled humidity atmosphere to establish a known water content. Three different humidities were selected; zero, 75 % and 100 % relative humidity. The SRPC-concrete was used in the dry condition only. The zero humidity, dry

specimens were dried for 24 hours at 100 °C then stored in a sealed container containing silica gel dessicant. It is possible that this treatment altered the microstructure of the material although the extent of any change is unknown. The remaining specimens were placed directly into sealed containers. The 75 % and 100 % relative humidities were achieved by placing a quantity of saturated sodium chloride solution or demineralised water respectively into the containers. The degree of water saturation was determined by monitoring weight loss during conditioning. The fractional weight losses incurred by conditioning, compared to the initial weight in a surface dry condition after removal from storage underwater, are given in Table 4. The data in Table 4 confirm that that the grouts have substantial porosity and show that both the preliminary and reference grouts lose water even during conditioning at 100 % relative humidity.

The possibility that the observed weight loss from the backfill grouts during conditioning at 100 % relative humidity was due to an experimental error was investigated by performing additional experiments. Six specimens of the reference backfill grout, in the form of discs 2 cm in thickness and 10 cm in diameter, were placed in a 100 % relative humidity atmosphere for a period in excess of 230 days. Three specimens were placed in a horizontal orientation stacked directly on top of one another. The remaining specimens were stood on edge; the vertical orientation. The overall weight losses were 4.6, 4.1 and 2.6 % for the specimens in the horizontal orientation and 5.0, 5.3 and 7.5 % for the specimens in the vertical orientation.

It appears that the specimens placed in the vertical orientation exhibit a greater weight loss than those in the horizontal orientation. This is consistent with the weight loss being due to gravity-driven draining since the "driving-force" for such draining would be proportional to the height of the "column" of water within the pore space. The horizontal specimen which gave the smallest weight loss was that placed at the base of the stack of three. The topmost specimen gave the largest weight loss. This is also consistent with draining, as the water from the upper specimens would partially drain into the bottom specimen. Overall, it can be concluded that the loss of water during conditioning is real effect and is consistent with draining due to gravity.

Analysis of the experimental data from the gas transport experiments was carried out using a numerical model of the gas migration process, as described in Section 3.3.2, and requires the measurement of the "gas-accessible" volume for each type of material and condition. This was measured by placing appropriate specimens into a sealed chamber at a known pressure and subsequently venting the gas into an additional, known volume. The resulting pressure drop, combined with the volumes of the system and the specimen, can be used to calculate the volume of porosity accessible by gas. This method has the advantage that the specimens are used in an intact, conditioned state and the measured porosity can be directly associated with that occupied during gas migration. The measured accessible volumes for all materials except the SRPC-concrete, expressed as equivalent fractional porosities, are given in Table 4. All measurements were made using a relatively low pressure of about 100 kPa. A further measurement was made on the 75 % relative humidity conditioned PFA/OPC-concrete using a pressure of about 3 MPa. The measured volume was within 2 % of that obtained from the low pressure measurement.

The gas-accessible volume porosity values for the backfill grouts are not significantly different from those obtained from weight loss measurements, as given in Table 4. The gas accessible porosity values were subject to some inaccuracy due to limitations in the measurements of the volumes. However, it appears from the comparison of the data in Table 4 that the PFA/OPC-concrete and BFS/OPC-grout have significantly lower gas accessible porosities than is indicated by other measurement techniques. The measurement of the fractional porosity of the materials is discussed further in Section 5.1.

3.1.3 Specimens Containing Interfaces

The influence of artefacts introduced by the construction process in the repository was assessed using specimens containing reinforcement bars and construction joints. It is expected that the reinforcement will be confined to the structural concrete in the repository. The backfill grout will be placed in a series of separate pours and hence "construction joints" between the different batches are likely to be the main interfaces within the backfill which may influence gas migration. The effect of interfaces on gas migration was investigated using specimens conditioned at both zero and 100 % relative humidity.

Specimens of the PFA/OPC-concrete were cast into moulds containing a section of reinforcing mesh oriented vertically in a cylindrical mould. The mix design and curing conditions utilised were identical to those discussed above. The mesh consisted of 4 mm diameter bars spaced at 50 mm intervals. The cylinders were sectioned between the horizontal members of the mesh to produce specimens containing two bars perpendicular to the flat faces of the slices. The arrangement of the reinforcement bars in the cylinder is illustrated in Figure 5. The interface between the reinforcement and the concrete was parallel to the direction of gas migration.

Simulated construction joints were produced in specimens of the preliminary backfill grout. Cast cylinders, cured identically to those described previously, were split approximately in half in the direction perpendicular to the flat faces and replaced in moulds prior to casting additional material of the same mix design as the original specimens. A further monolithic specimen was prepared from the additional material to act as a control. The specimens were subsequently cured at ambient temperature for at least 28 days. Sectioning produced specimens with the construction joint oriented parallel to the direction of gas migration. The actual backfill within an actual repository will have been subjected to significant compression due to the mass of the material placed. Hence, real construction joints may differ somewhat from those produced in the specimens. Compression should reduce the effective permeability of a joint and hence the transport of gas in the simulated joints represents an upper bound to the behaviour of real material.

3.2 Gas Diffusion Measurements

3.2.1 Experimental Apparatus

The general form of the experimental apparatus employed in these measurements is illustrated schematically in Figure 6. This apparatus allowed the sampling of a fixed volume of the gas from

one side of the cell. The actual cell used in the experiments is illustrated in Figure 7. Specimens were in the form of 100 mm discs approximately 20 mm in thickness mounted into a perspex holder using a cold-setting urethane compound (Devcon Flexane-94). Previous work has shown that this material provides an effective barrier to both aqueous and gaseous species and subsequent experiments have shown that the integrity of the seal is maintained for periods significantly in excess of a month [22].

The inter-diffusion of hydrogen and argon was measured for the SRPC-concrete in the dry condition using two different experimental techniques. The inter-diffusion coefficient was obtained directly by monitoring changes in gas composition and indirectly by the measurement of the transient pressure gradient induced during the diffusion process.

3.2.2 Gas Composition Monitoring

The diffusion of hydrogen into an argon carrier gas through a membrane of the SRPC-concrete was monitored by removing samples of the hydrogen-contaminated argon at regular intervals. The sampled volume was replaced with pure argon. The gas composition was measured using gas chromatography, with a sensitivity of better than 0.1 %. The volume of gas analysed was 75 cm^3, which, when losses during sampling are included, represents approximately half of the total volume of the carrier gas. Replacement of a significant fraction of the "contaminated" carrier gas by pure argon has the effect of increasing the concentration gradient across the specimen and lowering the hydrogen concentration at the onset of the subsequent sampling period. This effect had to be allowed for in the analysis of the experimental data.

Samples were taken every five minutes in the period up to an elapsed time of 35 minutes and every 10 minutes thereafter. The process of removing and replacing the sample cylinders took approximately two minutes. This time is a significant fraction of the total time elapsed between sampling events and results in some systematic error in the results.

3.2.3 Diffusion-induced Pressure Transients

During the measurement of gas composition changes it was observed that the transient pressure differences induced by the Kirkendall effect were of significant magnitude. These pressure transients were measured and analysed to determine an estimated inter-diffusion coefficient for hydrogen and argon as described below. The measurements were made using initial pressures of 100, 125, 155 and 175 kPa. It was assumed that the average pressure in the system remained equal to the initial pressure throughout the course of an experiment.

The inter-diffusion coefficient was estimated in the following way. The kinetic energies of the gases are equal and therefore, from the standard equation relating kinetic energy, mass and velocity, the velocity of hydrogen molecules will be $\sqrt{(40/2)}$ times that of argon, due to the different molecular masses; 2 for hydrogen and 40 for argon. Consequently, the unconstrained diffusion rate of hydrogen should be approximately 4.5 times that of argon. The effect of this difference in diffusion rates will be balanced by bulk flow under the induced pressure gradient.

The required bulk molecular flow rate will be equal to half the difference between the diffusive flow rates, that is (4.5-1)/2, or 1.75, times the argon diffusive flow rate. The overall effective interdiffusion rate will be equal to the average of the two diffusion rates, that is (4.5+1)/2, or 2.75, times the argon diffusive flow rate. Hence, the ratio of the bulk flow rate to the diffusive flow rate will be 1.75/2.75 or 0.64.

The actual bulk molecular flow rate can be calculated from the Darcy equation, suitably modified to allow for the effect of the compressibility of the gas, and the ideal gas approximation as discussed above. The diffusive flow rate can be derived from Fick's first law. The concentration of the gas molecules in the reservoir initially containing argon is also given by the ideal gas approximation and combining this with Fick's law for diffusion under a time invariant concentration gradient gives;

$$\frac{dn}{dt} = \frac{DA}{l} \frac{p_H}{RT} \qquad ....(6)$$

where dn/dt is now the diffusive molecular flow rate, D the inter diffusion coefficient and p_H the pressure in the reservoir initially containing hydrogen. The above equation assumes that the absolute amount of gas exchange between the reservoirs is relatively small and consequently that the hydrogen concentration is effectively zero in the argon reservoir. The ratio of the bulk and diffusive molecular flow rates is, as argued above, equal to 0.64. Hence, combining the equations for bulk and diffusive molecular flow gives;

$$D = \frac{k p_{av} \Delta p}{0.64 \, \mu p_H} \qquad ....(7)$$

This equation can be used to calculate the inter-diffusion coefficient. The derivation assumes that the peak in the pressure transient corresponds to steady-state diffusion.

3.3 Gas Permeability Measurements

3.3.1 Experimental Apparatus

The flow of gas under an imposed pressure gradient was measured by monitoring the decay of a pressure difference across a membrane of the material with elapsed time. This technique bears some similarities to that developed by Martin [15] except that in the present work the pressure was monitored on both sides of the membrane. The apparatus is illustrated schematically in Figure 6. Experimental measurements were carried out using a variety of gases. The permeability of the dry SRPC-concrete was measured using hydrogen and argon whereas that of the BFS/OPC and backfilling grouts and the flawed specimens was measured using helium and argon. The influence of gas type on gas migration was more fully investigated for the PFA/OPC-concrete using five

different gases; hydrogen, helium, methane, argon and carbon dioxide.

The experimental apparatus was designed to allow the maintenance of a constant humidity atmosphere adjacent to the specimen during an experiment. This was achieved by placing either desiccant, salt solution or pure water into the cell along with the specimen. The maintenance of a known humidity is more difficult to achieve in experiments where gas is flowing past the specimen. Hence, the pressure decay technique was adopted in preference to the alternative techniques discussed in Section 2.2.

Measurement cells were constructed for operation at both low (0-200 kPa) and high (0-10 MPa) applied pressures. The low pressure cells were identical to those utilised in the diffusion experiments, as shown in Figure 7. The higher pressure experiments were performed either with or without triaxial confinement of the specimens. In particular, it was found that triaxial stressing of the high porosity preliminary backfill grout caused a substantial permanent reduction in the volume of the specimens and some experimental error may have occurred. The specimen thickness was dependent on the measurement cell used. In the case of the triaxial cell specimens approximately 10 cm thick were used whilst in the "unconfined" cells the specimen thickness was approximately 2 cm. These two types of cell are illustrated in Figures 8 and 9 respectively. The construction of the low pressure cells gave a reduction in the area of specimen exposed in the lower pressure reservoir compared to that exposed in the high pressure reservoir. Where necessary, a correction by a factor of 1.13 has been applied to the data to allow for this effect.

Two variations on the basic experiment were performed. In the first, both reservoirs shown in Figure 6 were isolated and the pressures allowed to relax to an equilibrium level. Such experiments allowed measurements to be made at an approximately constant average pressure. In contrast, measurements were also performed with a continuously varying average pressure by holding one reservoir at a constant applied pressure. In both cases, the range of average pressure values was determined by the initial conditions and the volumes of the two reservoirs.

The permeability measurements were made at a range of different average pressures. Constant average pressures of 100 kPa and 1.5, 7, 15, 22 and 72 MPa were used in the measurements on the PFA/OPC-concrete whilst experiments on the grouts were constrained to a maximum average pressure of about 25 MPa to avoid specimen damage. The varying average pressure experiments were performed in two pressure ranges; 0 to 200 kPa and 0 to 3 MPa, denoted low and high pressure ranges respectively.

Between one and ten measurements were carried out for each set of conditions. The data generally exhibited very little variability between different runs on an individual specimen. It was considered that a measured permeability coefficient represented the sum of the permeability coefficient of the material and any additional contribution from short-circuit pathways such as cracks or incomplete sealing between specimen and container. Hence, it was not possible to obtain a measured permeability coefficient below the true permeability coefficient for the material. The best value of the permeability coefficient for a material was taken to be the lowest value obtained.

The elapsed time required for the completion of a particular experiment was determined by

the material being studied. These varied from about 10 seconds, in the case of dry preliminary backfill grout, to greater than one month for some of the materials in the 100 % relative humidity condition. The limit of accuracy of the experiments was ultimately controlled by the quality of the seals achieved in the measurement cells, both between the two reservoirs and to atmosphere. The effective lower and upper limits of resolution of the experimental apparatus were estimated as 10^{-21} and 10^{-14} m^2 respectively. Since the permeability coefficients are based on calculations of the rate of change of pressure, any experimental errors, such leaks between reservoirs or to atmosphere, will result in an over-estimate of the permeability coefficient. The presence of leaks to atmosphere can be detected in the closed system mode by checking for conservation of the total mass of gas as it flows from one reservoir to the other.

3.3.2 Analysis of Experimental Data

The flow of a single gas between the two reservoirs in the apparatus will be such that the pressure difference is reduced and eventually eliminated. The flow of a fluid in a homogeneous porous medium under a pressure gradient is governed by the Darcy equation given previously. The volumetric flow rate can be related to the molecular flow rate using the ideal gas approximation and the resulting version of the equation integrated across the whole specimen to give an expression for the molecular flow rate in terms of the applied pressures on either side of the membrane. The variation in pressure in one reservoir, in this instance that at the lower pressure, can be determined from this expression by the further application of the ideal gas approximation;

$$\frac{dp_1}{dt} = \frac{kA}{2\mu l V_1}\left[(p_2)^2 - (p_1)^2 \right] \qquad ....(8)$$

where dp_1/dt is the rate of pressure change in the low pressure reservoir, V_1 the volume of that reservoir and p_1 and p_2 the pressures in the low and high pressure reservoirs respectively. In a closed experiment, the change in pressure in the high pressure reservoir can be calculated from that measured in the lower pressure reservoir and hence p_2 obtained from p_1. Substituting for p_2 and integrating with respect to pressure and time gives an expression for the variation of pressure in the low pressure reservoir with time;

$$\frac{[(V'^2 - 1)\, p_1 - (V'+ 1)\, (\beta + V'\alpha)]\, [(\beta - \alpha)\, V' + \alpha - \beta]}{[(V'^2 - 1)\, p_1 - (V' - 1)\, (\beta + V'\alpha)]\, [(\beta + \alpha)\, V' + \alpha + \beta]}$$

$$= \exp\left[\frac{kA}{\mu l V_1}(\beta + V'\alpha)\, t \right] \qquad ....(9)$$

where V' is the ratio of the reservoir volumes (V_1/V_2) and α and β are the initial low and high pressures respectively. If the higher pressure is held constant, the effective value of V_2 is infinite and the ratio V' is zero. Applying this constraint to the equation above allows the determination of permeability coefficient from the experiments with variable average pressure. The variation in the pressure in the higher pressure reservoir can be obtained using an analogous method. This derivation predicts the exponential relaxation of an applied pressure difference with time which was observed experimentally by Martin [15].

The accuracy of the analysis given above depends on the assumption that the gas behaves as an ideal gas. The potential impact of deviation from the behaviour predicted by the ideal gas approximation is considered in Appendix 2. The effect is only significant for gases at high pressures and the deviation will cause errors in the permeability coefficients determined from high pressure experiments of up to perhaps 10 %.

The analytical solution for gas pressure variation given above assumes that steady state flow has been established. That is that the quantity of gas exiting the specimen into the lower pressure reservoir is equal to that entering the specimen from the higher pressure reservoir. For a compressible fluid in a medium with finite porosity this is not strictly true. Hence, the analytical solution is only applicable to materials where the error caused by the assumption of zero porosity is not significant. The errors become large in specimens of high porosity subject to a large pressure difference. In order that all the experimental data could be analysed, a numerical model of the variation in pressure with time was developed using a finite-element method. The value of the permeability coefficient obtained from the analytical solution was input as a starting value for the numerical calculation. Subsequently, the numerical model was run to produce a simulated data set of pressure versus time from which a new permeability coefficient was calculated using the analytical solution. This process was repeated until the simulated data set achieved a satisfactory match to the experimental data.

The measured permeability coefficients quoted in Section 4 below were obtained using this numerical method to extract the permeability coefficient from both constant and varying average pressure experiments. The analytical solution alone was used to calculate the infinite pressure permeability coefficients and Klinkenberg constants from the varying average pressure experiments. It is expected that these data will not be as accurate as those derived from the numerical solution.

The completion of an experiment is indicated by the achievement of a uniform pressure throughout the experimental apparatus. For materials with a low porosity, this pressure is equal to a volume-weighted average of the initial pressures in the two reservoirs. However, if the porosity is high, there is significant gas volume contained in the specimen and the final average pressure will include a contribution from the gas in the pore volume. The deviation of the final pressure from the weighted average of the initial pressures is considered in Appendix 3.
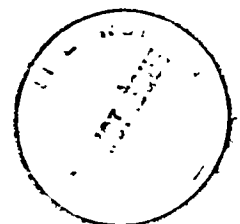
4 Experimental Results

4.1 Diffusion in SRPC-concrete

4.1.1 Gas Composition Monitoring

The measured variation in the hydrogen concentration as a function of time within the argon reservoir is shown in Figure 10. Each sampling event required that approximately half of the hydrogen was removed from the system and consequently the concentration was reduced after each sampling event. Figure 10 is constructed on the assumption that exactly half of the volume of the gas was removed during each sampling event. In the period between 10 and 25 minutes elapsed time, it appeared that the hydrogen removed was being completely replaced by the diffusive flow during the subsequent sampling period. This allowed the effective molecular flow rate to be estimated as 2×10^{-7} mol s^{-1}. The estimated hydrogen-argon inter-diffusion coefficient based on this flow rate is approximately 10^{-8} m^{2}s^{-1}.

4.1.2 Diffusion-induced Pressure Transients

The variation in the pressure difference between the two reservoirs due to the Kirkendall effect at an average pressure of 125 kPa is shown in Figure 11. The calculation of the inter-diffusion coefficient using the method given previously requires the permeability coefficient for the material. The appropriate values of the argon permeability coefficient (discussed below) and the calculated diffusion coefficient for each average pressure are given in Table 5. It is apparent from the results in the table that there is no systematic dependence of the measured diffusion coefficient on the average pressure at those pressures used in the experiments and hence the hydrogen-argon inter-diffusion coefficient is estimated to be 3×10^{-8} m^{2}s^{-1} for migration in dry SRPC-concrete.

4.2 Gas Permeability of Structural Concrete

4.2.1 Gas Migration at Constant Average Pressure

A typical pressure difference relaxation curve for a specimen of the PFA/OPC-concrete is shown in Figure 12. The results of all the experimental measurements of the permeability coefficient of the PFA/OPC-concrete are included in Appendix 4. Figure 13 shows a comparison of the gas permeability coefficients for the PFA/OPC-concrete obtained using hydrogen, helium, methane, argon and carbon dioxide as the migrating gases. Measurements were made on material conditioned at 0, 75% and 100% relative humidity. All experiments were performed at an average pressure of 100 kPa. Data for the 100 % relative humidity conditioned specimen are only available for helium and argon. If the Klinkenberg relationship is applicable to this data, the measured permeabilities at constant pressure will depend on the mean free path for each gas. The mean free path, λ, can be calculated in a number of ways, the equation used here is;

$$\lambda = \frac{2.02\,\mu}{\sqrt{pp}} \qquad\qquad ....(10)$$

where μ is the viscosity, p the pressure and ρ the density. The mean free paths for the gases used at a pressure of 100 kPa and a temperature of 25 °C are given in Table 6. The variation in the permeability coefficient with the type of gas for both the dry and 75 % relative humidity conditioned specimen at 100 kPa, given in Figure 13, is correlated with the mean free path of the gas given in Table 6. Linear regression on the two data sets gave correlations of $r^2 = 0.92$ and 0.75 for the dry and 75% relative humidity conditioned specimens respectively. The intercept as the mean free path tends to zero determined by linear regression gives the value of the infinite pressure permeability which equates with that in the Klinkenberg equation, since a mean free path of zero corresponds to a value of the Klinkenberg constant of zero. The infinite pressure permeability coefficients derived in this way are 1.3×10^{-17} m^2 for dry material and 2×10^{-20} m^2 for that conditioned at 75 % relative humidity.

4.2.2 Variation in Gas Permeability with Average Pressure

The values of the permeability coefficient of the SRPC-concrete in the dry condition for hydrogen and argon migration at a range of approximately constant average pressures between 0 and 150 kPa is shown in Figure 14. The data have been corrected by a factor of 1.13 to allow for the differing areas of the specimen exposed in the high and low pressure reservoirs as a result of the seal geometry. It is clear that the permeability coefficient is inversely dependent on average pressure. The permeability coefficient for hydrogen exceeds that for argon in the pressure range investigated. This is consistent with the observations made above and can be attributed to the increasing effect of Knudsen flow at lower pressures and the longer mean free path of hydrogen for a given pressure.

The Klinkenberg equation can be fitted to the data, as illustrated in Figure 14. The infinite pressure permeability coefficients thus determined are 3.6×10^{-18} and 4.0×10^{-18} m^2 from the hydrogen and argon data respectively. These values are close enough to be considered equal, within experimental error. The calculated values of the Klinkenberg constant are 6.6×10^5 Pa for hydrogen and 4.2×10^5 Pa for argon.

The dependence of the gas permeability for argon migration in the PFA/OPC-concrete (conditioned at zero humidity) on the average pressure is shown in Figure 15. Data are included for experiments performed at both constant and varying average pressures. The range of data obtained at each pressure is illustrated. It is apparent that the permeability coefficient decreases as the average pressure is increased. Plotting the best estimate permeability coefficient for the set of experiments performed at, approximately, a particular value of the average pressure against the reciprocal of average pressure indicated that the Klinkenberg relationship is probably applicable, although the correlation obtained was not strong ($r^2 = 0.78$). Linear regression gave the infinite

pressure permeability as 2.0×10^{-17} m^2 and the Klinkenberg constant as 190 kPa.

The change in permeability with average pressure shown in Figure 15 is most significant at low average pressures. The results of a series of measurements performed with the average pressure varying between 0 and 200 kPa in PFA/OPC-concrete conditioned at zero relative humidity, using each of the five different gases, are given in Table 6. There is a possible correlation between the Klinkenberg constant and the mean free path for each gas, calculated using the equation above, at a pressure of 100 kPa and a temperature of 25 °C ($r^2 = 0.60$).

The infinite pressure permeability coefficient should be a constant value, independent of the type of gas. The variation in the infinite pressure permeability coefficient with gas type is not strongly correlated with the mean free path ($r^2 = 0.50$) and it is assumed that the differences between the values shown in Table 6 are due to experimental error. The mean value of the infinite pressure permeability coefficient is $(3.7 \pm 0.6) \times 10^{-17}$ m^2. This value is reasonably consistent with the values of 1.3×10^{-17} and 2.0×10^{-17} m^2 determined above.

The results of the measurements carried out with a varying average pressure of argon on the PFA/OPC-concrete conditioned at 100 % relative humidity implied an infinite pressure permeability of $(7.6 \pm 2.3) \times 10^{-17}$ m^2. Comparison of this value with those given in Figure 13 indicate that the former must be subject to error as the permeability is apparently 3 orders of magnitude greater when measured in the varying average pressure experiment. The varying average pressure experiments were performed using higher pressure differences, up to 3 MPa. It is postulated that the high applied pressures gave rise to mechanical failure in the specimens when used in the non-triaxial high pressure cell. Consequently, the data for PFA/OPC-concrete in the 100% relative humidity condition have been omitted from Table 8.

4.3 Gas Permeability of Grouts

4.3.1 Gas Migration at Constant Average Pressure

Table 7 details the measured permeability coefficients for the migration of helium and argon at an average pressure of 100 kPa in all of the experimental materials in both the dry and 100 % relative humidity conditioned states. The data for the PFA/OPC-concrete are included for comparison. The data are derived from the experimental results given in Appendix 4. In some of the materials in the dry state, in particular the two types of backfill grout, the gas migration was so rapid that only variable average pressure experiments could be performed. In these cases the permeability coefficients for a constant average pressure of 100 kPa were calculated from the available data for varying average pressure, discussed below, using the Klinkenberg equation.

4.3.2 Variation in Gas Permeability with Average Pressure

The infinite pressure permeabilities for all of the experimental materials are shown in Table 8 for migration at low pressure in materials conditioned at 0 and 100 % relative humidity, with the exception of the value for the PFA/OPC-concrete in the 100 % relative humidity condition. It has been assumed that the infinite pressure permeability is a constant for all gases and hence the infinite

pressure permeability coefficients given are the average of the data for all gases studied in each material. Figure 16 illustrates the fit of the Klinkenberg equation to the variation in the measured permeability coefficient for the BFS/OPC-grout for average pressures in the range 0 to 100 kPa.

Table 9 gives the measured values of the Klinkenberg constant for all the experimental materials in the dry condition for both low and high average pressures. Where the table shows that the Klinkenberg constant is within experimental error of zero or negative, the change in permeability with pressure over the pressure range investigated was very small. A negative value may be the result of a systematic error in the data analysis when the change in permeability coefficient is small. In such circumstances, it must be assumed that the permeability coefficient is constant with average pressure and equal to the infinite pressure permeability coefficient.

The Klinkenberg constants for the materials in the 100 % relative humidity conditioned state were not measured for all materials and pressure ranges. When the values were measured, using high average pressures, in the range 0 to 3 MPa, the Klinkenberg constants were found to be negative or not significantly different from zero for all materials. The data were considered to indicate that there was little or no change in the permeability coefficient for average pressures in the high pressure range.

4.4 The Effect of Interfaces on Gas Permeability
4.4.1 Influence of Reinforcement on Gas Migration

The permeability coefficients for a constant average pressure of 100 kPa and the infinite pressure permeability coefficients for both the dry and 100 % relative humidity conditioned specimens are given in Table 10. These data can be directly compared with the data for pristine, that is unreinforced, PFA/OPC-concrete given in Tables 7 and 8.

The presence of the reinforcement bars appeared to increase the permeability coefficient of dry material (measured at a constant average pressure of 100 kPa) by a factor of between three and four. There was no significant difference between pristine and reinforced material for the 100 % relative humidity condition at a constant average pressure of 100 kPa. However, at a constant average pressure of about 1.6 MPa, the permeability coefficients for helium and argon were increased to 2×10^{-19} and 1×10^{-19} m^2 respectively. This represents an increase by about an order of magnitude compared to the data at obtained at 100 kPa. This increase in permeability with average pressure is not observed for the pristine material and must be attributed to the influence of the reinforcement.

The infinite pressure permeability coefficient for dry material is approximately a factor of five greater in the reinforced concrete. Comparable data for pristine material in the 100 % relative humidity condition are not available.

4.4.2 Influence of Construction Joints on Gas Migration

The experimental results obtained for the preliminary backfill grout containing a construction joint are given in Table 10. No data were obtained at constant average pressure in dry material as

the extremely high permeability made experiments too rapid. The control specimen gave a 100 kPa argon permeability coefficient of 6.3×10^{-16} m^2 for material in the 100 % relative humidity condition. The infinite pressure permeability coefficients for the control specimen were 2.3×10^{-13} and 4.6×10^{-16} m^2 for the dry and 100 % relative humidity conditions respectively. These data are significantly greater than those obtained for the normal specimens of the grout, given in Tables 7 and 8. It is apparent that the batch of grout used in the preparation of the construction joints is not consistent with the other specimens of this material.

The construction joint increased the 100 kPa permeability of 100 % relative humidity conditioned material by a factor of three compared to the control specimen and a factor of 70 compared to the pristine material. The infinite pressure permeability was equal to that of the control specimen for the dry condition and was approximately an order of magnitude greater for the 100 % relative humidity condition.

4.5 Variability in the Measurements

The contribution to experimental error arising from inter-specimen variability is mainly due to the variation in the number of short-circuit pathways in different specimens of the same material. In addition, some irreproducibility may occur between individual experimental runs on the same specimen and from differences in the intrinsic permeability coefficients of individual specimens of the same material. The total variability in the measurements of the permeability coefficient for a particular material under a fixed set of conditions can be quantified by the coefficient of variability of the data. This is equal to the ratio of the standard deviation to the mean for the data, usually expressed as a percentage.

The permeability coefficient measurements made at a constant average pressure of 100 kPa, summarised in Figure 13 and Table 7, generally exhibited overall coefficients of variability of between 10 and 40 %. The reproducibility of repeated measurements on an individual specimen was generally of the order of a few percent. In contrast, previous measurements of the aqueous diffusion coefficients for similar cementitious materials indicated a variability between repeated measurements of the same property of a single specimen of between about 10 and 30 % [16, 17, 22]. Hence, the measurement of gas permeability using this experimental technique seems to be inherently reproducible.

In contrast, the measured infinite pressure permeability coefficients, given in Table 8, had coefficients of variability of between about 30 and 200 %. The large variability in the infinite pressure permeability coefficients is due to the error produced when the Klinkenberg equation is fitted to data which exhibit a very small change in permeability over the pressure range investigated. This is particularly true of the backfill grouts.

5 Performance of Cementitious Materials

5.1 Specimen Porosities

Tables 3 and 4 give the porosities of the experimental materials as obtained using three different methods; weight loss during conditioning, mercury intrusion porosimetry and gas accessible volume measurement. The methods are discussed in detail in Sections 3.1.1 and 3.1.2.

A theoretical maximum fractional porosity for the materials can be determined from the amount of water in the original mix prior to hydration, assuming that the volume of air entrained in the materials is negligible. A water-saturated material with a "porosity" of 1 must have an initial water content of 1000 kg m^{-3}. Consequently, the theoretical maximum porosity of a real mix will be given by the ratio of 1000 to the actual water content. The maximum porosities of the materials are 0.19 for the PFA/OPC-concrete, 0.54 for the BFS/OPC-grout, 0.69 for the preliminary backfill grout and 0.63 for the reference backfill grout. In all cases, the theoretical maximum porosities exceed the largest measured value for the porosity; generally that obtained from weight loss measurements. The discrepency must be due to water incorporated into the hydrated cement phases during initial curing prior to the placement of the specimens into water tanks.

Consideration of the data given in Tables 3 and 4 shows that the measured gas-accesible volumes after drying for the denser materials, the PFA/OPC-concrete and the BFS/OPC-grout, are not consistent with the weight loss, MIP or theoretical maximum porosities. Figures 1 and 2 show that these materials have a relatively large proportion of pores with radii less than 10 nm. This cannot be explained by the retention of water in very fine porosity as this would be indicated by the weight loss measurements. However, the fine porosity may represent "ink-bottle" pores where the entrance to regions of the porosity is constricted. Such constrictions may either hinder direct gas access or be blocked by retained water. In the latter case, the retention of a small volume of water may prevent gas access to a large fraction of the total porosity.

The measured porosities for the backfill grouts in the dry condition from the different techniques are generally consistent. The porosities obtained by MIP are slightly lower than those obtained from weight loss and gas-accessible volume. The reason for the apparent lack of penetration of mercury into some of the pore structure is not known.

The measurements of porosity from gas-accessible volumes in the specimens conditioned at 100 % relative humidity show that some porosity is apparently present in materials which are supposed to be water-saturated. The negative measured value of the gas-accessible volume porosity for the PFA/OPC-concrete conditioned at 75 % relative humidity demonstrates that these data are subject to experimental error and the non-zero measured porosities for the PFA/OPC-concrete and the BFS/OPC-grout may not be significant. However, for the backfill grouts there is significant accessible porosity after conditioning at 100 % relative humidity. This is discussed further in Section 5.5.

It is apparent that none of the measured values of the fractional porosity can be considered to be truely representative of the porosity of a material. The weight loss measurements may include

additional water lost from the hydrated cement phases whereas the MIP and gas-accessible volume data may be influenced by damage to the pore structure during drying. The gas-accessible volumes porosities are probably the most significant since they can be directly related to the migration of gases within the materials.

5.2 Gas Migration in Structural Concretes

5.2.1 Gas Diffusion in Structural Concretes

The best value of the hydrogen-argon inter-diffusion coefficient for the SRPC-concrete in a dry condition, 3×10^{-8} m^{2}s^{-1}, is similar in magnitude to the values obtained by other workers and discussed previously in Section 2.2.2. The gas migration parameters measured for the other materials indicate that the parameters for the high porosity backfilling grouts exceed those for the structural materials by an order of magnitude or more. Consequently, the value of the diffusion coefficient for the SRPC-concrete represents a lower limit to the diffusion coefficients for the other materials, in particular the backfilling grouts. Gas migration by diffusion will only be significant during the operating phase of the repository. In these circumstances, the gases generated within the backfilled structure may migrate by inter-diffusion with gases within the air in open, operational vaults.

5.2.2 Bulk Gas Flow in Dry Material

The experimental data shown in Figure 13 demonstrate that the permeability coefficient for the PFA/OPC-concrete measured at a constant average pressure of 100 kPa is dependent on the mean free path of the gas. Experiments conducted with a varying average pressure show that the permeability coefficient for a particular gas in both the SRPC- and PFA/OPC-concretes decreases with increasing average pressure, as shown by the data in Table 6 and Figure 14. This variation is also demonstrated by the compilation of the data for argon migration in dry PFA/OPC-concrete shown in Figure 15. These observations are consistent with previous observations by other workers, as discussed in Section 2.2.1, which demonstrate that the gas permeability of structural concretes is influenced by Knudsen flow at lower pressures [8].

The data for the SRPC-concrete, shown in Figure 14, demonstrate that this material exhibits a significantly lower permeability than does the PFA/OPC-concrete. This is at variance with the general expectation that the mass transport characteristics of a PFA-modified material will be lower than those of an unmodified cement [22]. The infinite pressure permeability coefficient given in Table 8 for the SRPC-concrete is an order of magnitude lower than that given for the PFA/OPC-concrete. The measured fractional porosities of the two materials, given in Table 3, are similar. The observed difference in performance may be the result of differing degrees of damage to the pore structures of the two materials during drying.

The contribution of Knudsen flow to the flow of a given gas, as described in Section 2.1, is characterised by the Knudsen number; the ratio of the mean free path to the radius of the pores in which the gas is flowing. A Knudsen number significantly greater than unity indicates that

Knudsen flow will be important. The mean free path is dependent on the nature of migrating gas, as shown above. Consequently, the contribution from Knudsen flow at a given pressure will depend on the gas flowing, as shown by the data in Figure 13. The average pore radius for the PFA/OPC-concrete, given in Table 3, is 0.011 μm whilst the mean free path at 100 kPa and 25 °C varies between 0.070 and 0.305 μm for the gases used in these experiments. Hence, the Knudsen numbers are in the range 6 to 28 and a significant contribution from Knudsen flow at 100 kPa would be expected.

The data shown in Figure 15 demonstrate that the change in the argon permeability coefficient of the PFA/OPC-concrete for an increase in the average pressure from 100 kPa to 7.5 MPa is a decrease by about a factor of 2.5. Comparison of the infinite pressure permeability coefficients for dry material given in Table 6 for the different gases with the permeability coefficients obtained at a constant average pressure of 100 kPa given in Figure 13 also indicates that the permeability decreases by at most a factor of two as the pressure is increased over this range. The majority of this decrease occurs in the 0 to 1 MPa pressure range, as shown in Figure 15.

5.2.3 Bulk Gas Flow in Water-saturated Material

The behaviour of the PFA/OPC-concrete in the partially or fully water saturated condition is qualitatively similar to that in a dry condition. Figures 12 and 13 demonstrate that the permeability coefficient is dependent on the type of gas for concrete conditioned at 75 % relative humidity, although the measured permeability coefficients are significantly lower than those of dry material. The reduction in the measured permeability coefficient for material conditioned at high relative humidities must be due to the effective blocking of pores which remained filled with water after conditioning. The relationship between the radius of the largest filled pore, r_p, and relative humidity, H, is given by the Kelvin equation [3];

$$-\ln (H) = \frac{2\sigma}{r_p} \frac{V_m}{RT} \qquad ....(11)$$

where σ and V_m are the surface tension and molar volume of water respectively. A relative humidity of 75 % gives a maximum filled pore radius of about 4 nm whilst at a relative humidity of 100 % all pores should be filled with water. Hence, at 75 % relative humidity the majority of the porosity should be available for gas migration. The reduction in the permeability coefficient for 75 % relative humidity conditioned materials apparent in the experimental results hence indicates that gas migration is significantly influenced by the finer porosity and that much of the pore volume may not form interconnected networks with constrictions larger than 4 nm.

The material conditioned at 100 % relative humidity demonstrated a further decrease in the permeability coefficient. The Kelvin equation predicts that all porosity is water-filled for this condition and hence a reduction is expected. However, the only mechanism available for gas

migration in material that is fully water-saturated will be solution-diffusion, where dissolved gas molecules diffuse in the pore solution, as discussed in Section 2.2.3. The calculation of an equivalent permeability coefficient for the solution-diffusion mechanism of gas migration is described in Appendix 5. An equivalent permeability coefficient of about 2×10^{-23} m^2 is obtained for the migration of oxygen. It is assumed that the other gases will exhibit similar values, with the possible exception of carbon dioxide, which has a significantly greater solubility. This value is significantly less than that obtained for helium migration in the PFA/OPC-concrete, 7×10^{-20} m^2, and it must be concluded that either there was leakage across the specimen or that some interconnected porosity remains open in the specimens conditioned at 100 % relative humidity.

5.3 Gas Migration in Grouts

Table 7 shows that the permeability coefficients at 100 kPa for the three different grouts in the dry condition are of similar magnitude and are an order of magnitude or more greater than those measured for the PFA/OPC-concrete. The permeability coefficients for the grouts are decreased by two or three orders of magnitude for the 100 % relative humidity conditioned specimens compared to the dry materials. The permeability coefficient for the BFS/OPC-grout in the 100 % relative humidity conditioned state is substantially lower than those of the other grouts and is comparable in magnitude to that of the structural concrete.

Comparison of the data obtained using helium and argon as the migrating gases in dry materials shows that there is no significant dependence on gas type for the preliminary backfill grout. Hence, there is apparently little or no Knudsen flow occurring at 100 kPa. Some dependence on gas type is exhibited by the BFS/OPC- and reference backfill grouts. The observed variation in behaviour must be due to the differences in pore sizes between the grouts.

Comparison of the permeability coefficients extrapolated to infinite pressure, given in Table 8, with those obtained at 100 kPa average pressure (Table 7) indicates that there is no consistent relationship between the two. This demonstrates that the permeability coefficients of these materials are not strongly dependent on average pressure at pressures of 100 kPa and above. The values of the Klinkenberg constants for these materials were extracted from the data. However, the results were found to be extremely variable and some values were negative, indicating an increase in the permeability coefficient with increasing average pressure. Hence, the permeability coefficients for the high porosity grouts can be considered to be approximately constant over the range of average pressures studied here.

The difference between the behaviour of the grouts and that of the PFA/OPC-concrete must be due to differences in the pore structures of the materials. Table 3 shows that the average pore sizes of the preliminary and reference backfill grouts are 0.7 and 0.4 µm respectively. These values are such that the Knudsen numbers for the two materials will be significantly less than unity at an average pressure of 100 kPa and hence no significant contribution from Knudsen flow would be expected in these materials at this, or greater, pressure.

5.4 Comparison with Water Permeability Coefficients

Since the viscous flow of fluids is governed by the Darcy equation, the permeability coefficient should be equal for all fluids. The flow of gases is complicated by the Klinkenberg effect and compressibility, but the infinite pressure permeability coefficients for dry material should be equal to the permeability coefficients for liquids such as water [2, 3, 8]. The data for material conditioned at 100 % relative humidity cannot be directly compared to those for water flow.

The water permeability coefficients for both the SRPC- and PFA/OPC-concretes have been shown to be less than about 10^{-21} m^2 [22]. Table 7 indicates that the infinite pressure permeability coefficients for the concretes are more then four orders of magnitude greater than this. Although, the water permeability measurements were complicated by the continued hydration of the materials it is unlikely that the difference can be explained by this effect.

The water permeability coefficient of the preliminary backfill grout has been measured as about 4×10^{-16} m^2 [31]. This value is approximately two orders of magnitude lower than the infinite pressure permeability coefficient of the dry grout given in Table 8. In contrast, the water permeability of the reference backfill grout, at 2×10^{-16} m^2 [32], is close to the infinite pressure permeability coefficient. No water permeability data are available for the BFS/OPC-grout.

The data discussed above demonstrate completely different relationships between water and gas permeability coefficients. Only the reference backfill grout shows the close agreement between the two data expected initially. The reasons for these differences in the behaviour of the materials are uncertain, and may reflect differences in pore structure under dry and wet conditions, that is the presence of water not only fills pore space but changes its characteristics.

5.5 Interaction between Gas and Water in Cementitious Materials

Comparison of the permeability coefficients obtained for the experimental materials in the dry and 100 % relative humidity conditioned states demonstrates that the influence of water within the pore structure of cementitious materials is crucial in determining gas migration rates. The comparison between the effective permeability coefficient for the solution-diffusion migration mechanism and the measured permeability coefficients demonstrates that none of the experimental materials can be considered to be fully water saturated under any of the experimental conditions in this study.

As discussed in Section 2.1, the only mechanism available for gas migration in fully water-saturated material is solution-diffusion. The equivalent permeability coefficient for solution-diffusion derived in Appendix 5, about 10^{-23} m^2, is significantly lower than the lowest permeability coefficients measured for any of the 100 % relative humidity conditioned materials. Hence it appears that the gas migration observed in this study may differ significantly from that expected for the truly water-saturated condition.

The application of a pressure difference to a water saturated porous material will result in the expulsion of water from pores which exceed a particular size. The expulsion of a fluid from a capillary requires the application of an excess pressure denoted the capillary pressure. The

capillary pressure, p, for a pore of radius r_p, assuming an angle of contact between the fluid and the capillary wall of 90°, is given by [2];

$$p = \frac{2\sigma}{r_p} \qquad ....(12)$$

where σ is the surface tension, equal to 0.073 Nm^{-1} for water. The approximate capillary pressures for the average pore radius of both the PFA/OPC-concrete and the BFS/OPC-grout are 13 MPa whereas those for preliminary and reference backfill grouts are 210 and 320 kPa respectively.

In the low pressure experiments, the maximum applied pressure is 200 kPa. This pressure can expel water from pores of the order of 0.7 µm. The MIP measurements of pore size distributions for the two backfill grouts demonstrate that both materials exhibit a significant volume of porosity with pore radii above this value, as shown in Figures 3 and 4. Hence, water expulsion may occur in the 100 % relative humidity conditioned specimens even in the low pressure experiments. Measurements made on the backfill grouts using higher applied pressures may exhibit significant water expulsion effects. This would result in measured permeability coefficients in excess of those expected for fully saturated material based on the solution-diffusion model of gas migration. In addition, the increased expulsion of water at higher pressures may give an increase in permeability with applied pressure.

The above discussion assumes that the average pore radius obtained from the MIP measurements is the maximum pore size available. This is unlikely to be true and, although the pore size distributions of the high-porosity grouts are substantially skewed towards the larger pore sizes, there will be significant porosity with radii in excess of the average values. The experimental results appear to demonstrate that the migration of gas is significantly affected by the presence of these larger pores.

Similar effects would be expected for the PFA/OPC-concrete and the BFS/OPC-grout. However, the finer pore structure would mitigate the effect and hence the measured permeability coefficients for 100 % relative humidity conditioned material should be closer to the value predicted by the solution-diffusion model. This is demonstrated by the comparison between the measured permeability coefficients for these materials and those measured for the backfill grouts.

The weight losses measured during conditioning at 100 % relative humidity for both the preliminary and reference backfill grouts indicate that full water saturation may not have been achieved prior to the commencement of the experiments. It is possible that the water within the larger pores in these materials drains under the influence of gravity. Thus, the data obtained for 100 % relative humidity conditioned specimens may not be representative of the behaviour of fully water saturated material.

The retention of water within a capillary is governed by the balance between the capillary

pressure and the gravitational force exerted by the weight of the water. Consequently, water will only be retained in pores of a given radius if the pore length does not exceed a particular value. This length can be calculated by equating the capillary pressure to the hydrostatic pressure of a column of water;

$$h = \frac{2\sigma}{r_p \rho g} \qquad ....(13)$$

where h is the maximum pore length which can remain water filled and g the acceleration due to gravity. The maximum pore lengths are 21 and 32 m for the preliminary and reference backfill grout average pore radii respectively. Since the specimen thicknesses are only a few centimetres, it is apparent that the weight loss cannot be explained by gravitational draining.

If the movement of water under the influence of gravity is occurring, despite the argument above, it may provide an additional means whereby the migration of gas within a repository could occur. In particular, the movement of water may allow a consequent migration of gas as a "bubble".

6 The Effects of Stress Generation in Cementitious Materials

6.1 Model of Cracking in Cementitious Materials

The effects of the stress generated by gas pressurisation have been studied using a simple model of a spherical gas source in spherical repository. The model is illustrated schematically in Figure 17. The ultimate effect of stress will be the formation of a crack. If the region of gas generation shown in Figure 17 is considered to be a void then backfill cracking at the void surface will occur if the tangential hoop stress exceeds the tensile strength of the backfill. Hence, in the model the crucial stress for determining the cracking of the material is considered to be the tangential hoop stress at the surface of the void.

Analytical solutions exist for the tangential hoop stress and radial stress at a given radius for a spherical pressure vessel [33]. The repository model can be considered to be equivalent to such a situation. The standard result for a pressure vessel gives a tangential hoop equal to half the excess pressure in the vessel. The principal difference between a pressure vessel and the repository model is the presence of porosity in the backfill. The effect of the porosity of the backfill material has been included into the model by modifying the value used for the radial stress.

$$-S_r = (1-\varepsilon) \Delta p \qquad ....(14)$$

where S_r is the radial stress, Δp is the excess pressure in the void and ε is the fractional porosity of the material. This approach is rather simplistic, but, as discussed below, it can be shown to be a good approximation for the conditions applicable to the behaviour of a repository. Incorporating the Equation 14 into the standard expression for the tangential hoop stress, S_θ, gives;

$$S_\theta = \frac{\Delta p}{2} \left[1 + \frac{2v\varepsilon}{(1-v)} \right] \qquad ....(15)$$

where v is the Poisson's ratio for the backfill. This expression can be used to calculate the hoop stress using appropriate parameters. The backfill is considered to fail if the calculated stress exceeds the tensile strength of the material.

The value of the pressure excess depends on the relative rates of gas generation and migration. The value of the pressure in the void can be determined using the Darcy equation (Equation 1) and integrating between the void radius, R, and the outer radius of the repository, ζ. This gives an expression for the pressure produced in the void, p_v;

$$p_v^2 - p^2 = \left[\frac{1}{R} - \frac{1}{\zeta} \right] \frac{Q\mu p_0}{2\pi k} \qquad ....(16)$$

where p is the hydrostatic pressure outside the repository, Q the rate of gas generation measured at standard pressure p_0 (equal to 101325 Pa), μ the gas viscosity and k the permeability coefficient for the backfill. The excess pressure is equal to the difference between the pressure in the void and the hydrostatic pressure. If it is assumed that the outer radius is effectively infinite, Equations 15 and 16 combined to yield an expression for the tangential hoop stress generated at the void surface;

$$2S_\theta = \left[1 + \frac{2v\varepsilon}{(1-v)} \right] \left[-p + \sqrt{p^2 + \frac{Q\mu p_0}{2\pi Rk}} \right] \qquad ....(17)$$

This equation is used to calculate the tangential hoop stresses due to the generation of gas discussed in Section 6.2.

6.2 Sensitivity to Material Properties and Conditions

6.2.1 Basis of Calculations

The sensitivity of the tangential hoop stress, calculated using the analytical approximation given in Equation 17, to the material parameters required by the model was investigated. The effect of a particular parameter was assessed by fixing all remaining parameters at typical values and varying the parameter of concern over an appropriate range. The typical parameters were selected to reasonably approximate the reference backfill grout in a water saturated condition. It is apparent from the analytical approximation that the calculated stress in this model is independent of the Young's modulus of the material. The gas viscosity was assumed to be equal to that of argon at a value of 2.2×10^{-5} Pas.

The tangential hoop stress at the void surface calculated from the typical values of the model parameters is 238 kPa. The compressive strength of the reference backfill grout is 6.0 MPa. If the tensile strength is assumed to be one tenth of the compressive strength, that is 600 kPa, then the tensile strength is not exceeded by the hoop stress for the typical conditions and the reference backfill grout will not crack.

6.2.2 Gas Generation Rate

The anticipated maximum gas generation rate is approximately one repository volume of gas per year, measured at standard temperature and pressure. The model illustrated in Figure 17 is intended to represent the venting of gas from a hypothetical single waste drum with an approximate volume of 1 m³. Hence, the typical value of the generation rate was taken to be 1 m³ per year at standard temperature and pressure. The range of generation rates was specified as 0 to 5 m³ per year. The variation in stress with gas generation rate is shown in Figure 18. The stress is increased as the gas generation rate is increased.

6.2.3 Hydrostatic Pressure

Current radioactive waste disposal strategies envisage the placement of a repository at a depth of up to 1000 m below ground level. This indicates a potential range of hydrostatic pressures of between 100 kPa and 10 MPa if the rock overlying the repository is fully saturated by the groundwater. Figure 18 demonstrates that the stress is inversely dependent on the hydrostatic pressure and hence the lower pressure of 100 kPa was adopted as the typical value to represent a plausible worst case. The reduction in stress with increasing hydrostatic pressure is attributed to the compressibility of the gas. As the pressure increases the volumetric flow rate is decreased. This behaviour implies that a repository will be more susceptible to gas generated cracking before re-saturation by groundwater as the effective hydrostatic pressure within the repository will be lower. The hydrostatic pressure due to the overlying rock cannot be exerted on the backfill since, prior to re-saturation, there will be insufficient fluid in the backfill to fully transmit the pressure.

6.2.4 Fractional Porosity

The data given in Table 3 indicate a range of fractional porosities of between about 0.1 and 0.6 for the experimental materials. The relationship between the measured values of fractional porosity and that available for gas flow is not known. The typical value was taken as 0.5, close to the values given for the backfill grouts in Table 3. The analytical solution demonstrates that gas generated stress is linearly dependent on the fractional porosity of the material, assuming constant permeability. The stress increases by a factor of 0.5 as the porosity is varied between zero and unity. The effect of the fractional porosity on the stress may not be adequately modelled by the analytical approximation and the dependence of stress on porosity may not be as simple as indicated here.

6.2.5 Void Radius

The model is intended to simulate the effects of gas vented from waste drums. The size of a vent, either engineered as a design feature or due to drum corrosion, cannot exceed the size of a drum; approximately 1 m. The typical value of 0.05 m was selected to represent an engineered vent of 10 cm diameter. Figure 18 demonstrates that the stress generated at the surface of the void is strongly dependent on the void radius. The requirement for a void dimension is a limitation in the overall model and Figure 18 shows that the void radius is crucial in determining the stress.

6.2.6 Poisson's Ratio

The expected value of the Poisson's ratio for an ideal material is 0.5. The values for real materials tend to be between about 0.2 and 0.4 and hence a range of 0 to 0.5 was investigated. The typical value was taken to be 0.2. The stress increased by a factor of two as the Poisson's ratio was varied between 0 and 0.5. Variation in this parameter is not of primary importance in determining the stress.

6.2.7 Permeability Coefficient

As has been discussed previously, the repository is likely to become water saturated at some stage after closure and hence the gas permeability will be influenced by the presence of water. Figure 18 demonstrates that the stress is strongly dependent on permeability for permeability coefficients below about 10^{-16} m^2. Table 7 shows that the permeability coefficients for water saturated materials are likely to lie below this value and hence will be crucial in determining the stress. The value of the permeability coefficient used as the typical value was 10^{-18} m^2, somewhat below the measured permeability coefficient for the reference backfill grout in the 100 % relative humidity conditioned state.

6.3 Summary of the Predictions of Gas-induced Cracking in a Repository

The comparative performance of the cementitious materials studied in this work is summarised in Figure 19. As discussed above, the crucial parameters in determining the calculated level of tangential hoop stress at the void surface are the void radius and the permeability coefficient of the surrounding material. Figure 19 shows the calculated stress for permeability coefficients between 10^{-22} and 10^{-14} m^2 for voids of 0.02, 0.1 and 0.5 m radius using the typical values for the remaining parameters. The measured ranges of the permeability coefficients for the cementitious materials are also illustrated, plotted at stress values equal to the estimated tensile strength of each material based on one tenth of the compressive strength. If the tensile strength of the material at an appropriate permeability is exceeded by the calculated stress then the material is predicted to crack at the void.

Figure 19 indicates that, assuming that the permeability coefficients are equal to those measured in this work, the two backfill grouts can adequately disperse gas and hence will not crack. In contrast, the PFA/OPC-concrete and the BFS/OPC-grout appear to have insufficient permeability in the saturated state to prevent cracking.

6.4 Behaviour of Gas in a Repository

The behaviour of the backfill grouts during conditioning at 100 % relative humidity demonstrates that the specimens used in the experiments may not be truly representative of complete water saturation. The range of permeability coefficients indicated in Figure 19 shows that the presence of additional water may compromise the assertions made above. However, it is shown in Appendix 5 that the ultimate lower limit of the permeability coefficient, equivalent to the solution-diffusion mechanism of gas migration, is of the order of 10^{-23} m^2. This limit applies to any water saturated material, including the backfill grouts. If the permeability coefficient is as low as 10^{-23} m^2, extrapolation from the data given in Figure 19 shows that the stress generated by gas pressurisation will exceed the tensile strength of the backfill and extensive gas-induced cracking would occur.

The presence of significant gas-induced cracking in the backfill may result in a large increase in the effective gas permeability of the material. The measurements of the permeability of

specimens of the preliminary grout containing a construction joint demonstrate that such an interface increases the permeability coefficient to about 10^{-15} m^2. If a similar increase in the permeability occurs after the backfill cracks initially, the gas pressure should be relieved and no further cracking take place. This assumes that the gas can effectively disperse into the geosphere in the vicinity of the repository. Hence, it is possible that a series of cracks may occur in the backfill which link the regions of gas generation to the surrounding geosphere. The exact geometry and number of these cracks cannot be predicted by the current model, which simply predicts whether the gas-induced stress will exceed the tensile strength of a porous material.

The relative significance of any gas-induced cracking of the backfill will depend on the number of cracks in the backfill caused by other mechanisms. If the backfill is dominated by the presence of a large number of cracks caused by another mechanism, such as construction joints, shrinkage or rock movement, the addition of further cracks due to gas pressurisation will not significantly affect the overall behaviour of the repository. In addition, the presence of cracks prior to any pressurisation may increase the effective permeability of the backfill and aid the dispersion of the gas generated within the repository. Hence, the effects of gas generation in repository which is subject to substantial cracking from other sources will be limited.

It is apparent that if the backfill is not subject to substantial cracking from other sources the effects of gas pressurisation may have some significance. In particular, cracks might then occur in the backfill where none were previously present. The consideration of other mechanisms of cracking is beyond the scope of this study.

7 Conclusions

The gas permeability coefficients for a range of potential repository construction materials have been determined for specimens in dry and in both partially and fully water saturated conditions. It has been shown that the permeability of the structural PFA/OPC-concrete is dependent on both gas type and average pressure under all conditions. The permeability coefficient is approximately independent of average pressure at pressures above about 1 MPa. These effects are attributable to an additional component of gas flow caused by significant Knudsen flow at lower average pressures. The permeability coefficient is significantly reduced for water saturated conditions due to a reduction in the volume of porosity available for gas flow.

Gas flow in the two high porosity backfill materials is not significantly dependent on the average pressure in the range 100 kPa to 3 MPa. Some differences are observed for measurements carried out using helium and argon. The contribution of Knudsen flow to gas migration in these materials is small at the average pressures studied due to the generally larger pore size when compared with the structural concrete. The permeability coefficient is significantly reduced when the materials are water saturated, but it remains several orders of magnitude greater than that observed in the PFA/OPC-concrete. The BFS/OPC-grout, typical of the encapsulation materials placed within waste packages, has a similar permeability coefficient to those measured for the backfill grouts when dry but exhibits a significantly lower permeability, close to that of the concrete, when water saturated. Some dependence on average pressure is observed. The properties of this material may be affected by damage during drying.

The observed permeability coefficients for water saturated materials are all significantly greater than the permeability coefficient predicted by the solution-diffusion mechanism of gas migration. This may be due to the movement or displacement of the water within the pore structure. Such an effect would result in an increase in the permeability coefficient at higher applied pressures.

The presence of interfaces within the cementitious materials, such as construction joints and reinforcement bars, results in an increase in the permeability of the materials when water is present. No significant increase was observed in dry materials.

A simple model of the development of cracking in cementitious materials in repositories has been developed. The model identifies the gas permeability coefficient as a crucial parameter in determining the likelihood of cracking through gas generation in voids. Initial calculations indicate that the backfill grouts studied in this work should be able to release gas at a sufficient rate to avoid cracking.

Acknowledgements

References

1. Proceedings of joint NEA/CEC Workshop, "Sealing of Radioactive Waste Repositories", Paris (1989).

2. R.E. Cunningham and R.J.J. Williams, "Diffusion in gases and porous media", Plenum Press, New York (1980).

3. F.A.L. Dullien, "Porous media - Fluid transport and pore structure", Academic Press, New York (1979).

4. C.H. Geankoplis, "Mass transport phenomena", Holt, New York (1972).

5. C.N. Satterfield, "Mass transfer in heterogeneous catalysis", MIT Press, Cambridge, Massachusetts (1970).

6. R.E. Collins, "Flow of fluids through porous media", Renhold Pub. Co., New York (1960).

7. L.J. Klinkenberg, *Drilling and Production Practice* (1941), 200.

8. P.B. Bamforth, *Mag. Concrete Res.* **39** (1987), 3.

9. M. Knudsen, *Ann. Phys.* **28** (1909), 75.

10. J. Crank, "The mathematics of diffusion", Clarendon Press, Oxford (1956).

11. K.P. McCarty and E.A. Mason, *Phys. Fluids* **3** (1960), 908.

12. R.B. Evans III, G.M. Watson and E.A. Mason, *J. Chem. Phys.* **35** (1961), 2076.

13. S. Goto and D.M. Roy, *Cement Concrete Res.* **11** (1981), 575.

14. R.H. Mills, *Mat. Res. Soc. Symp. Vol. 85* (1987), 135.

15. G.R. Martin, *Mag. Concrete Res.* **38** (1986), 90.

16. J.G. Cabrera and C.J. Lynsdale, *Mag. Concrete Res.* **40** (1988), 177.

17. H. Grube and C.D. Lawrence, Proc. RILEM Seminar on "The Durability of Concrete Structures under Normal Outdoor Exposure", Hannover (1984).

18. H. Grube and C.D. Lawrence, private communication.

19. J.W. Figg, *Mag. Concrete Res.* **25** (1973), 213.

20. L. Chou Chen and D.L. Katz, *ACI Journal* (1978), 673.

21. M. Daimon, T. Akiba and R. Kondo, *J. Am. Ceram. Soc.* **54** (1971), 423.

22. A.W. Harris, A. Atkinson, A.K. Nickerson and N.M. Everitt, Nirex Safety Study Report NSS/R125, Harwell Laboratory (1988).

23. C.R. Wilding, personal communication.

24. C.D. Lawrence, personal communication.

25. K. Tuutti, in "Corrosion of steel in concrete", Swedish Cement and Concrete Research Institute, Stockholm (1982), 146.

26. M.V.J. Culot, H.G. Olson and K.J. Schiager, *Health Phys.* **30** (1976), 263.

27. R.F. Holub, R.F. Droullard, T.B. Borak, W.C. Inkret, J.G. Morse and J.F. Baxter, *Health Phys.* **49** (1985), 267.

28. C.L. Page, N.R. Short and A. El Tarras, *Cement Conc. Res.* **11** (1981), 395.

29. A. Atkinson and A.K. Nickerson, *J. Mater. Sci.* **19** (1984), 3068.

30. C.L. Page and P. Lambert, *J. Mater. Sci.* **22** (1987), 942.

31. A.W. Harris and A.K. Nickerson, Nirex Safety Study Report NSS/R189, Harwell Laboratory (1989).

32. A.W. Harris, unpublished data.

33. T. Roark and C. Young, "Formulas for stress and strain (5th Edition)", McGraw-Hill (1975).

34. R.C. Weest (ed.), "The handbook of physics and chemistry (68th Edition)", CRC Press, Florida, USA (1988).

Appendix 1 - Ionic Conductivity Measurements

The ionic conductivities of specimens saturated with a 3 M solution of sodium chloride were measured. Cylinders measuring 100 mm in diameter and 300 mm in length were exposed to the solution for a minimum of 28 days prior to measurement. The magnitude of the impedence was measured using a Hewlett-Packard HP-4276A LCZ meter operating at 10 kHz. Contact was made to the ends of the cylinders using silver electrodes with a layer of absorbent material soaked in the solution to ensure a good contact. The sides of the specimens were dried to prevent short circuits. In all cases the load was found to be almost purely resistive. The measured ionic conductivites are given in Table 11 [22, 31, 32].

An equivalent sodium-chloride ion inter-diffusion coefficient by comparing the ratio of the measured specimen conductivity to that of the free solution with the known diffusion coefficient of aqueous sodium chloride. The free solution conducitivity was measured as 16.8 $\Omega^{-1}m^{-1}$ using a Mullard E7591/B platinum conductivity cell. The solution diffusion coefficient was assumed to be 2×10^{-5} m^2s^{-1} [22]. The calculated diffusion coefficients are also given in Table 11.

Comparison of the measured conductivities with the porosities given in Table 3 demonstrates that a change in the porosity from about 0.1 to 0.5 apparently results in an increase in conductivity by about three orders of magnitude. Table 3 shows that differences in the average pore size are significantly greater then those in porosity and hence it is probable that the mass transport properties of the cementitious materials are determined by the pore size rather than the fractional porosity. It must be assumed that the pore size distribution also influences mass transport but the quantitative comparison of pore size distributions is not possible. Overall, it can be concluded that the aqueous phase mass transport properties of these materials are determined by the pore structure, as would be expected.

Appendix 2 - The Ideal Gas Approximation

The methods used to analyse the experimental data assume that the gases involved conform to the ideal gas approximation. The implications of deviations from ideal behaviour are considered in this appendix.

The behaviour of a real gas can be modelled by the Van der Waals modification to the ideal gas law [34]. The behaviour of a gas is described by;

$$\left[p + \frac{n^2 \gamma}{V^2} \right] \left[V - n\delta \right] = nRT \qquad \text{....(18)}$$

where p is the pressure, V the volume, T the absolute temperature, n the number of moles of gas and R the gas constant. The constants γ and δ are dependent on the type of gas involved. The magnitude of the influence of any deviation from ideal behaviour is illustrated by calculating the change in pressure during the isothermal compression and expansion of 1 mole of gas at room temperature (25 °C). The resulting pressures and the percentage deviations from the values calculated from the ideal gas approximation are shown in Table 12.

It is apparent that deviations from the ideal gas law are only significant during the compression of the gases. This is particularly true for carbon dioxide, where a one hundredfold reduction in volume results in a pressure which is almost half that predicted by the ideal gas approximation. The maximum pressures used in the experiments are of the order of 3 MPa. At such pressures, the effect of deviation from ideal behaviour is to give an under- or over-estimate of the quantity of gas in the high pressure reservoir by perhaps up to 10 %. Consequently, the molecular flow rate differs from that expected and the true permeability coefficient must also be different from that calculated from the high pressure reservoir data. Hence, the calculated permeability coefficients derived from high pressure data may be up to about 10 % in error.

The effect of the deviation from ideal gas behaviour is negligible for experiments performed at pressures of the order of 100 kPa. Hence the data quoted in Table 7 are not affected.

Appendix 3 - Prediction of Final Pressures

If the volume of the pore space in a specimen is negligible, the average pressure at the completion of a constant average pressure experiment, when the entire system has reached an equilibrium pressure, is given by a volume-weighted average of the initial pressures in the reservoirs. Since the volumes of the two reservoirs are not exactly equal, the final pressure may not be exactly the same as the simple mean of the two initial average pressures.

The impact of the volume of the pore space can be included by calculating a pore volume based on the porosity and volume of the specimen, V_p. The final pressure is then given by;

$$p_{final} = \frac{p_1 V_1 + p_2 V_2 + p_p V_p}{V_1 + V_2 + V_p} \qquad ....(19)$$

where V_1 and V_2 the reservoir volumes, p_1 and p_2 are the initial reservoir pressures and p_p the average pressure in the pore space. Since the gas within the pore space is compressible, the pressure gradient is not linear. The calculation of the average pressure in the pore space must allow for this non-linearity. The variation in pressure with position can be determined from the Darcy equation and integrated over the thickness of the specimen. This gives the following expression for the average pressure in the pore space;

$$p_p = \frac{2}{3} \frac{(p_1)^3 - (p_2)^3}{(p_1)^2 - (p_2)^2} \qquad ....(20)$$

Equation 20 indicates that the average pressure in the pore space for a low pressure of 100 kPa and a high pressure of 3 MPa is 20.02 MPa. In contrast, the average pressure if a linear pressure gradient is assumed is 15.50 MPa.

In many of the experiments the volume of the pore space can be significant. This is particularly true for specimens in the dry condition, where the pore space volume can exceed the volumes of the reservoirs. Hence, a simple average of the initial pressures will underestimate the expected final pressure.

Appendix 4 - Experimental Data

The results of the 370 experimental measurements of the permeability coefficient are tabulated in this appendix. The data are divided into sections according to material, humidity condition and migrating gas. The specimen number, average pressure during the experiment, run type and the permeability coefficient are given for each experiment.

The quoted overall average pressure is the mean of the measured pressures in each reservoir at the commencement and termination of the experiment. The run type is designated 1, 2 or 3. These values correspond to the following;

Run type 1 - Constant average pressure run.

Run type 2 - Varying average pressure run with constant high pressure.

Run type 3 - Varying average pressure run with constant low pressure.

In the case of a varying average pressure experiment, the quoted average pressure is determined as described above. The calculated permeability coefficient for such an experiment is that applicable to the quoted average pressure and can be directly compared to the data obtained from constant average pressure experiments.

Two values of the permeability coefficient, k, are given for each experiment. The value obtained from the analytical solution to the variation in pressure with time and the value calculated from the simulation of the behaviour of materials with non-zero porosity. The analytical solution value is used as the initial datum for the simulation for each experiment. The simulation value is considered to be a more accurate result and hence is quoted as the "best" permeability coefficient.

PFA/OPC-concrete
Dry condition - hydrogen migration

Sample	Pressure / 100 kPa	Run type	Analyt. k / m^2	Best k / m^2
G4	1.0	1	6.10×10^{-17}	7.07×10^{-17}
G4	1.0	1	5.74×10^{-17}	6.69×10^{-17}
G4	1.5	2	4.28×10^{-17}	5.16×10^{-17}
G36	1.0	1	7.56×10^{-17}	8.94×10^{-17}
G36	1.5	2	4.31×10^{-17}	5.25×10^{-17}
G37	1.0	1	1.01×10^{-16}	1.18×10^{-16}
G37	1.5	2	7.47×10^{-17}	9.02×10^{-17}
G38	1.0	1	8.55×10^{-17}	9.97×10^{-17}
G38	1.5	2	6.29×10^{-17}	7.62×10^{-17}
G39	1.0	1	6.79×10^{-17}	8.06×10^{-17}
G39	1.5	2	5.05×10^{-17}	6.13×10^{-17}

PFA/OPC-concrete
Dry condition - helium migration

Sample	Pressure / 100 kPa	Run type	Analyt. k / m^2	Best k / m^2
G36	1.1	1	1.04×10^{-16}	1.25×10^{-16}
G36	1.5	2	7.80×10^{-17}	9.46×10^{-17}
G37	1.1	1	1.30×10^{-16}	1.54×10^{-16}
G37	1.6	2	1.01×10^{-16}	1.22×10^{-16}
G38	1.1	1	1.11×10^{-16}	1.33×10^{-16}
G38	1.5	2	8.68×10^{-17}	1.05×10^{-16}
G39	1.1	1	8.86×10^{-17}	1.07×10^{-16}
G39	1.5	2	6.93×10^{-17}	8.43×10^{-17}
G65	1.0	1	5.20×10^{-17}	6.43×10^{-17}
G64	1.0	1	3.15×10^{-17}	8.43×10^{-17}
G64	1.0	1	2.84×10^{-17}	7.51×10^{-17}
HG6	15.3	1	4.81×10^{-17}	5.23×10^{-17}
HG6	16.6	1	4.10×10^{-17}	4.46×10^{-17}
HG6	16.5	1	3.57×10^{-17}	4.49×10^{-17}
HG6	16.0	1	3.46×10^{-17}	4.34×10^{-17}
HG6	8.7	3	3.98×10^{-17}	5.21×10^{-17}
HG6	24.0	2	3.29×10^{-17}	5.34×10^{-17}
HG6	24.1	2	4.22×10^{-17}	5.08×10^{-17}
HG7	16.6	1	3.84×10^{-17}	4.14×10^{-17}
HG7	16.6	1	3.11×10^{-17}	3.88×10^{-17}
HG7	16.3	1	4.57×10^{-17}	4.95×10^{-17}
HG7	16.1	1	4.33×10^{-17}	4.71×10^{-17}
HG7	15.1	1	3.44×10^{-17}	4.32×10^{-17}
HG7	24.4	2	4.48×10^{-17}	5.40×10^{-17}
HG7	24.4	2	3.09×10^{-17}	5.01×10^{-17}
HG7	8.8	3	4.08×10^{-17}	5.35×10^{-17}

PFA/OPC-concrete
Dry condition - methane migration

Sample	Pressure / 100 kPa	Run type	Analyt. k / m^2	Best k / m^2
G36	1.6	2	3.40×10^{-17}	4.12×10^{-17}
G36	1.1	1	4.59×10^{-17}	5.47×10^{-17}
G37	1.6	2	4.67×10^{-17}	5.64×10^{-17}
G37	1.1	1	5.99×10^{-17}	7.05×10^{-17}
G38	1.6	2	3.43×10^{-17}	4.16×10^{-17}
G38	1.1	1	4.98×10^{-17}	5.89×10^{-17}

Sample	Pressure / 100 kPa	Run type	Analyt. k / m^2	Best k / m^2
G39	1.6	2	2.81×10^{-17}	3.41×10^{-17}
G39	1.1	1	3.72×10^{-17}	4.47×10^{-17}

PFA/OPC-concrete
Dry condition - argon migration

Sample	Pressure / 100 kPa	Run type	Analyt. k / m^2	Best k / m^2
G4	1.0	1	4.74×10^{-17}	5.54×10^{-17}
G4	1.5	2	3.46×10^{-17}	4.20×10^{-17}
G4	1.0	1	4.52×10^{-17}	5.27×10^{-17}
G36	1.1	1	5.31×10^{-17}	6.31×10^{-17}
G36	1.5	2	4.24×10^{-17}	5.17×10^{-17}
G37	1.1	1	7.53×10^{-17}	8.81×10^{-17}
G37	1.5	2	5.66×10^{-17}	6.87×10^{-17}
G38	1.1	1	5.73×10^{-17}	6.74×10^{-17}
G38	1.6	2	4.35×10^{-17}	5.32×10^{-17}
G39	1.1	1	4.33×10^{-17}	5.17×10^{-17}
G39	1.5	2	3.72×10^{-17}	4.55×10^{-17}
G65	1.1	1	2.25×10^{-17}	2.81×10^{-17}
G65	0.9	1	2.36×10^{-17}	2.91×10^{-17}
G64	1.0	1	2.83×10^{-17}	3.52×10^{-17}
G64	1.0	1	2.88×10^{-17}	3.51×10^{-17}
HG6	15.9	1	2.74×10^{-17}	3.42×10^{-17}
HG6	15.5	1	2.63×10^{-17}	3.28×10^{-17}
HG6	16.2	1	3.15×10^{-17}	3.40×10^{-17}
HG6	15.4	1	3.13×10^{-17}	3.38×10^{-17}
HG6	8.1	3	1.71×10^{-17}	3.19×10^{-17}
HG6	23.6	2	2.42×10^{-17}	3.93×10^{-17}
HG6	8.6	3	1.89×10^{-17}	3.61×10^{-17}
HG6	23.2	2	1.90×10^{-17}	3.10×10^{-17}
HG6	48.5	1	1.37×10^{-17}	1.71×10^{-17}
HG6	72.6	2	1.33×10^{-17}	2.16×10^{-17}
HG7	16.3	1	2.80×10^{-17}	3.57×10^{-17}
HG7	16.4	1	3.52×10^{-17}	3.82×10^{-17}
HG7	16.7	1	2.42×10^{-17}	3.03×10^{-17}
HG7	16.2	1	3.24×10^{-17}	3.53×10^{-17}
HG7	24.1	2	2.81×10^{-17}	4.61×10^{-17}
HG7	23.8	2	4.16×10^{-17}	5.01×10^{-17}
HG7	8.6	3	2.94×10^{-17}	3.91×10^{-17}
HG7	8.7	3	1.79×10^{-17}	3.44×10^{-17}
HG7	48.7	1	1.35×10^{-17}	1.69×10^{-17}
HG7	24.9	3	8.99×10^{-18}	1.83×10^{-17}
HG7	73.3	2	1.15×10^{-17}	1.88×10^{-17}

PFA/OPC-concrete
Dry condition - carbon dioxide migration

Sample	Pressure / 100 kPa	Run type	Analyt. k / m^2	Best k / m^2
G36	1.0	1	2.70×10^{-17}	3.21×10^{-17}
G36	1.5	2	2.12×10^{-17}	2.59×10^{-17}
G37	1.0	1	3.24×10^{-17}	3.81×10^{-17}
G37	1.5	2	2.51×10^{-17}	3.05×10^{-17}
G38	1.1	1	2.55×10^{-17}	3.01×10^{-17}
G38	1.5	2	1.97×10^{-17}	2.41×10^{-17}
G39	1.1	1	2.20×10^{-17}	2.62×10^{-17}
G39	1.5	2	1.69×10^{-17}	2.06×10^{-17}
HG6	3.6	3	8.39×10^{-17}	1.52×10^{-16}

Sample	Pressure / 100 kPa	Run type	Analyt. k / m^2	Best k / m^2
HG6	6.2	1	2.75×10^{-17}	3.53×10^{-17}
HG6	3.6	3	2.53×10^{-17}	4.57×10^{-17}
HG6	8.6	2	2.31×10^{-17}	3.74×10^{-17}
HG7	5.8	1	1.56×10^{-17}	2.03×10^{-17}
HG7	8.2	2	1.22×10^{-17}	1.95×10^{-17}
HG7	3.4	3	1.90×10^{-17}	3.43×10^{-17}

PFA/OPC-concrete
75 % relative humidity condition - hydrogen migration

Sample	Pressure / 100 kPa	Run type	Analyt. k / m^2	Best k / m^2
G2	1.0	1	1.39×10^{-18}	1.59×10^{-18}
G2	1.0	1	1.36×10^{-18}	1.56×10^{-18}
G3	1.0	1	4.49×10^{-19}	5.16×10^{-19}
G3	1.0	1	4.53×10^{-19}	5.21×10^{-19}

PFA/OPC-concrete
75 % relative humidity condition - helium migration

Sample	Pressure / 100 kPa	Run type	Analyt. k / m^2	Best k / m^2
G2	1.0	1	1.78×10^{-18}	2.05×10^{-18}
G2	1.0	1	2.05×10^{-18}	2.35×10^{-18}
G1	0.9	1	4.42×10^{-19}	5.09×10^{-19}
G3	1.0	1	6.67×10^{-19}	7.66×10^{-19}
G3	1.0	1	7.69×10^{-19}	8.84×10^{-19}
G67	9.5	1	9.75×10^{-19}	9.75×10^{-19}
G67	13.8	1	1.38×10^{-18}	1.38×10^{-18}
G67	10.6	1	4.94×10^{-18}	4.94×10^{-18}

PFA/OPC-concrete
75 % relative humidity condition - methane migration

Sample	Pressure / 100 kPa	Run type	Analyt. k / m^2	Best k / m^2
G2	1.0	1	9.35×10^{-19}	1.07×10^{-18}
G2	1.0	1	9.72×10^{-19}	1.12×10^{-18}
G3	1.1	1	2.19×10^{-19}	2.52×10^{-19}
G3	1.0	1	2.28×10^{-19}	2.62×10^{-19}

PFA/OPC-concrete
75 % relative humidity condition - argon migration

Sample	Pressure / 100 kPa	Run type	Analyt. k / m^2	Best k / m^2
G1	1.0	1	1.16×10^{-19}	1.34×10^{-19}
G2	1.0	1	6.78×10^{-19}	7.79×10^{-19}
G2	1.0	1	7.48×10^{-19}	8.60×10^{-19}
G2	1.1	1	1.12×10^{-18}	1.29×10^{-18}
G2	1.0	1	6.42×10^{-19}	7.38×10^{-19}
G1	1.0	1	1.31×10^{-19}	1.51×10^{-19}
G1	1.0	1	1.41×10^{-19}	1.63×10^{-19}
G3	1.0	1	2.61×10^{-19}	3.00×10^{-19}
G3	1.0	1	2.62×10^{-19}	3.02×10^{-19}
G3	1.0	1	2.57×10^{-19}	2.95×10^{-19}
G3	1.0	1	1.81×10^{-19}	2.08×10^{-19}
HG8	8.0	3	1.67×10^{-19}	1.67×10^{-19}
G66	1.0	1	8.44×10^{-20}	8.44×10^{-20}

Sample	Pressure / 100 kPa	Run type	Analyt. k / m²	Best k / m²
G66	16.2	1	1.62×10^{-19}	1.62×10^{-19}
G67	1.0	1	5.82×10^{-20}	5.82×10^{-20}

PFA/OPC-concrete
75 % relative humidity condition - argon migration

Sample	Pressure / 100 kPa	Run type	Analyt. k / m²	Best k / m²
G2	1.0	1	1.25×10^{-19}	1.55×10^{-19}
G2	1.1	1	2.18×10^{-19}	2.50×10^{-19}
G3	1.0	1	6.14×10^{-20}	7.05×10^{-20}
G3	1.1	1	8.25×10^{-20}	9.48×10^{-20}

PFA/OPC-concrete
100 % relative humidity condition - helium migration

Sample	Pressure / 100 kPa	Run type	Analyt. k / m²	Best k / m²
G18	1.0	1	6.11×10^{-20}	7.02×10^{-20}
HG11	15.7	1	6.25×10^{-22}	6.25×10^{-22}
G3	18.9	1	4.20×10^{-22}	4.20×10^{-22}

PFA/OPC-concrete
100 % relative humidity condition - argon migration

Sample	Pressure / 100 kPa	Run type	Analyt. k / m²	Best k / m²
G16	1.0	1	5.27×10^{-21}	6.06×10^{-21}
G17	1.0	1	9.86×10^{-22}	1.13×10^{-21}
G18	1.0	1	3.59×10^{-20}	4.12×10^{-20}
G19	1.0	1	1.20×10^{-21}	1.38×10^{-21}
DG15	8.6	3	1.08×10^{-17}	1.08×10^{-17}
DG15	16.1	1	2.60×10^{-17}	2.60×10^{-17}
DG15	23.7	2	3.88×10^{-17}	3.88×10^{-17}
G70	8.5	3	7.09×10^{-17}	7.09×10^{-17}
G70	16.1	1	4.82×10^{-17}	4.82×10^{-17}
G70	23.6	2	5.60×10^{-17}	5.60×10^{-17}
G71	16.2	1	4.85×10^{-19}	4.85×10^{-19}

BFS/OPC-grout
Dry condition - helium migration

Sample	Pressure / 100 kPa	Run type	Analyt. k / m^2	Best k / m^2
G20	1.5	2	5.28×10^{-16}	6.45×10^{-16}
G20	0.5	3	1.83×10^{-15}	2.40×10^{-15}
G21	1.5	2	5.18×10^{-16}	6.35×10^{-16}
G21	0.5	3	1.57×10^{-15}	2.04×10^{-15}
G22	1.5	2	4.80×10^{-16}	5.88×10^{-16}
G22	0.5	3	1.32×10^{-15}	1.70×10^{-15}
G23	1.5	2	4.36×10^{-16}	5.34×10^{-16}
G23	0.5	3	1.56×10^{-15}	2.03×10^{-15}
G72	0.5	3	5.42×10^{-15}	7.28×10^{-15}
G72	1.5	2	3.45×10^{-15}	4.42×10^{-15}
G73	0.5	3	4.86×10^{-15}	6.75×10^{-15}
G73	1.5	2	2.70×10^{-15}	3.49×10^{-15}
G72	8.5	3	1.39×10^{-15}	1.67×10^{-15}
G72	24.1	2	1.17×10^{-15}	1.33×10^{-15}
G73	8.2	3	2.00×10^{-15}	2.45×10^{-15}
G73	23.7	2	2.11×10^{-15}	2.38×10^{-15}

BFS/OPC-grout
Dry condition - argon migration

Sample	Pressure / 100 kPa	Run type	Analyt. k / m^2	Best k / m^2
G20	1.5	2	3.99×10^{-16}	4.87×10^{-16}
G20	1.0	1	4.36×10^{-16}	5.17×10^{-16}
G21	1.5	2	3.61×10^{-16}	4.42×10^{-16}
G21	1.0	1	3.80×10^{-16}	4.53×10^{-16}
G22	1.5	2	3.17×10^{-16}	3.88×10^{-16}
G22	1.0	1	3.44×10^{-16}	4.09×10^{-16}
G23	1.5	2	2.88×10^{-16}	3.54×10^{-16}
G23	1.0	1	3.29×10^{-16}	3.93×10^{-16}
G73	0.6	3	2.80×10^{-15}	3.89×10^{-15}
G73	1.6	2	2.08×10^{-15}	2.69×10^{-15}
G72	0.6	3	3.59×10^{-15}	4.82×10^{-15}
G72	1.6	2	2.85×10^{-15}	3.65×10^{-15}
G73	23.6	2	7.93×10^{-16}	8.98×10^{-16}
G73	8.1	3	1.01×10^{-15}	1.23×10^{-15}
G72	8.2	3	8.45×10^{-16}	1.02×10^{-15}
G72	25.2	2	6.38×10^{-16}	7.22×10^{-16}

BFS/OPC-grout
75 % relative humidity condition - argon migration

Sample	Pressure / 100 kPa	Run type	Analyt. k / m^2	Best k / m^2
G24	1.0	1	6.14×10^{-18}	7.43×10^{-18}
G24	1.0	1	5.81×10^{-18}	6.77×10^{-18}
G25	1.0	1	3.80×10^{-18}	4.65×10^{-18}
G25	1.0	1	5.97×10^{-18}	6.99×10^{-18}
G26	1.0	1	3.62×10^{-18}	4.44×10^{-18}
G26	1.0	1	2.91×10^{-18}	3.40×10^{-18}
G27	1.0	1	5.11×10^{-18}	6.21×10^{-18}
G27	1.0	1	6.17×10^{-18}	7.19×10^{-18}

BFS/OPC-grout
100 % relative humidity condition - helium migration

Sample	Pressure / 100 kPa	Run type	Analyt. k / m^2	Best k / m^2
G40	1.0	1	1.54×10^{-17}	1.77×10^{-17}
G40	1.0	1	1.59×10^{-17}	1.83×10^{-17}
G41	1.0	1	3.67×10^{-19}	4.22×10^{-19}
G41	1.0	1	3.47×10^{-19}	3.99×10^{-19}
G42	1.0	1	8.99×10^{-19}	1.03×10^{-18}
G42	1.0	1	8.38×10^{-19}	9.64×10^{-19}

BFS/OPC-grout
100 % relative humidity condition - argon migration

Sample	Pressure / 100 kPa	Run type	Analyt. k / m^2	Best k / m^2
G30	1.0	1	5.27×10^{-17}	6.06×10^{-17}
G30	1.0	1	3.61×10^{-17}	4.15×10^{-17}
G31	1.0	1	1.21×10^{-17}	1.39×10^{-17}
G31	1.0	1	1.43×10^{-17}	1.64×10^{-17}
G32	1.0	1	1.98×10^{-17}	2.27×10^{-17}
G32	1.0	1	3.99×10^{-17}	4.58×10^{-17}
G33	0.9	1	7.74×10^{-17}	8.89×10^{-17}
G33	1.0	1	6.21×10^{-17}	7.14×10^{-17}
G40	1.0	1	5.09×10^{-18}	5.85×10^{-18}
G40	1.0	1	1.42×10^{-17}	1.63×10^{-17}
G41	1.0	1	1.53×10^{-19}	1.76×10^{-19}
G41	1.0	1	1.87×10^{-19}	2.15×10^{-19}
G42	1.0	1	6.29×10^{-20}	7.23×10^{-20}
G42	1.0	1	6.43×10^{-19}	7.39×10^{-19}
G43	1.0	1	7.96×10^{-22}	9.15×10^{-22}
HG4	16.5	1	5.43×10^{-18}	5.43×10^{-18}
HG4	16.2	1	4.69×10^{-18}	4.69×10^{-18}
HG4	8.6	3	5.04×10^{-18}	5.04×10^{-18}
HG4	23.8	2	5.40×10^{-18}	5.40×10^{-18}

Preliminary design backfill grout
Dry condition - helium migration

Sample	Pressure / 100 kPa	Run type	Analyt. k / m^2	Best k / m^2
G13	1.5	2	1.62×10^{-14}	2.28×10^{-14}
G13	1.5	2	1.65×10^{-14}	2.32×10^{-14}
G13	1.5	2	1.59×10^{-14}	2.23×10^{-14}
G14	1.5	2	1.58×10^{-14}	2.21×10^{-14}
G14	1.5	2	1.60×10^{-14}	2.24×10^{-14}
HG12	24.4	2	2.08×10^{-15}	4.49×10^{-15}
HG12	10.1	3	2.61×10^{-15}	6.60×10^{-15}
HG13	24.4	2	2.13×10^{-15}	4.59×10^{-15}
HG13	10.2	3	2.52×10^{-15}	6.37×10^{-15}
HG13	10.2	3	1.12×10^{-15}	6.37×10^{-15}

Preliminary design backfill grout
Dry condition - argon migration

Sample	Pressure / 100 kPa	Run type	Analyt. k / m^2	Best k / m^2
G6	1.5	2	1.34×10^{-14}	1.89×10^{-14}
G6	1.5	2	1.34×10^{-14}	1.90×10^{-14}
G6	1.5	2	1.32×10^{-14}	1.87×10^{-14}
G6	1.5	2	1.33×10^{-14}	1.88×10^{-14}
G13	1.5	2	1.13×10^{-14}	1.59×10^{-14}
G13	1.5	2	1.08×10^{-14}	1.53×10^{-14}
G16	1.5	2	1.07×10^{-14}	1.50×10^{-14}
G16	1.5	2	1.07×10^{-14}	1.49×10^{-14}
G16	1.5	2	1.03×10^{-14}	1.45×10^{-14}
G16	1.5	2	1.05×10^{-14}	1.47×10^{-14}
G44	1.5	2	2.10×10^{-14}	3.71×10^{-14}
G44	1.5	2	2.05×10^{-14}	3.57×10^{-14}
G45	1.5	2	1.41×10^{-14}	2.48×10^{-14}
G45	1.5	2	1.47×10^{-14}	2.58×10^{-14}
HG12	23.7	2	1.96×10^{-15}	4.16×10^{-15}
HG12	23.7	2	8.29×10^{-16}	4.01×10^{-15}
HG12	9.0	3	1.76×10^{-15}	4.50×10^{-15}
HG12	9.0	3	7.47×10^{-16}	4.52×10^{-15}
HG13	23.7	2	1.92×10^{-15}	4.08×10^{-15}
HG13	23.7	2	8.07×10^{-16}	3.90×10^{-15}
HG13	9.0	3	1.84×10^{-15}	4.71×10^{-15}
HG13	9.0	3	7.64×10^{-16}	4.64×10^{-15}
G94	1.7	2	2.00×10^{-14}	3.27×10^{-14}

Preliminary design backfill grout
Dry condition - carbon dioxide migration

Sample	Pressure / 100 kPa	Run type	Analyt. k / m^2	Best k / m^2
HG12	7.7	2	1.59×10^{-15}	3.38×10^{-15}
HG12	3.2	3	1.29×10^{-15}	3.22×10^{-15}

Preliminary design backfill grout
100 % relative humidity condition - helium migration

Sample	Pressure / 100 kPa	Run type	Analyt. k / m^2	Best k / m^2
G8	1.0	1	1.39×10^{-16}	1.72×10^{-16}
G8	1.0	1	1.38×10^{-16}	1.70×10^{-16}

Sample	Pressure / 100 kPa	Run type	Analyt. k / m^2	Best k / m^2
G8	1.0	1	1.39×10^{-16}	1.71×10^{-16}
G8	0.5	1	2.56×10^{-16}	3.16×10^{-16}
G8	1.5	1	2.07×10^{-16}	2.54×10^{-16}
HG14	16.9	1	3.31×10^{-17}	6.67×10^{-17}
HG14	16.9	1	3.29×10^{-17}	6.71×10^{-17}
HG14	9.0	3	2.33×10^{-17}	9.71×10^{-17}
HG14	24.9	2	2.61×10^{-17}	8.69×10^{-17}
HG15	16.2	1	4.46×10^{-17}	9.01×10^{-17}
HG15	8.6	3	3.30×10^{-17}	1.38×10^{-16}
HG15	24.2	2	3.29×10^{-17}	1.11×10^{-16}
G98	1.0	1	5.02×10^{-16}	6.26×10^{-16}
G98	0.5	3	9.91×10^{-16}	1.47×10^{-15}
G98	1.5	2	4.66×10^{-16}	6.21×10^{-16}

Preliminary design backfill grout
100 % relative humidity condition - argon migration

Sample	Pressure / 100 kPa	Run type	Analyt. k / m^2	Best k / m^2
G8	1.0	1	7.68×10^{-17}	9.36×10^{-17}
G8	1.0	1	8.78×10^{-17}	1.08×10^{-16}
G8	1.0	1	9.68×10^{-17}	1.18×10^{-16}
G8	1.0	1	1.01×10^{-16}	1.23×10^{-16}
G10	1.0	1	8.75×10^{-17}	1.07×10^{-16}
G10	1.5	1	6.77×10^{-17}	8.36×10^{-17}
G9	1.5	1	4.81×10^{-17}	5.93×10^{-17}
G9	1.0	1	5.49×10^{-17}	6.77×10^{-17}
G11	1.3	1	4.65×10^{-17}	5.75×10^{-17}
G11	1.2	1	6.96×10^{-17}	8.55×10^{-17}
HG15	16.4	1	3.11×10^{-17}	6.35×10^{-17}
HG15	24.9	2	2.68×10^{-17}	8.82×10^{-17}
HG15	9.0	3	3.18×10^{-17}	1.32×10^{-16}
HG14	15.5	1	2.00×10^{-17}	4.08×10^{-17}
HG14	16.0	1	1.78×10^{-17}	3.64×10^{-17}
HG14	8.5	3	7.31×10^{-18}	3.05×10^{-17}
HG14	24.2	2	1.45×10^{-17}	4.79×10^{-17}
G98	1.0	1	2.73×10^{-16}	3.41×10^{-16}
G98	0.5	3	5.64×10^{-16}	8.29×10^{-16}
G98	1.6	2	2.86×10^{-16}	3.81×10^{-16}
G14	0.5	3	6.85×10^{-16}	1.01×10^{-15}

Reference design backfill grout
Dry condition - helium migration

Sample	Pressure / 100 kPa	Run type	Analyt. k / m^2	Best k / m^2
G109	0.6	3	8.83×10^{-15}	1.45×10^{-14}
G109	1.5	2	2.66×10^{-15}	4.02×10^{-15}
G110	0.6	3	1.60×10^{-15}	2.33×10^{-15}
G110	1.6	2	2.34×10^{-15}	3.25×10^{-15}
G111	0.6	3	1.54×10^{-14}	2.27×10^{-14}
G111	1.5	2	2.46×10^{-15}	3.40×10^{-15}
G108	0.6	3	8.24×10^{-15}	1.36×10^{-14}
G108	1.5	2	2.68×10^{-15}	4.05×10^{-15}
G108	8.1	3	2.73×10^{-15}	3.66×10^{-15}
G109	8.1	3	2.45×10^{-15}	3.28×10^{-15}

Reference design backfill grout
Dry condition - argon migration

Sample	Pressure / 100 kPa	Run type	Analyt. k / m^2	Best k / m^2
G111	1.5	2	1.66×10^{-15}	2.24×10^{-15}
G111	0.6	3	3.94×10^{-15}	6.47×10^{-15}
G110	1.5	2	1.68×10^{-15}	2.27×10^{-15}
G110	0.5	3	3.98×10^{-15}	6.49×10^{-15}
G109	1.5	2	1.56×10^{-15}	2.34×10^{-15}
G109	0.6	3	3.73×10^{-15}	6.15×10^{-15}
G108	0.5	3	3.51×10^{-15}	6.63×10^{-14}
G108	1.5	2	1.53×10^{-15}	2.29×10^{-15}
G109	7.7	3	1.48×10^{-15}	1.99×10^{-15}
G109	23.6	2	2.81×10^{-15}	3.43×10^{-15}
G108	7.7	3	1.63×10^{-15}	2.18×10^{-15}

Reference design backfill grout
100 % relative humidity condition - helium migration

Sample	Pressure / 100 kPa	Run type	Analyt. k / m^2	Best k / m^2
G100	1.0	1	6.27×10^{-17}	7.46×10^{-17}
G100	1.0	1	6.08×10^{-17}	7.28×10^{-17}
G101	1.0	1	7.82×10^{-17}	9.28×10^{-17}
G101	1.0	1	9.70×10^{-17}	1.15×10^{-16}
G103	11.1	1	5.11×10^{-17}	5.54×10^{-17}
G103	16.2	2	7.17×10^{-17}	8.26×10^{-17}
G103	6.1	3	5.76×10^{-17}	6.87×10^{-17}

Reference design backfill grout
100 % relative humidity condition - argon migration

Sample	Pressure / 100 kPa	Run type	Analyt. k / m^2	Best k / m^2
G100	1.0	1	3.47×10^{-17}	4.18×10^{-17}
G100	1.0	1	3.55×10^{-17}	4.27×10^{-17}
G100	1.0	1	3.77×10^{-17}	4.50×10^{-17}
G101	1.1	1	4.21×10^{-17}	5.05×10^{-17}
G101	1.0	1	4.95×10^{-17}	5.90×10^{-17}
G101	1.0	1	5.23×10^{-17}	6.22×10^{-17}
G103	10.8	1	4.18×10^{-17}	4.55×10^{-17}
G103	16.4	2	3.59×10^{-17}	4.13×10^{-17}
G103	6.1	3	4.29×10^{-17}	5.13×10^{-17}

Sample		Run type	Analyt. k / m^2	Best k / m^2
G102	23.7	2	5.83×10^{-17}	6.24×10^{-17}
G102	8.3	3	6.12×10^{-17}	6.95×10^{-17}

Reference design backfill grout
100 % relative humidity condition - carbon dioxide migration

Sample	Pressure / 100 kPa	Run type	Analyt. k / m^2	Best k / m^2
G103	11.0	1	6.08×10^{-17}	6.48×10^{-17}
G103	16.0	2	4.65×10^{-17}	5.37×10^{-17}
G103	6.0	3	1.22×10^{-16}	1.45×10^{-16}

PFA/OPC-concrete containing reinforcement bars
Dry condition - helium migration

Sample	Pressure / 100 kPa	Run type	Analyt. k / m^2	Best k / m^2
G82	1.0	1	1.76×10^{-16}	1.87×10^{-16}
G82	1.5	2	1.49×10^{-16}	1.67×10^{-16}
G82	0.5	3	3.14×10^{-16}	3.78×10^{-16}
G82	24.1	2	1.92×10^{-16}	2.06×10^{-16}
G82	8.7	3	1.81×10^{-16}	2.06×10^{-16}
G83	8.8	3	1.89×10^{-16}	2.14×10^{-16}
G83	24.5	2	2.91×10^{-16}	3.13×10^{-16}
G83	1.5	2	3.54×10^{-16}	3.95×10^{-16}
G83	0.5	3	7.84×10^{-16}	9.45×10^{-16}

PFA/OPC-concrete containing reinforcement bars
Dry condition - argon migration

Sample	Pressure / 100 kPa	Run type	Analyt. k / m^2	Best k / m^2
G82	1.1	1	1.18×10^{-16}	1.26×10^{-16}
G82	1.5	2	1.06×10^{-16}	1.18×10^{-16}
G82	0.6	3	1.43×10^{-16}	1.71×10^{-16}
G82	16.2	1	1.04×10^{-16}	1.04×10^{-16}
G82	23.9	2	1.25×10^{-16}	1.33×10^{-16}
G82	8.6	3	1.09×10^{-16}	1.23×10^{-16}
G83	8.5	3	1.77×10^{-16}	2.01×10^{-16}
G83	23.5	2	1.58×10^{-16}	1.70×10^{-16}
G83	1.0	1	2.74×10^{-16}	2.92×10^{-16}
G83	0.5	3	4.19×10^{-16}	5.01×10^{-16}
G83	1.5	2	2.64×10^{-16}	2.95×10^{-16}

PFA/OPC-concrete containing reinforcement bars
100 % relative humidity condition - helium migration

Sample	Pressure / 100 kPa	Run type	Analyt. k / m^2	Best k / m^2
G46	1.0	1	1.51×10^{-20}	1.73×10^{-20}
G47	1.0	1	4.25×10^{-21}	4.88×10^{-21}
G48	1.0	1	3.35×10^{-20}	3.85×10^{-20}
G87	15.2	1	2.04×10^{-19}	2.04×10^{-19}

PFA/OPC-concrete containing reinforcement bars
100 % relative humidity condition - argon migration

Sample	Pressure / 100 kPa	Run type	Analyt. k / m^2	Best k / m^2
G46	1.0	1	2.58×10^{-20}	2.97×10^{-20}
G47	1.0	1	5.02×10^{-21}	5.77×10^{-21}
G48	1.0	1	2.41×10^{-20}	2.77×10^{-20}
G86	8.4	3	2.45×10^{-16}	2.45×10^{-16}
G87	13.2	1	2.15×10^{-19}	2.15×10^{-19}
G87	20.8	2	1.40×10^{-19}	1.40×10^{-19}
G87	16.6	1	1.10×10^{-19}	1.10×10^{-19}

Preliminary design backfill grout containing construction joint
Dry condition - argon migration

Sample	Pressure / 100 kPa	Run type	Analyt. k / m^2	Best k / m^2
G88	1.7	2	2.19×10^{-14}	3.59×10^{-14}

Preliminary design backfill grout containing construction joint
100 % relative humidity condition - helium migration

Sample	Pressure / 100 kPa	Run type	Analyt. k / m^2	Best k / m^2
G92	1.5	2	3.67×10^{-15}	5.09×10^{-15}
G92	0.5	3	4.79×10^{-15}	7.53×10^{-15}
G93	1.5	2	2.18×10^{-15}	2.90×10^{-15}
G93	0.5	3	7.99×10^{-15}	1.16×10^{-14}

Preliminary design backfill grout containing construction joint
100 % relative humidity condition - argon migration

Sample	Pressure / 100 kPa	Run type	Analyt. k / m^2	Best k / m^2
G92	1.1	1	1.96×10^{-15}	2.32×10^{-15}
G92	1.5	2	2.48×10^{-15}	3.43×10^{-15}
G92	0.6	3	3.25×10^{-15}	4.97×10^{-15}
G92	1.6	2	2.00×10^{-15}	2.77×10^{-15}
G92	0.6	3	1.89×10^{-15}	2.92×10^{-15}
G93	1.1	1	1.62×10^{-15}	2.02×10^{-15}
G93	0.5	3	3.05×10^{-15}	4.47×10^{-15}
G93	1.5	2	1.39×10^{-15}	1.85×10^{-15}
G93	1.5	2	2.01×10^{-15}	2.65×10^{-15}
G93	0.6	3	3.66×10^{-15}	5.14×10^{-15}
G92	8.1	3	1.80×10^{-15}	2.31×10^{-15}
G92	26.6	2	1.33×10^{-15}	1.56×10^{-15}

Appendix 5 - Solution-diffusion Equivalent Permeability Coefficient

A water-saturated porous material can be considered to be effectively impermeable if an applied gas pressure difference does not exceed the capillary pressure for the connected porosity and the gas pressure is unable to displace water from the pore space. In such a situation, the only available mechanism for the migration of gas across the material is by dissolution and subsequent diffusion in the aqueous phase. The rate of gas migration by this mechanism can be used to calculate an equivalent effective permeability coefficient as follows.

Since, according to Henry's law, the concentration of a dissolved ideal gas is directly proportional to the gas pressure in equilibrium with the solution, the change in concentration of dissolved gas across a porous membrane is proportional to the change in pressure. Hence, the concentration gradient of the dissolved gas, dc/dx, can be assumed to be related to the pressure gradient, dp/dx, by the following;

$$\frac{dc}{dx} = \frac{c_0}{p_0}\frac{dp}{dx} \qquad ....(21)$$

where c_0 is the concentration of dissolved gas measured at atmospheric pressure, p_0. In a steady state, the molecular flow of the dissolved gas as a function of the concentration gradient in the aqueous phase and the volumetric flow rate as a function of the pressure gradient are given by Fick's first law and the Darcy equation respectively (Equations 1 and 4 in the main text). If the gas is assumed to be ideal, the Darcy equation can be combined with the ideal gas law to give an expression for the molecular flow rate as a function of the pressure gradient (Equation 6 in the main text). Substituting Equation 21 into Equation 4 and combining with Equation 6 gives an expression for the equivalent permeability coefficient, k_{sd};

$$k_{sd} = D\frac{c_0}{p_0}\frac{\mu RT}{P_{av}} \qquad ....(22)$$

where D is the diffusion coefficient for the dissolved gas and p_{av} the linear average of the pressures either side of the specimen.

The diffusion coefficient for dissolved oxygen has been measured by Page and Lambert [30]. A typical value is 2×10^{-12} m^{2}s^{-1}. The solubility of oxygen in cold water at atmospheric pressure is in the range 3.16 to 4.89 cm^3 per 100 cm^3 of water, corresponding to solution concentrations of 1.3 to 2.0 mol m^{-3}. At an average pressure of 100 kPa, the equivalent permeability coefficient for oxygen derived from these values has a maximum value of 2×10^{-23} m^2.

	PFA/OPC-concrete	BFS/OPC-grout	Preliminary grout	Reference grout	Interface specimens
Dry	H_2, He, CH_4, Ar, CO_2	He, Ar	He, Ar, CO_2	He, Ar	He, Ar
75 % RH	H_2, He, CH_4, Ar, CO_2	Ar			
100 % RH	He, Ar	He, Ar	He, Ar	He, Ar	He, Ar

	PFA/OPC-concrete	BFS/OPC-grout	Preliminary grout	Reference grout	Interface specimens
Dry	He, Ar, CO_2	He, Ar	He, Ar, CO_2	He, Ar	He, Ar
75 % RH	He, Ar, CO_2				
100 % RH	He, Ar	Ar	He, Ar	He, Ar, CO_2	Ar

Table 1   Summary of the permeability measurements performed in this work. The upper table refers to low pressure experiments (average pressure about 100 kPa) and the lower table to experiments performed with higher average pressures. In addition, measurements were carried out using hydrogen and argon in dry SRPC-concrete.

Material	Water-cement ratio	Aggregate-cement ratio	Total cement content / kg m^{-3}
SRPC-concrete	0.45	4.0	413
PFA/OPC-concrete	0.475	4.55	400
BFS/OPC-grout	0.4	0	1350

Table 2   Water-cement and aggregate-cement ratios and total cementcontent used
in the manufacture of the experimental materials. Data for backfill
grouts are unavailable. All ratios are by weight.

Material	Strength / MPa	Density / kg m^{-3}	Percentage Porosity		Average pore radius / μm
			Wt. loss	MIP	
SRPC-concrete	64.0	2478	13	-	-
PFA/OPC-concrete	61.0	2430	12	11	0.011
BFS/OPC-grout	32.0	1890	40	29	0.011
Preliminary grout	0.9	1460	66	56	0.70
Reference grout	6.0	1755	54	44	0.45

Table 3   Physical properties of the experimental materials. Average pore radius
values obtained using mercury intrusion porosimetry (MIP). MIP
measurements were not performed on the SRPC-concrete.

Material	Dry		75 % RH		100 % RH	
	Wt.	GAV	Wt.	GAV	Wt.	GAV
PFA/OPC-concrete	14.3	2.9	1.2	-2.3	0	6.9
BFS/OPC-grout	44.4	23.1	2.0	3.8	0	3.7
Preliminary grout	66.3	67.2	56.0	-	35.9	42.6
Reference grout	55.1	54.9	25.1	33.4	11.4	12.7

Table 4 Fractional porosities obtained from the weight loss for each material during conditioning in the given relative humidity atmosphere (Wt.) and from the measurement of gas accessible volumes (GAV). Negative value is due to inaccuracy in the measurement.

Average Pressure / 100kPa	$k / 10^{-17} \, m^2$	$D / 10^{-8} \, m^2 s^{-1}$
1.00	1.66	3.32
1.25	1.40	3.26
1.55	1.18	3.74
1.75	1.08	2.50

Table 5 Calculated values of the hydrogen-argon inter-diffusion coefficient for the dry SRPC-concrete at the average pressures shown. The appropriate values of the argon permeability coefficient, derived from Figure 4, used in the calculation are also given.

Gas	Mean free path at 100 kPa / μm	k_∞ / 10^{-17} m^2	b / 100 kPa	
			Low pressure	High pressure
Hydrogen	0.194	4.9±1.1	1.9±1.1	-
Helium	0.305	5.2±0.9	1.9±0.8	0.9±1.0
Methane	0.086	4.6±1.6	0.3±0.3	-
Argon	0.110	2.4±0.3	1.6±0.3	2.6±3.7
Carbon Dioxide	0.070	1.9±0.2	0.5±0.2	5.6±3.4

Table 6 Results of the measurements of gas flow in dry PFA/OPC-concrete using varying average pressure. Data given are the means of the best-fit values for the Klinkenberg equation. Low pressure data obtained for average pressures in the range 0 to 200 kPa. High pressure data obtained for average pressures in the range 0 to 7.5 MPa. Quoted errors are standard errors.

Material	Dry		100 % Relative Humidity	
	Helium	Argon	Helium	Argon
SRPC-concrete	-	2×10^{-17}	-	-
PFA-concrete	6×10^{-17}	3×10^{-17}	7×10^{-20}	$\leq 10^{-21}$
BFS-grout	5×10^{-16}	4×10^{-16}	4×10^{-19}	$\leq 10^{-21}$
Prelim. grout	2×10^{-14}	10^{-14}	2×10^{-16}	4×10^{-17}
Reference grout	3×10^{-15}	2×10^{-15}	7×10^{-17}	4×10^{-17}

Table 7 Measured permeability coefficients for a constant average pressure of 100 kPa in the experimental materials. All data are expressed as k / m^2.

Material	Dry	100 % Relative Humidity
SRPC-concrete	$(3.8\pm0.1)\times10^{-18}$	-
PFA/OPC-concrete	$(3.7\pm0.6)\times10^{-17}$	-
BFS/OPC-grout	$(5.3\pm1.0)\times10^{-16}$	$(5.9\pm0.4)\times10^{-18}$
Preliminary grout	$(4.4\pm1.1)\times10^{-14}$	$(4.4\pm0.8)\times10^{-16}$
Reference grout	$(4.4\pm1.1)\times10^{-16}$	$(4.6\pm5.0)\times10^{-16}$

Table 8　Measured values of the infinite pressure permeability coefficient. Data for the dry conditioned specimens obtained for pressures in the range 0 to 100 kPa only. Quoted errors are standard errors. All data are expressed as k / m^2.

Material	Low Pressure (100 kPa)		High Pressure (>100 kPa)	
	Helium	Argon	Helium	Argon
PFA/OPC-concrete	1.9±0.8	1.6±0.3	0.9±1.0	2.6±3.7
BFS/OPC-grout	0.5±0.3	-(0.3±0.1)	1.2±0.6	-(1.8±3.7)
Preliminary grout	-(0.4±0.2)	-(0.8±0.2)	2.3±0.3	1.1±0.2
Reference grout	20.6±9.5	6.0±1.9	2.2±0.7	-(3.7±1.9)

Table 9　Measured values of the Klinkenberg constant for materials in the dry condition obtained using varying average pressure experiments. Where quoted the errors are standard errors. All data expressed as b / 10^5 Pa.

			Rebar in Concrete	Joint in Backfill
k measured at 100 kPa	Dry	Helium	2×10^{-16}	-
		Argon	10^{-16}	4×10^{-14}
	100 % RH	Helium	5×10^{-21}	3×10^{-15}
		Argon	6×10^{-21}	2×10^{-15}
Infinite Pressure Permeability	Dry		$(2.0 \pm 0.7) \times 10^{-16}$	2.19×10^{-13}
	100 % RH		1.08×10^{-19}	$(4.4 \pm 1.9) \times 10^{-15}$

Table 10 Measured values of the permeability coefficients for the flawed specimens. The constant average pressure data were obtained from experiments at an average pressure of 100 kPa. Where quoted, errors are standard errors. All data are expressed as k / m².

Material	$\sigma / 10^{-3} \, \Omega^{-1} m^{-1}$	$D / 10^{-13} \, m^2 s^{-1}$
SRPC-concrete	21.1 ± 0.8	25 ± 1
PFA/OPC-concrete	6.7	8.0
BFS/OPC-grout	13.0	15.5
Preliminary grout	2100	2500
Reference grout	430	510

Table 11 Ionic conductivities for the experimental materials saturated by a 3 M sodium chloride solution. Calculated equivalent sodium-chloride ion inter-diffusion coefficients are also given. Where quoted, errors are standard errors.

Occupied Volume / m^3	Hydrogen	Helium	Methane	Argon	Carbon Dioxide
2.0	0.012	0.012	0.012	0.012	0.012
0.02	1.239 (0.1)	1.239 (0.1)	1.235 (-0.2)	1.237 (-0.1)	1.232 (-0.5)
2×10^{-4}	136.7 (10.4)	139.6 (12.8)	101.2 (-18.3)	113.9 (-8.0)	67.6 (-45.0)

Table 12 Pressure of 1 mole of gas when occupying quoted volume, calculated from the Van der Waals equation. Percentage deviation from the pressure predicted by the ideal gas approximation for the same volumes are given in brackets. There is no significant deviation for a volume of $2 \, m^3$. Pressures expressed as p / 100 kPa.
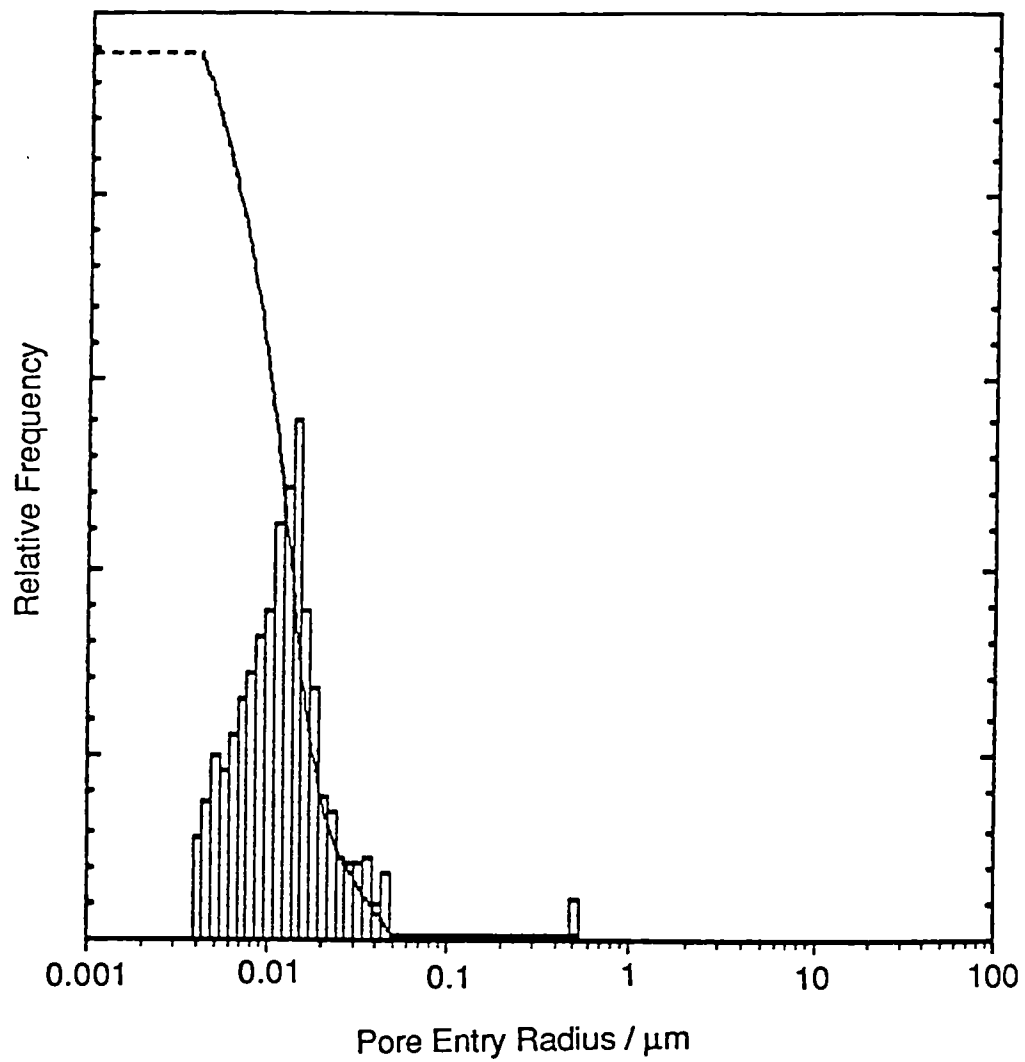
Figure 1 Pore entry radius distribution for the PFA/OPC-concrete as determined by mercury intrusion porosimetry.
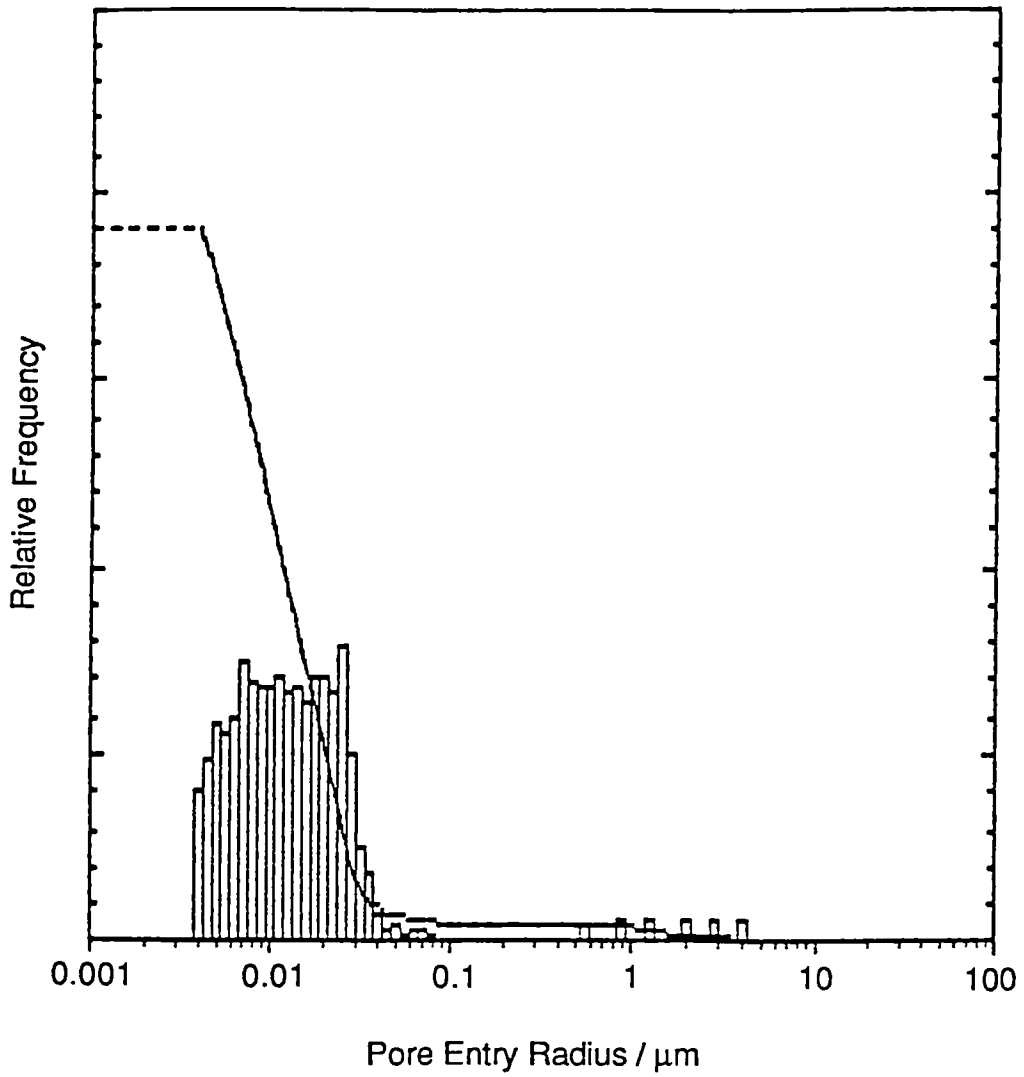
Figure 2 Pore entry radius distribution for the BFS/OPC-grout as determined by mercury intrusion porosimetry.
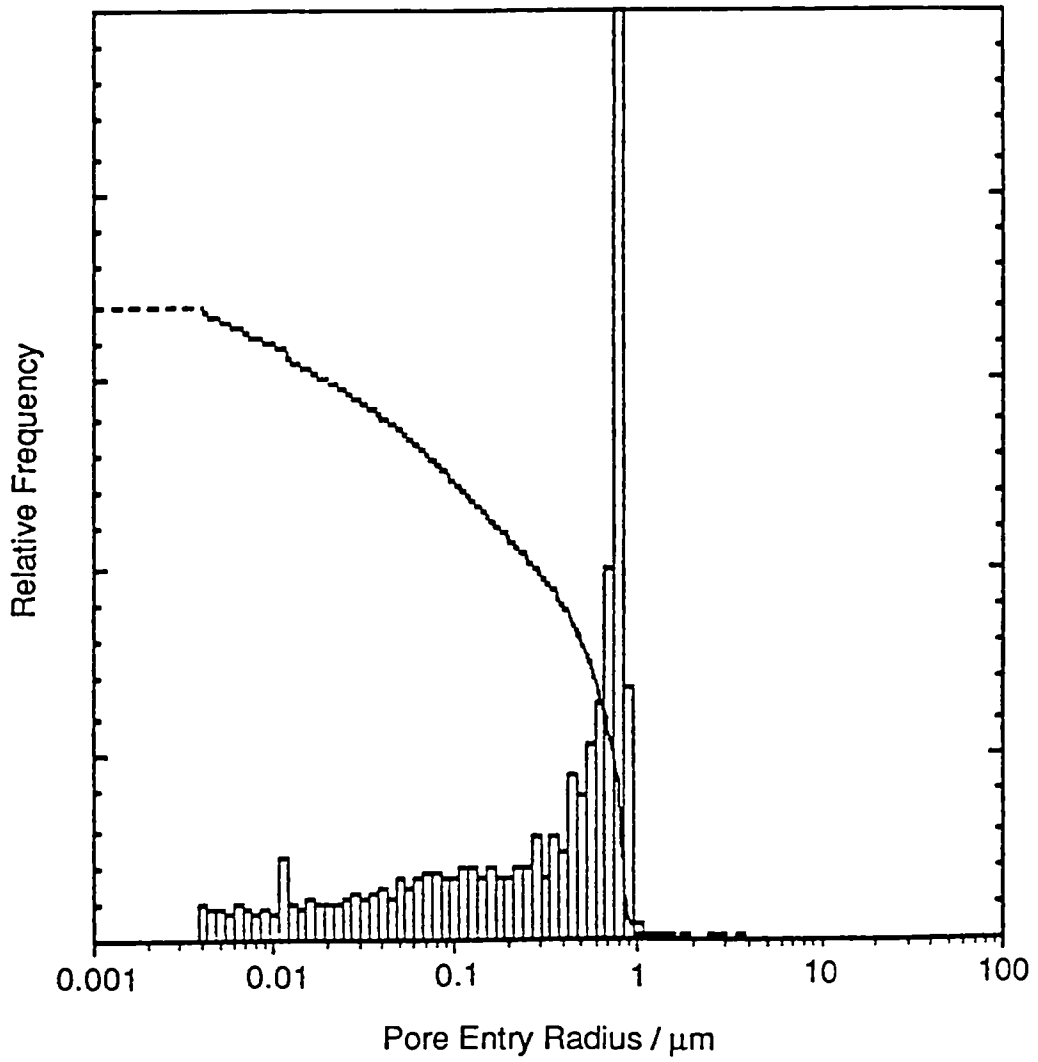
Figure 3   Pore entry radius distribution for the preliminary design backfill grout as determined by mercury intrusion porosimetry.
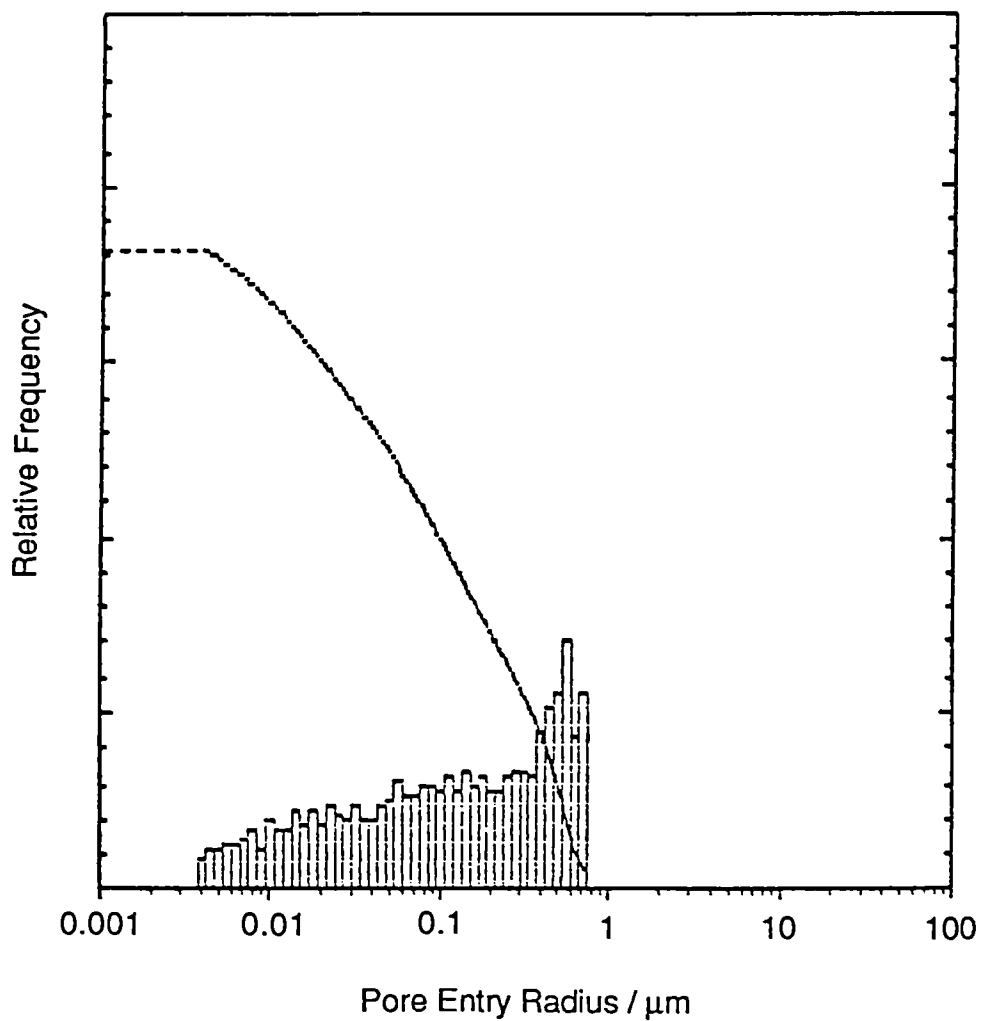
Figure 4   Pore entry radius distribution for the reference backfill grout as determined by mercury intrusion porosimetry.
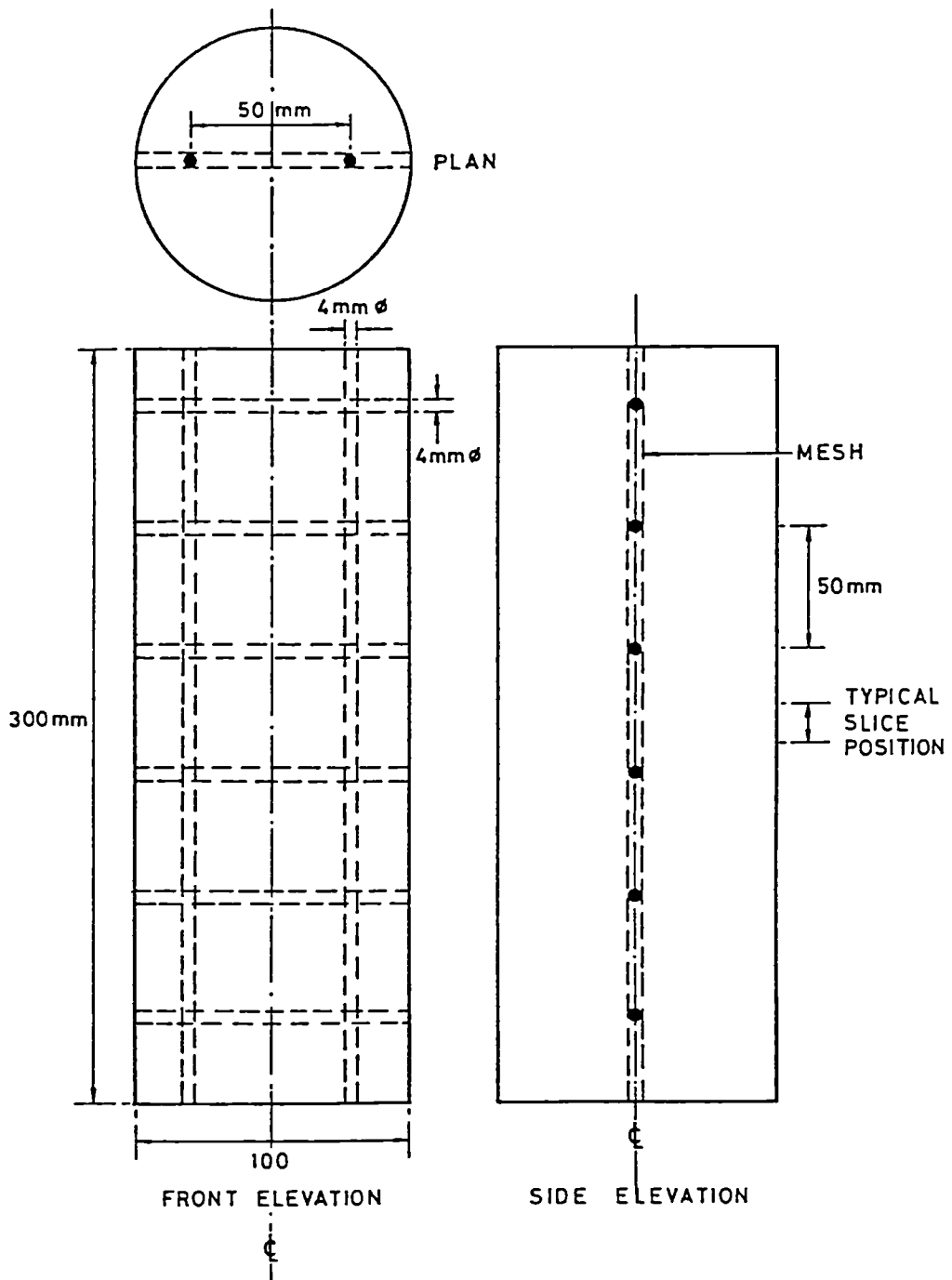
Figure 5   Illustration of the arrangement of reinforcement bars in
PFA/OPC-concrete cylinder used to produce specimens for the
assessment of the effect of interfaces on gas migration.
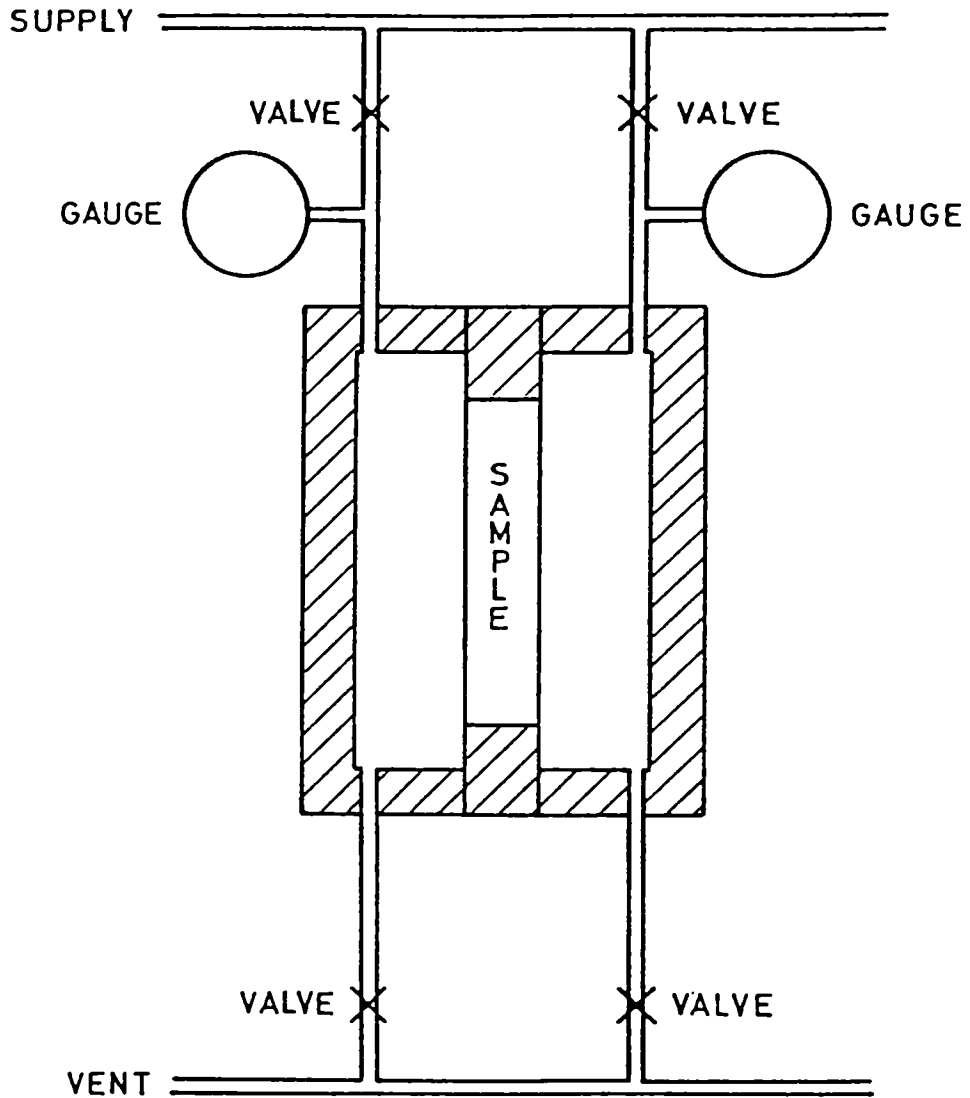
Figure 6   Schematic diagram of the experimental apparatus for the measurement of gas migration.
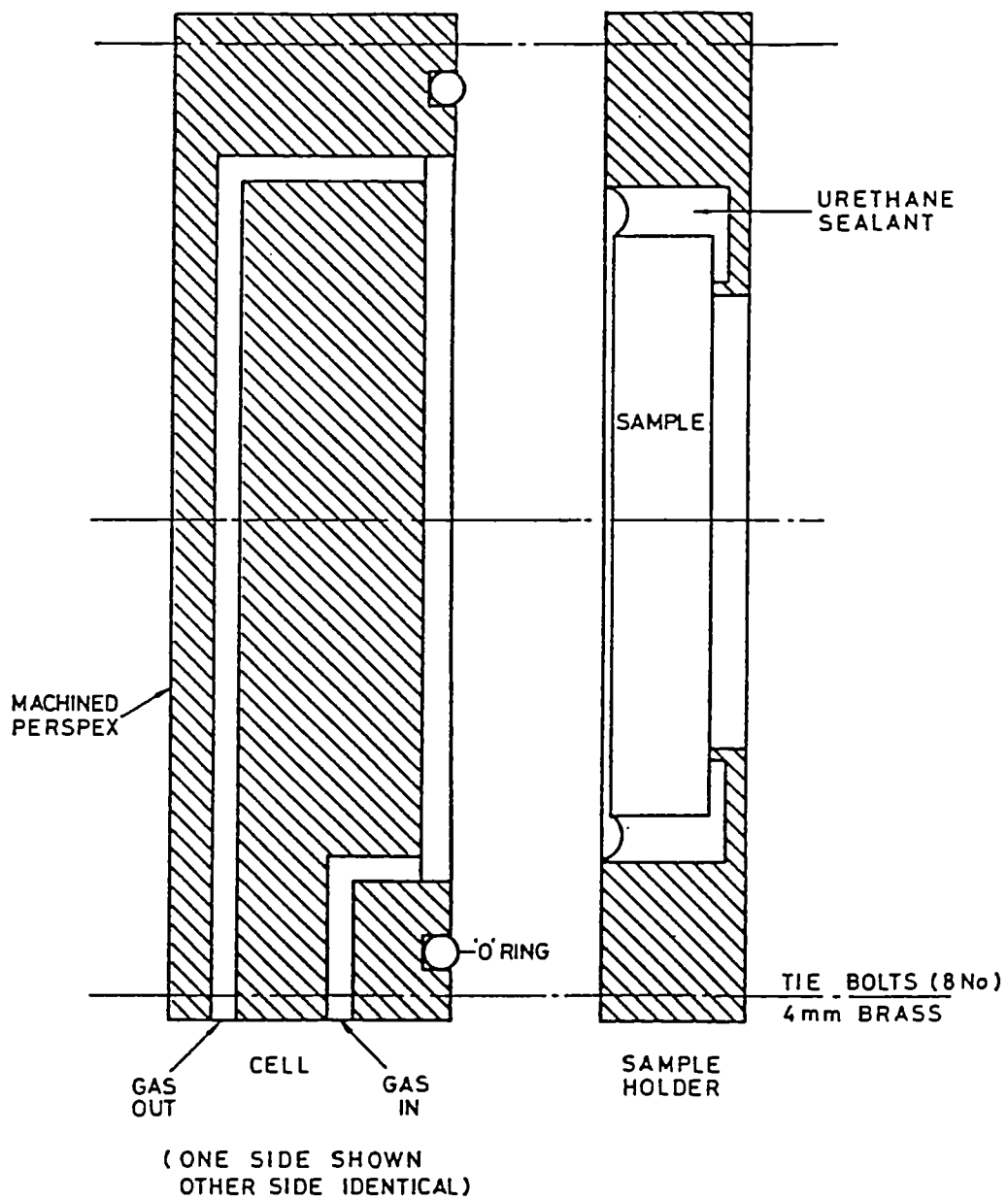
Figure 7   Low pressure permeability and diffusion measurement cell. One half of the cell is shown, the other half is an identical mirror image. Cell is constructed from perspex.
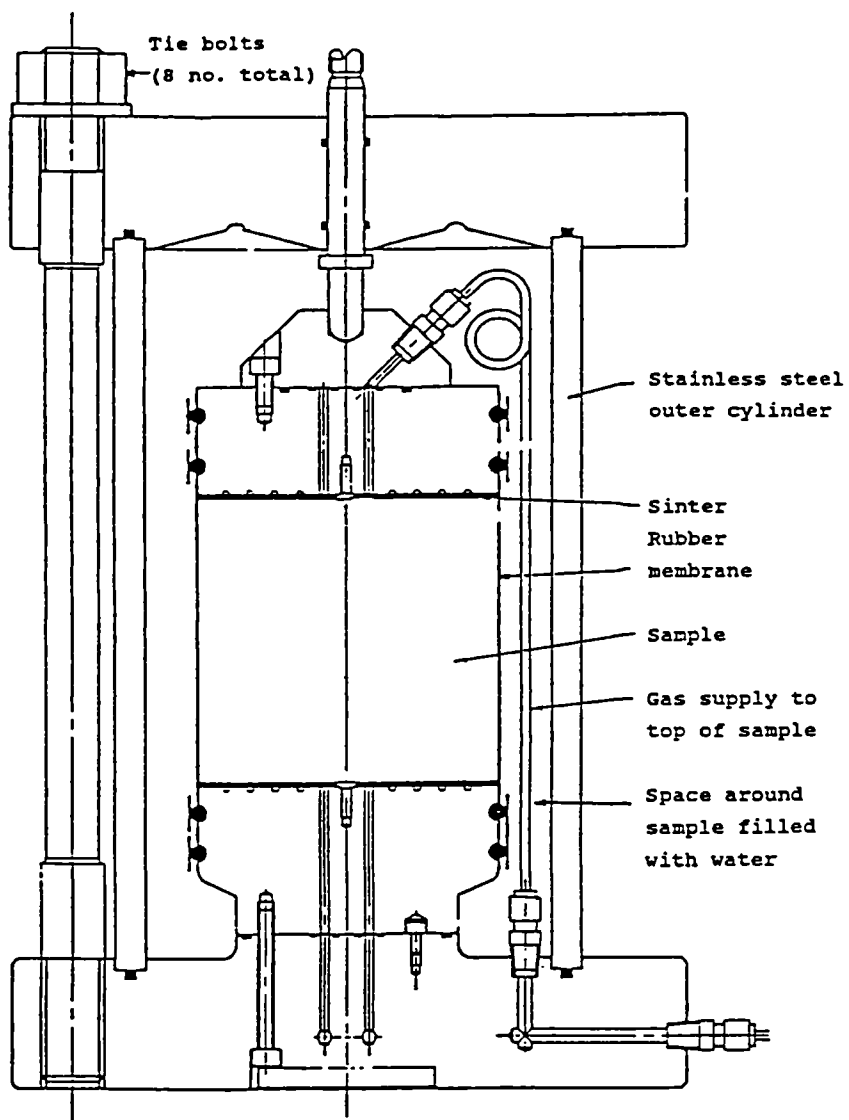
Figure 8   Triaxially-confined high pressure permeability measurement cell.
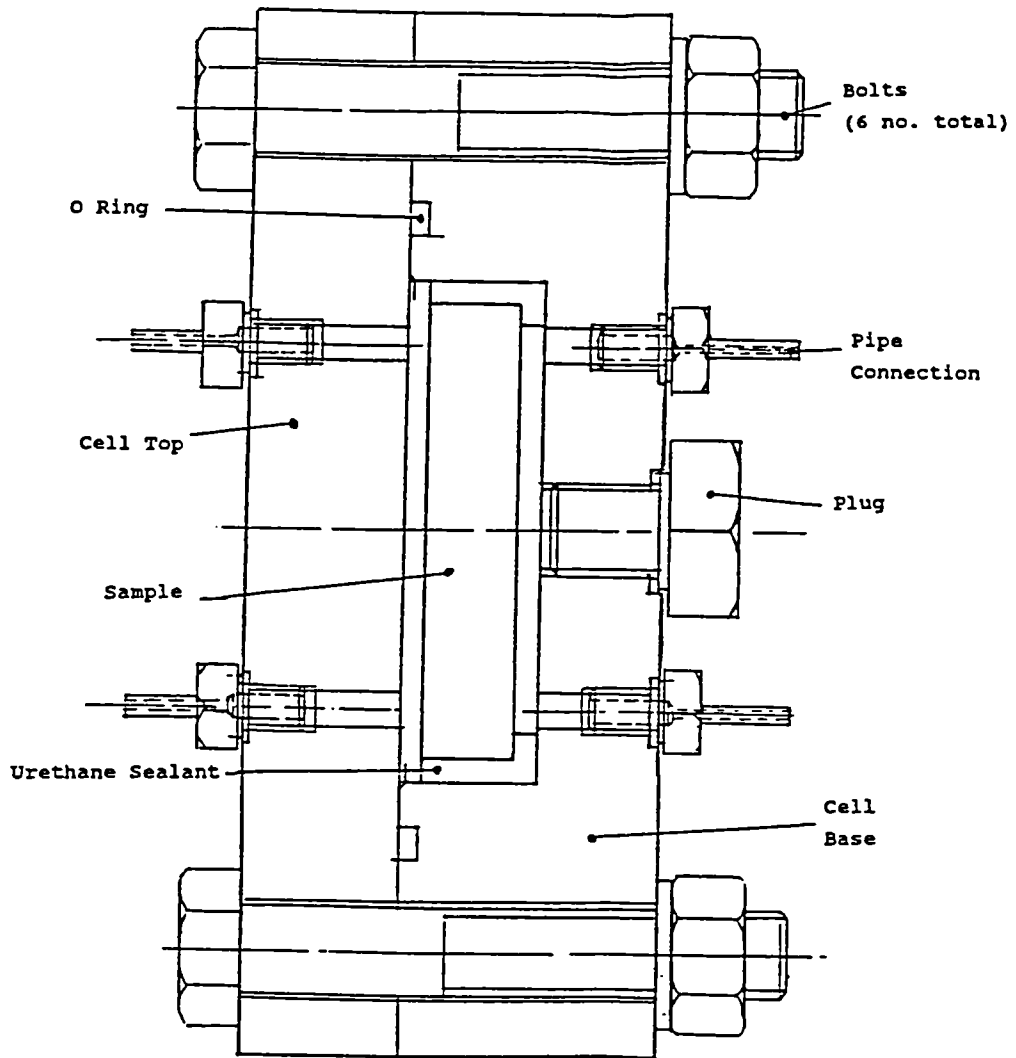
Figure 9 "Unconfined" high pressure permeability measurement cell. The urethane sealant is the same as that used in the low pressure cell.
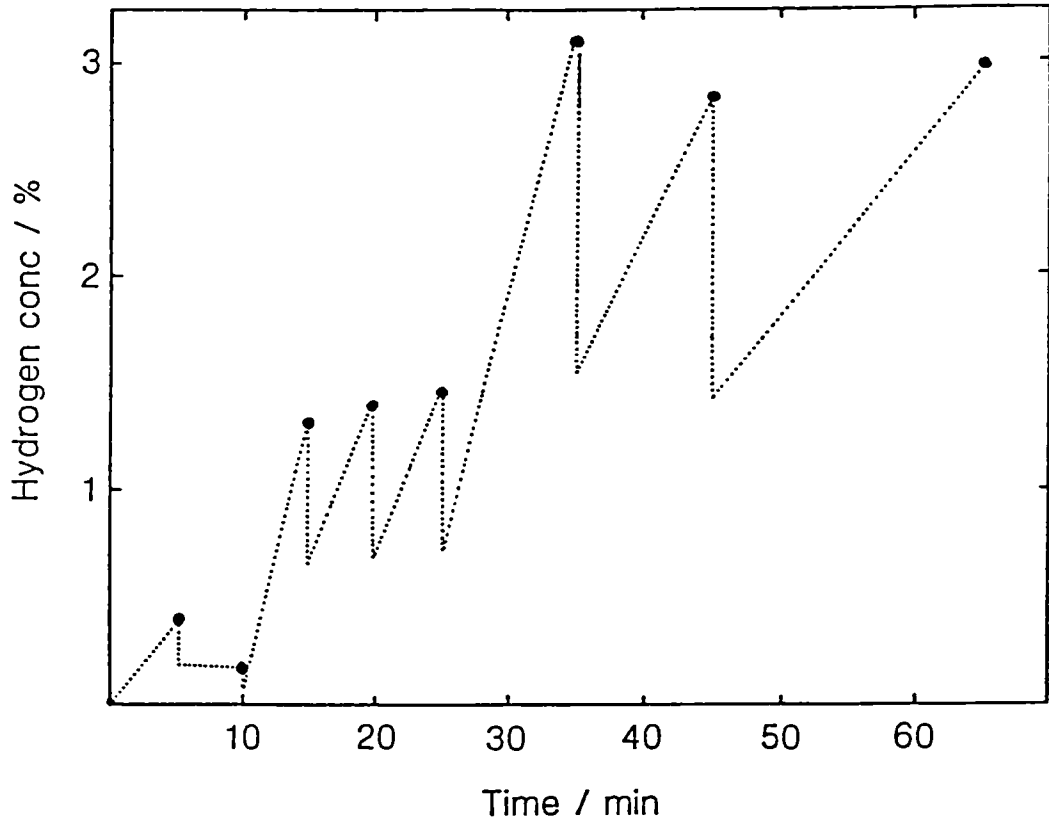
Figure 10   Variation in the concentration of hydrogen in the reservoir initially containing argon with time after diffusion through dry SRPC-concrete Reconstruction assumes half the volume is sampled for each measurement.
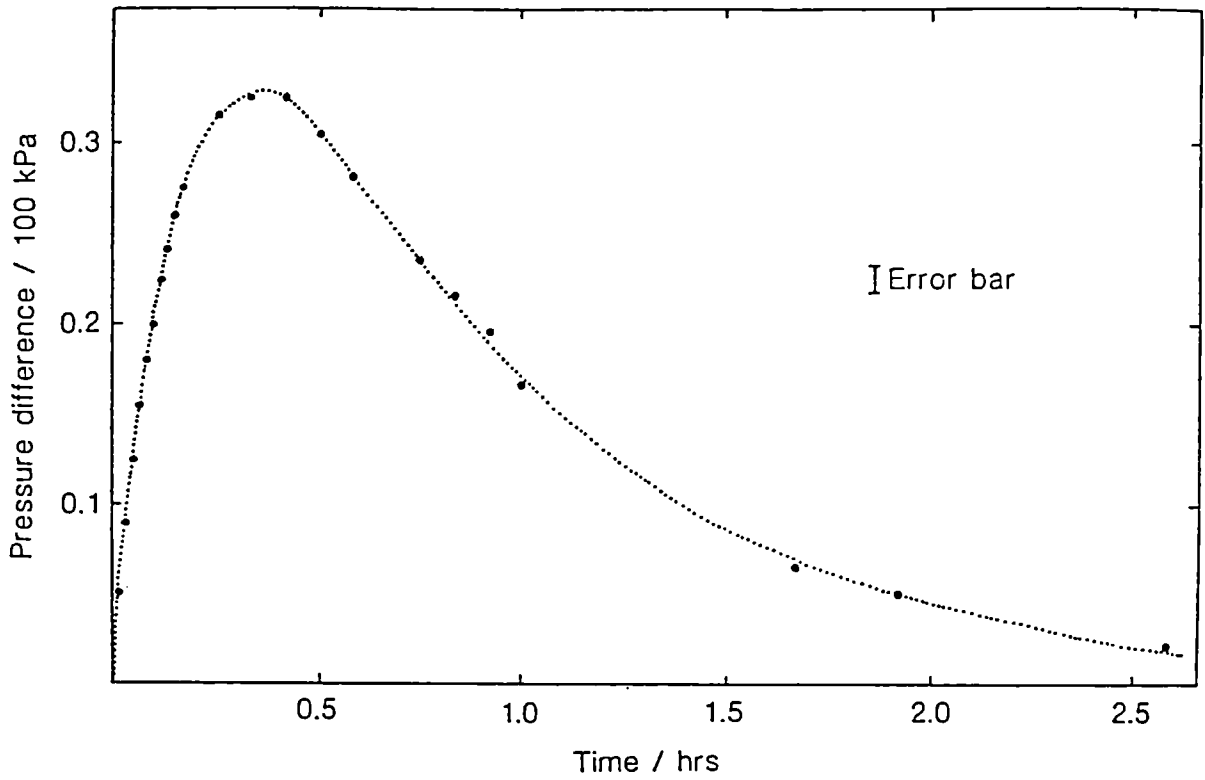
Figure 11 Variation in the pressure difference across SRPC-concrete caused by the Kirkendall effect during hydrogen-argon inter-diffusion. Initial pressure was a constant 125 kPa.
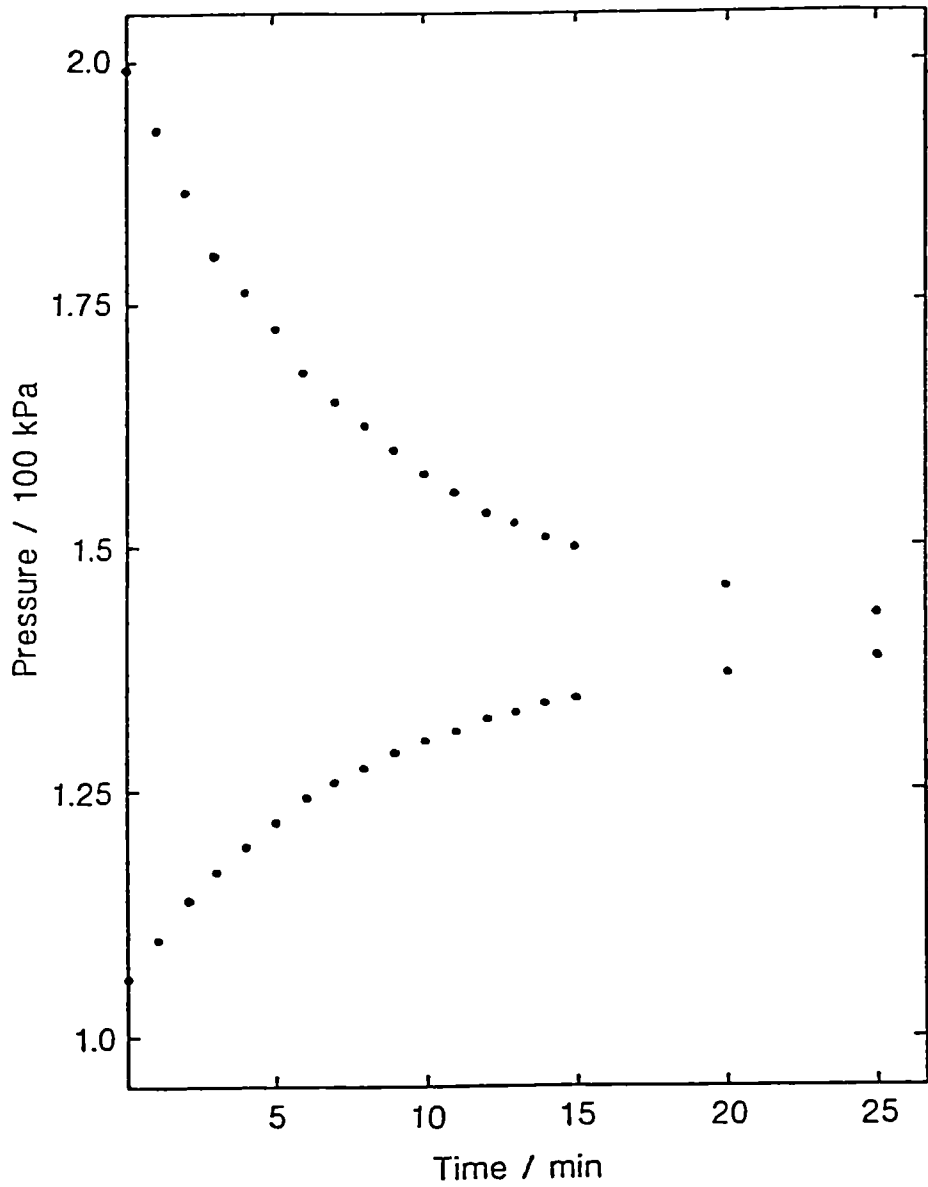
Figure 12   Typical variation in pressure observed during the measurement of the permeability of PFA/OPC-concrete. The migrating gas was argon.
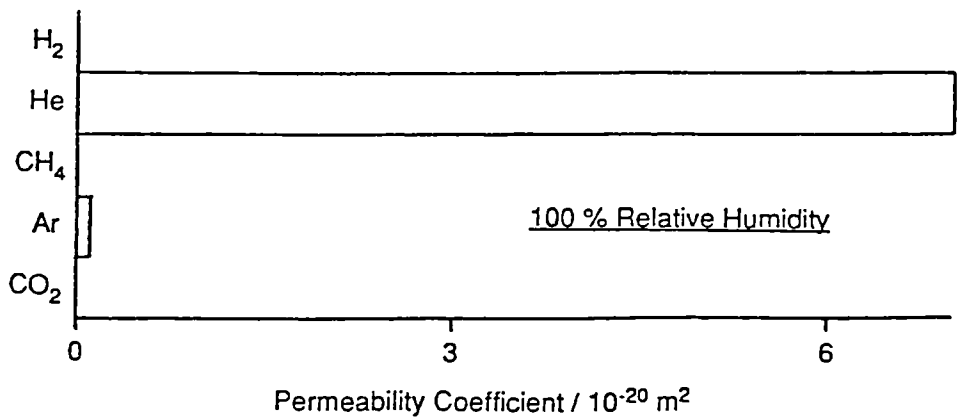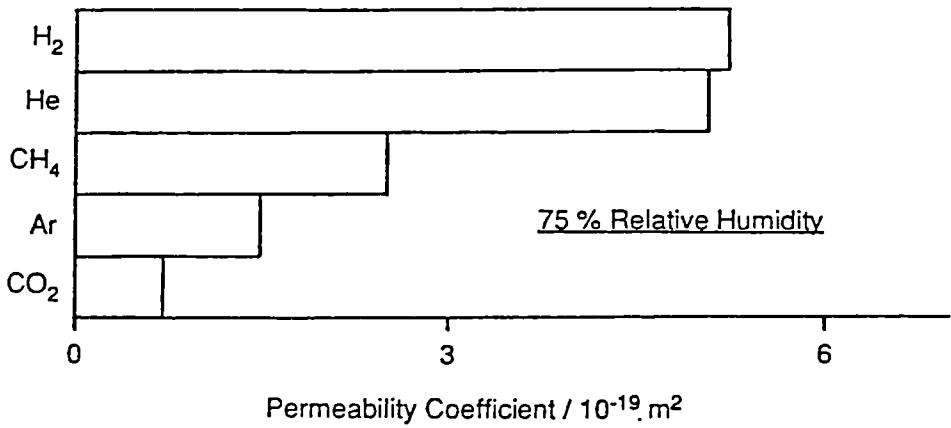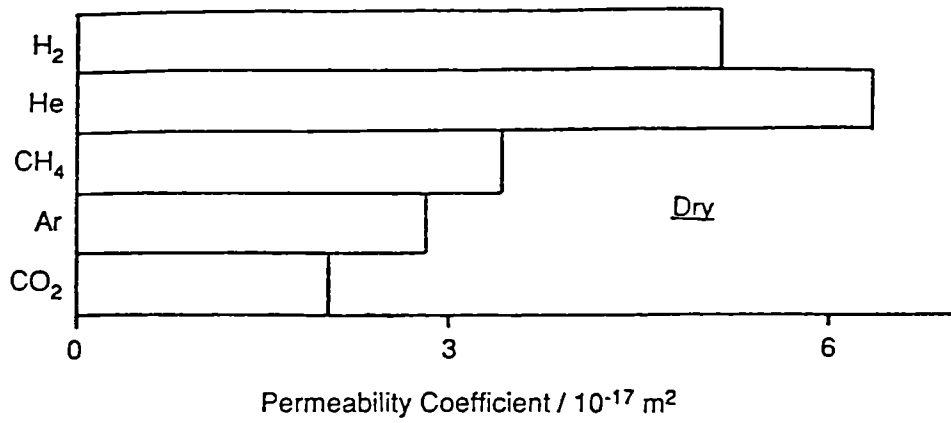
Figure 13   Summary of the permeability coefficients measured for PFA/OPC-concrete conditioned under dry, 75 % relative humidity and 100 % relative humidity conditions. All measurements were performed using a constant average pressure of 100 kPa.
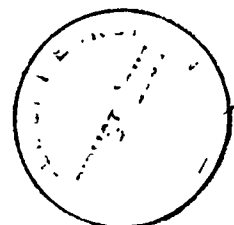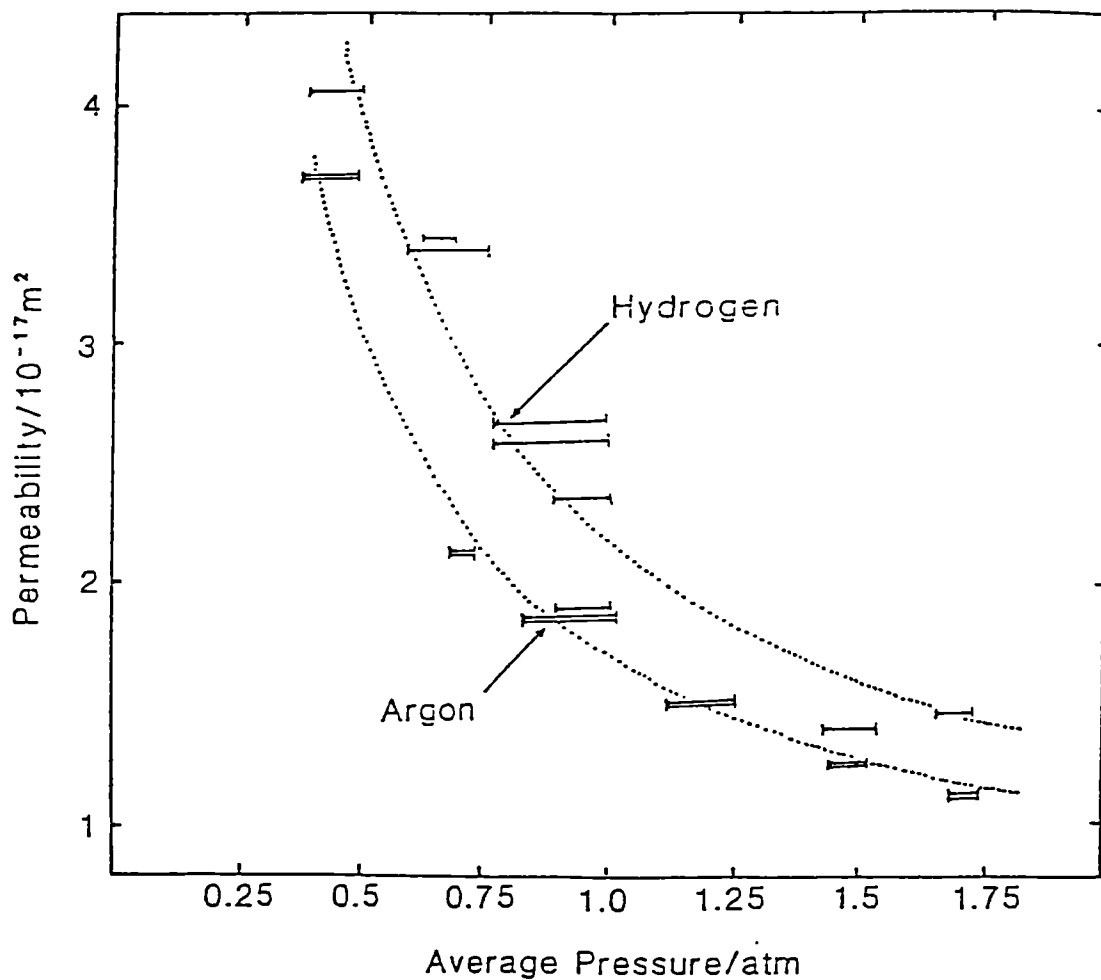
Figure 14 Variation in the permeability coefficients for hydrogen and argon in dry SRPC-concrete with average pressure. The curves demonstrate the fit of the Klinkenberg equation to the data. The permeability coefficients are expressed as $k / 10^{-17}$ m^2. Error bars illustrate the slight variation in average pressure which occurred during individual experiments.
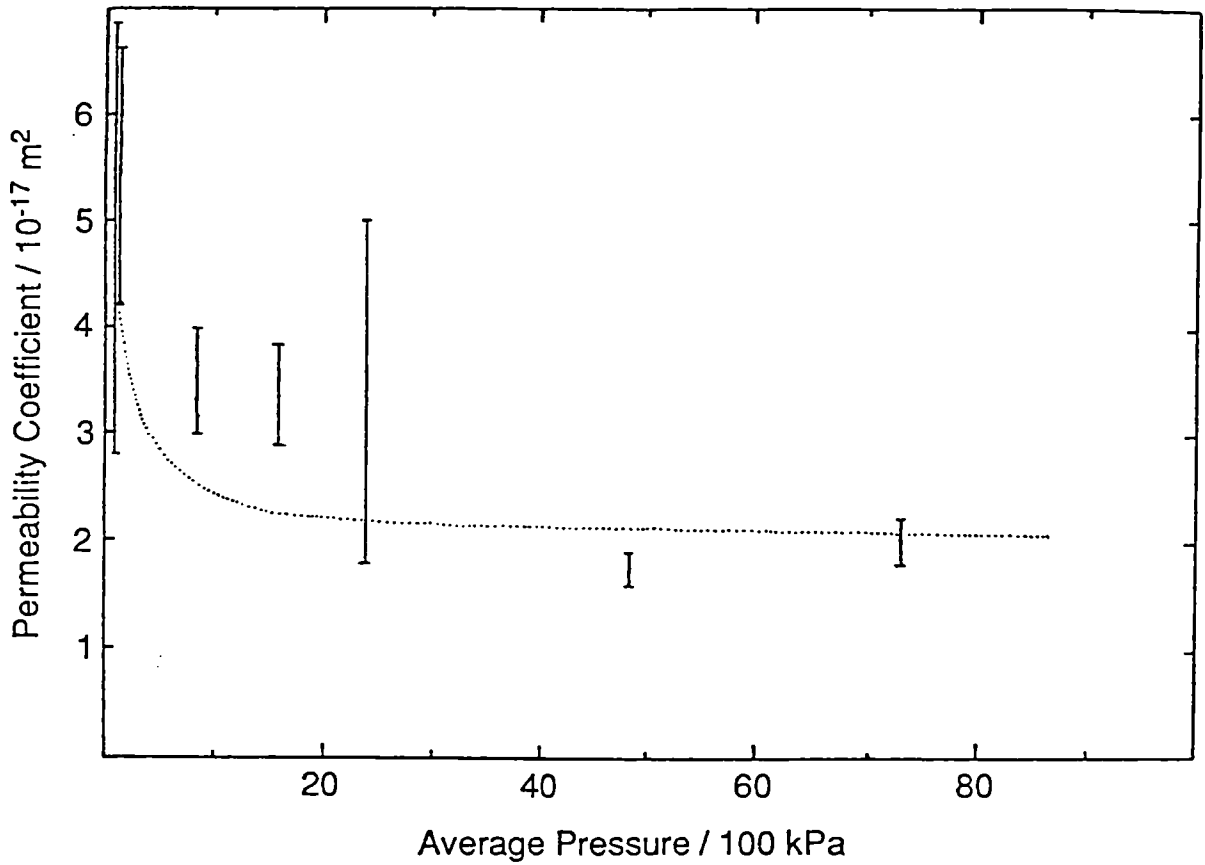
Figure 15   Variation in the permeability coefficient for argon in dry
PFA/OPC-concrete with average pressure. Each point is the mean of
several experiments carried out at the same average pressure. The
permeability coefficients are expressed as $k / 10^{-17}$ m^2.
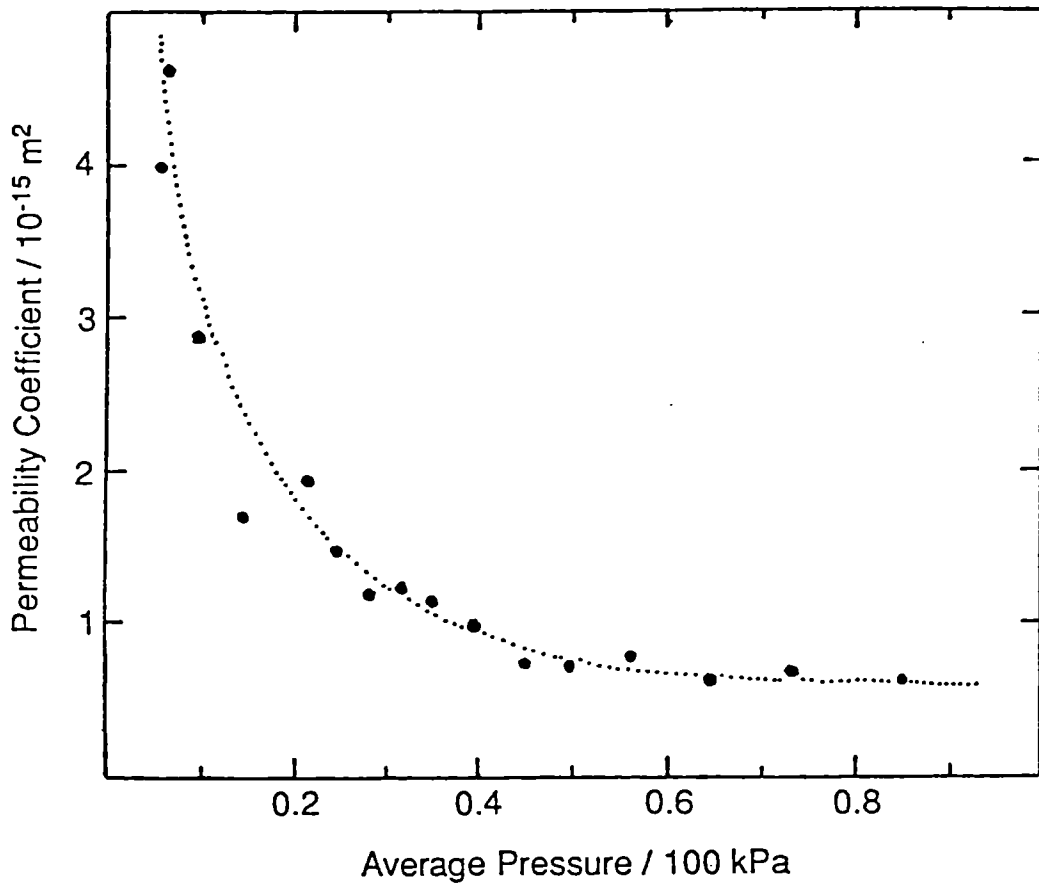
Figure 16 Variation in permeability coefficient with average pressure in the BFS/OPC-grout during a single varying average pressure experiment. Measured values of the infinite pressure permeability coefficient and Klinkenberg constant were 3.64×10^{-16} m^2 and 7.31×10^4 Pa respectively.
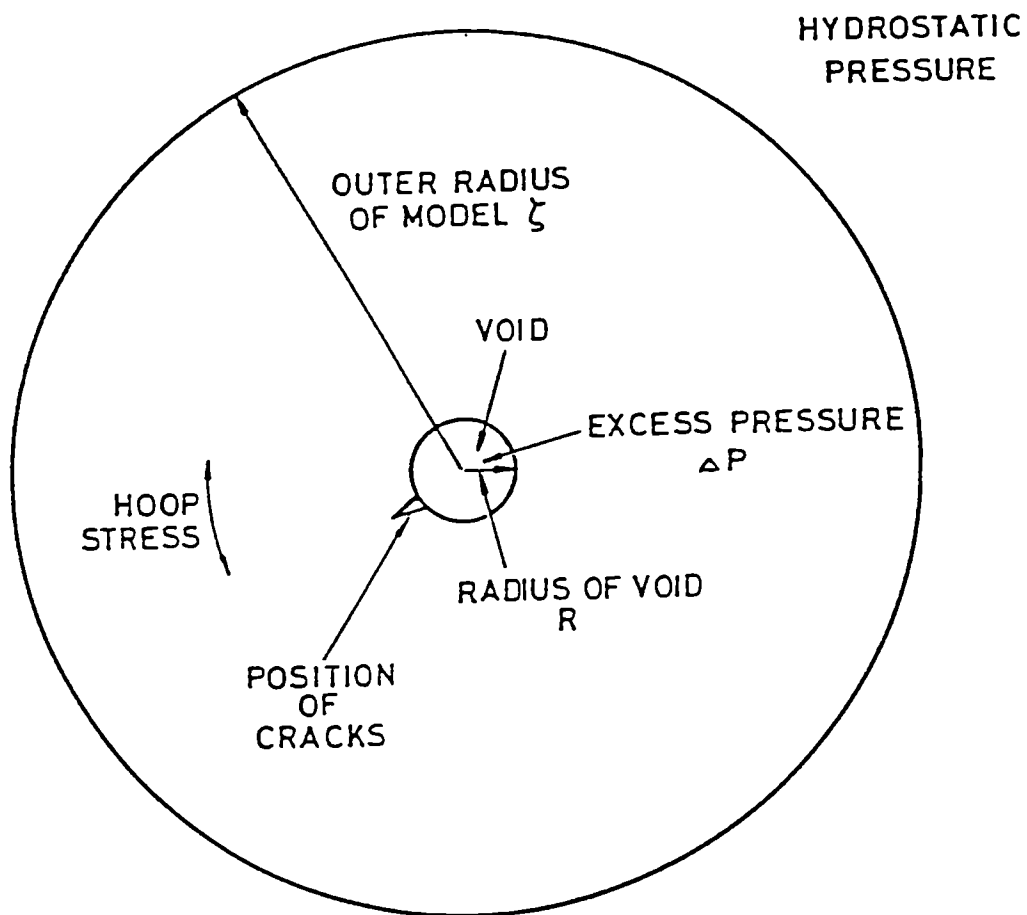
Figure 17 Illustration of the spherical repository approximation used as the basis for the model of stress and crack generation in backfill.
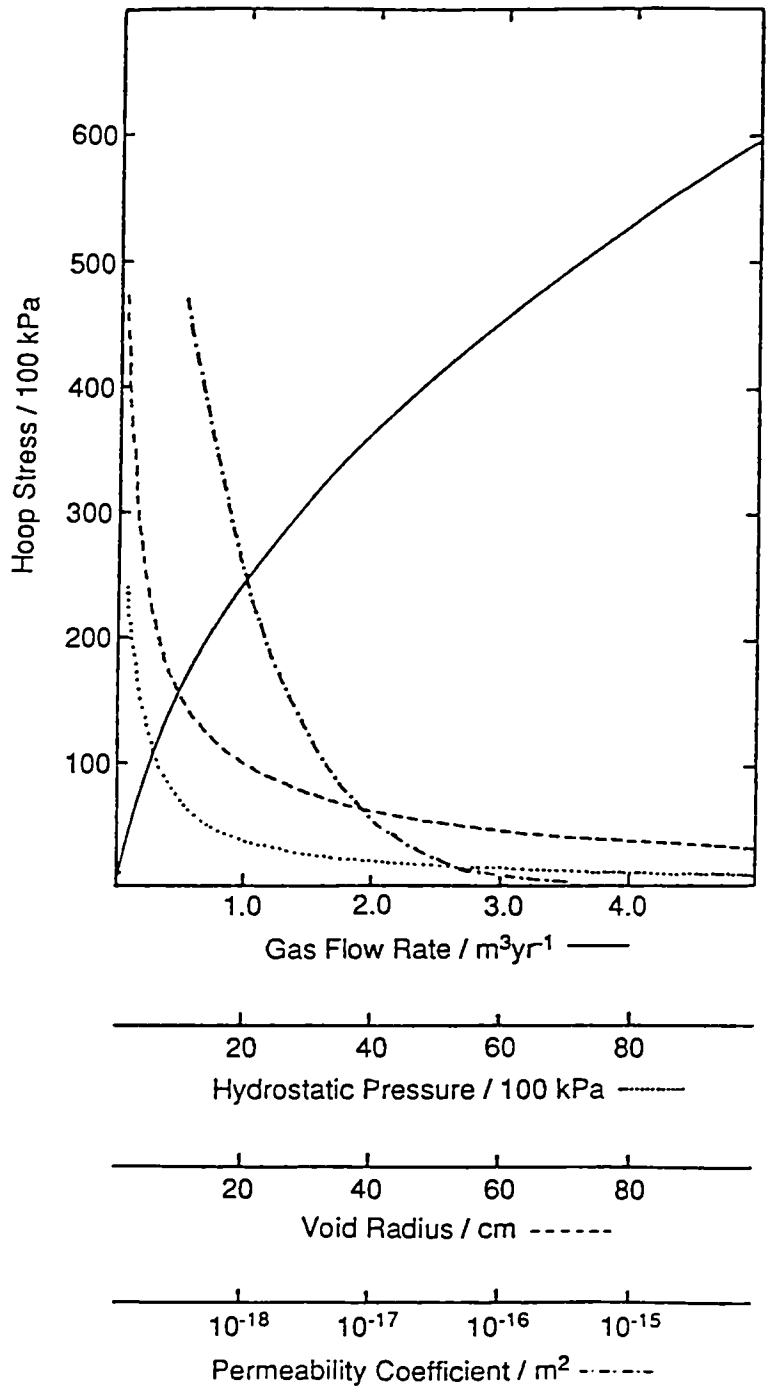
Figure 18 Variation in spherical hoop stress at the void surface with gas generation rate, hydrostatic pressure, void radius and backfill permeability coefficient, calculated from the analytical solution to the stress generation model.
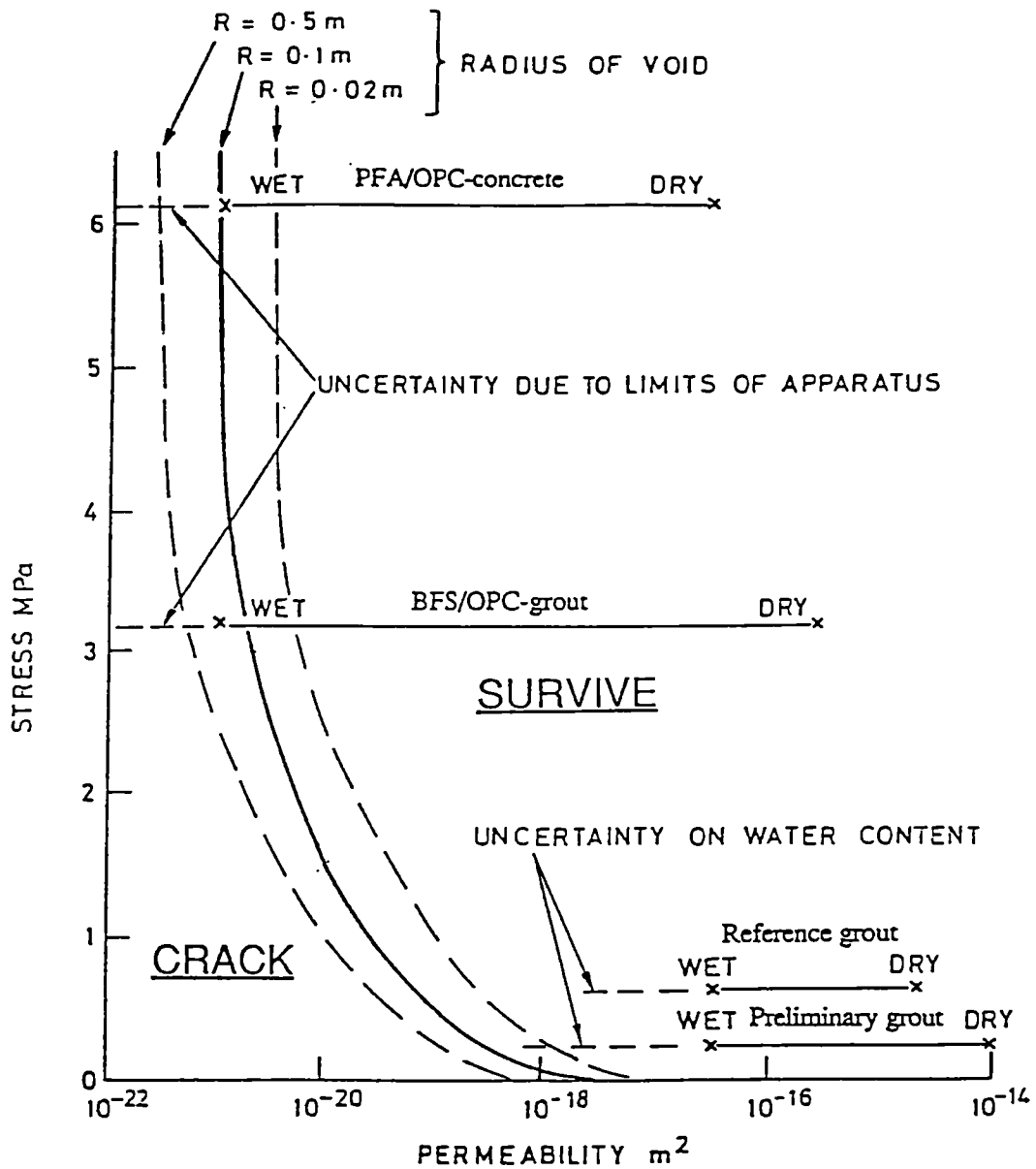
Figure 19 Summary of the conclusions of the stress generation model. The variation in tangential hoop stress at the void surface for three different void radii is plotted against permeability coefficient. The estimated tensile strengths for the materials investigated in this work are also plotted against the range of the permeability coefficients. A material is considered to crack if the calculated stress exceeds the tensile strength, as shown by the regions labelled "survive" and "crack".

The performance of the cementitious materials within a radioactive waste repository as a physical barrier to the migration of radionuclides depends on the maintenance of the integrity of the barrier. Potentially, this can be compromised by physical damage to the barrier caused by pressurization as gas is generated within the repository. The maintenance of chemical homogeneity within the material used for backfilling the repository may also be compromised as a consequence of gas pressurization through the formation of additional cracks and the reaction of cementitious materials with gases such as carbon dioxide. Consequently, the migration of gas within repository construction materials may be a significant parameter in both the design of a repository and the provision of a safety-case for disposal. The migration of hydrogen, helium, methane, argon and carbon dioxide has been studied for materials selected to be typical of repository structural concretes and grouts that are being considered for backfilling and waste encapsulation. The apparent permeability of these materials to gas has been shown to be dependent on gas type and average pressure in the structural concrete due to the effects of Knudsen flow at pressures of the order of 100 kPa. This is not observed in the grouts due to the significantly greater pore size. The permeability coefficients of the grouts are several orders of magnitude greater than those of the concrete. Gas migration is strongly influenced by the degree of water saturation of the materials. The presence of interfaces within the materials results in an increase in permeability at higher degrees of water saturation. A simple model has been developed to simulate the effects of gas pressurization. The tangential hoop stress at the surface of a void is calculated and comparison with the expected tensile strength of the materials is used to assess the potential for cracking. The backfill grouts seem to have sufficient permeability to disperse gas without crack formation.

Venta y suscripciones • Salg og abonnement • Verkauf und Abonnement • Πωλήσεις και συνδρομές
Sales and subscriptions • Vente et abonnements • Vendita e abbonamenti
Verkoop en abonnementen • Venda e assinaturas

BELGIQUE / BELGIË

**Moniteur belge /
Belgisch Staatsblad**
Rue de Louvain 42 / Leuvenseweg 42
B-1000 Bruxelles / B-1000 Brussel
Tél. (02) 512 00 26
Fax (02) 511 01 84

Autres distributeurs /
Overige verkooppunten

**Librairie européenne/
Europese boekhandel**
Rue de la Loi 244/Wetstraat 244
B-1040 Bruxelles / B-1040 Brussel
Tél. (02) 231 04 35
Fax (02) 735 08 60

Jean De Lannoy
Avenue du Roi 202 /Koningslaan 202
B-1060 Bruxelles / B-1060 Brussel
Tél. (02) 538 51 69
Télex 63220 UNBOOK B
Fax (02) 538 08 41

Document delivery:

Credoc
Rue de la Montagne 34 / Bergstraat 34
Bte 11 / Bus 11
B-1000 Bruxelles / B-1000 Brussel
Tél. (02) 511 69 41
Fax (02) 513 31 95

DANMARK

J. H. Schultz Information A/S
Herstedvang 10-12
DK-2620 Albertslund
Tlf. (45) 43 63 23 00
Fax (Sales) (45) 43 63 19 69
Fax (Management) (45) 43 63 19 49

DEUTSCHLAND

Bundesanzeiger Verlag
Breite Straße
Postfach 10 80 06
D-W-5000 Köln 1
Tel. (02 21) 20 29-0
Telex ANZEIGER BONN 8 882 595
Fax 2 02 92 78

GREECE/ΕΛΛΑΔΑ

G.C. Eleftheroudakis SA
International Bookstore
Nikis Street 4
GR-10563 Athens
Tel. (01) 322 63 23
Telex 219410 ELEF
Fax 323 98 21

ESPAÑA

Boletín Oficial del Estado
Trafalgar, 29
E-28071 Madrid
Tel. (91) 538 22 95
Fax (91) 538 23 49

Mundi-Prensa Libros, SA
Castelló, 37
E-28001 Madrid
Tel. (91) 431 33 99 (Libros)
          431 32 22 (Suscripciones)
          435 36 37 (Dirección)
Télex 49370-MPLI-E
Fax (91) 575 39 98

Sucursal:

Librería Internacional AEDOS
Consejo de Ciento, 391
E-08009 Barcelona
Tel. (93) 488 34 92
Fax (93) 487 76 59

**Llibreria de la Generalitat
de Catalunya**
Rambla dels Estudis, 118 (Palau Moja)
E-08002 Barcelona
Tel. (93) 302 68 35
     302 64 62
Fax (93) 302 12 99

FRANCE

**Journal officiel
Service des publications
des Communautés européennes**
26, rue Desaix
F-75727 Paris Cedex 15
Tél. (1) 40 58 75 00
Fax (1) 40 58 77 00

IRELAND

Government Supplies Agency
4-5 Harcourt Road
Dublin 2
Tel. (1) 61 31 11
Fax (1) 78 06 45

ITALIA

Licosa SpA
Via Duca di Calabria, 1/1
Casella postale 552
I-50125 Firenze
Tel. (055) 64 54 15
Fax 64 12 57
Telex 570466 LICOSA I

GRAND-DUCHÉ DE LUXEMBOURG

Messageries Paul Kraus
11, rue Christophe Plantin
L-2339 Luxembourg
Tél. 499 88 88
Télex 2515
Fax 499 88 84 44

NEDERLAND

SDU Overheidsinformatie
Externe Fondsen
Postbus 20014
2500 EA 's-Gravenhage
Tel. (070) 37 89 911
Fax (070) 34 75 778

PORTUGAL

Imprensa Nacional
Casa da Moeda, EP
Rua D. Francisco Manuel de Melo, 5
P-1092 Lisboa Codex
Tel. (01) 69 34 14

**Distribuidora de Livros
Bertrand, Ld.ª**
Grupo Bertrand, SA
Rua das Terras dos Vales, 4-A
Apartado 37
P-2700 Amadora Codex
Tel. (01) 49 59 050
Telex 15798 BERDIS
Fax 49 60 255

UNITED KINGDOM

HMSO Books (Agency section)
HMSO Publications Centre
51 Nine Elms Lane
London SW8 5DR
Tel. (071) 873 9090
Fax 873 8463
Telex 29 71 138

ÖSTERREICH

**Manz'sche Verlags-
und Universitätsbuchhandlung**
Kohlmarkt 16
A-1014 Wien
Tel. (0222) 531 61-0
Telex 112 500 BOX A
Fax (0222) 531 61-39

SUOMI

Akateeminen Kirjakauppa
Keskuskatu 1
PO Box 128
SF-00101 Helsinki
Tel. (0) 121 41
Fax (0) 121 44 41

NORGE

Narvesen information center
Bertrand Narvesens vei 2
PO Box 6125 Etterstad
N-0602 Oslo 6
Tel. (2) 57 33 00
Telex 79668 NIC N
Fax (2) 68 19 01

SVERIGE

BTJ
Tryck Traktorwägen 13
S-222 60 Lund
Tel. (046) 18 00 00
Fax (046) 18 01 25

SCHWEIZ / SUISSE / SVIZZERA

OSEC
Stampfenbachstraße 85
CH-8035 Zürich
Tel. (01) 365 54 49
Fax (01) 365 54 11

CESKOSLOVENSKO

NIS
Havelkova 22
13000 Praha 3
Tel. (02) 235 84 46
Fax 42-2-264775

MAGYARORSZÁG

Euro-Info-Service
Pf. 1271
H-1464 Budapest
Tel./Fax (1) 111 60 61/111 62 16

POLSKA

Business Foundation
ul. Krucza 38/42
00-512 Warszawa
Tel. (22) 21 99 93, 628-28-82
International Fax&Phone
(0-39) 12-00-77

ROUMANIE

Euromedia
65, Strada Dionisie Lupu
70184 Bucuresti
Tel./Fax 0 12 96 46

BULGARIE

D.J.B.
59, bd Vitocha
1000 Sofia
Tel./Fax 2 810158

RUSSIA

**CCEC (Centre for Cooperation with
the European Communities)**
9, Prospekt 60-let Oktyabria
117312 Moscow
Tel. 095 135 52 87
Fax 095 420 21 44

CYPRUS

**Cyprus Chamber of Commerce and
Industry**
Chamber Building
38 Grivas Dhigenis Ave
3 Deligiorgis Street
PO Box 1455
Nicosia
Tel. (2) 449500/462312
Fax (2) 458630

TURKIYE

**Pres Gazete Kitap Dergi
Pazarlama Dağitim Ticaret ve sanayi
AŞ**
Narlıbahçe Sokak N. 15
Istanbul-Cağaloğlu
Tel. (1) 520 92 96 - 528 55 66
Fax 520 64 57
Telex 23822 DSVO-TR

ISRAEL

ROY International
PO Box 13056
41 Mishmar Hayarden Street
Tel Aviv 61130
Tel. 3 496 108
Fax 3 544 60 39

CANADA

Renouf Publishing Co. Ltd
Mail orders — Head Office:
1294 Algoma Road
Ottawa, Ontario K1B 3W8
Tel. (613) 741 43 33
Fax (613) 741 54 39
Telex 0534783

Ottawa Store:
61 Sparks Street
Tel. (613) 238 89 85

Toronto Store:
211 Yonge Street
Tel. (416) 363 31 71

UNITED STATES OF AMERICA

UNIPUB
4611-F Assembly Drive
Lanham, MD 20706-4391
Tel. Toll Free (800) 274 4888
Fax (301) 459 0056

AUSTRALIA

Hunter Publications
58A Gipps Street
Collingwood
Victoria 3066
Tel. (3) 417 5361
Fax (3) 419 7154

JAPAN

Kinokuniya Company Ltd
17-7 Shinjuku 3-Chome
Shinjuku-ku
Tokyo 160-91
Tel. (03) 3439-0121

Journal Department
PO Box 55 Chitose
Tokyo 156
Tel. (03) 3439-0124

SINGAPORE

Legal Library Services Ltd
STK Agency
Robinson Road
PO Box 1817
Singapore 9036

**AUTRES PAYS
OTHER COUNTRIES
ANDERE LÄNDER**

**Office des publications officielles
des Communautés européennes**
2, rue Mercier
L-2985 Luxembourg
Tél. 499 28 1
Télex PUBOF LU 1324 b
Fax 48 85 73/48 68 17

CD-NA-14194-EN-C